

AD-A113 975

ELECTROCHEMICAL TECHNOLOGY CORP SEATTLE WA
DETERMINATION OF THE EFFECT OF COMPOSITION, STRUCTURE AND ELECT--ETC(U)
OCT 81 R T RUGGERI, T R BECK

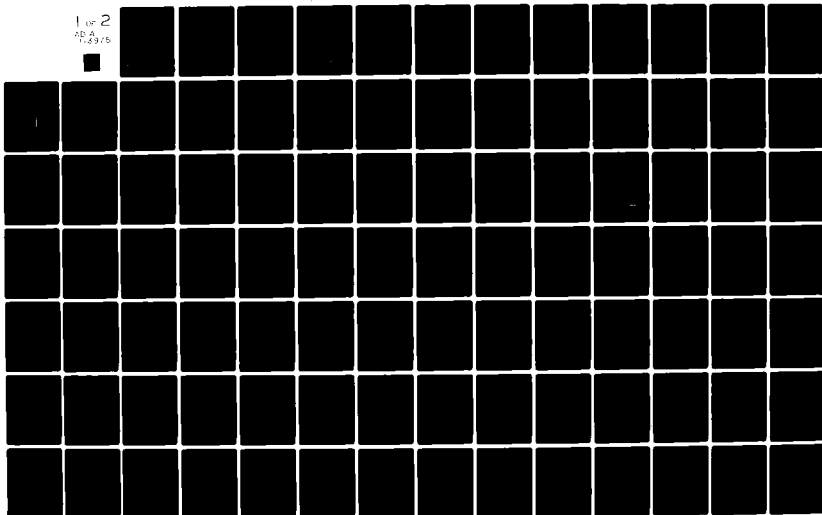
F/G 11/3

N00014-79-C-0021

NL

UNCLASSIFIED

1 of 2
ADA
1-8975



AD A113975

Contract No. N00014-79-C-0021

12

DETERMINATION OF THE EFFECT OF COMPOSITION,
STRUCTURE AND ELECTROCHEMICAL MASS TRANSPORT
PROPERTIES ON ADHESION AND CORROSION
INHIBITION OF PAINT FILMS.

Final Report
October 30, 1981

Prepared for
UNITED STATES NAVY
Navel Ocean Research and Development Activity
Bay St. Louis, Mississippi 39520

By:
ELECTROCHEMICAL TECHNOLOGY CORP.
3935 Leary Way N.W.
Seattle, WA 98107

DTIC FILE COPY

DTIC
ELECTE
APR 28 1982
E

ROBERT T. RUGGERI

THEODORE R. BECK, Principal Investigator

82 04 28 057

This document has been approved
for public release and sale; its
distribution is unlimited.

Unclassified

SECURITY CLASSIFICATION OF THIS PAGE (When Data Entered)

REPORT DOCUMENTATION PAGE		READ INSTRUCTIONS BEFORE COMPLETING FORM
1. REPORT NUMBER	2. GOVT ACCESSION NO.	3. RECIPIENT'S CATALOG NUMBER
	AD A113975	
4. TITLE (and Subtitle) Determination of the Effect of Composition, Structure, and Electrochemical Mass Transport Properties on Adhesion and Corrosion Inhibition of Paint Films		5. TYPE OF REPORT & PERIOD COVERED Final Nov. 1, 1980 to Oct. 31, 1981
		6. PERFORMING ORG. REPORT NUMBER
7. AUTHOR(s) R. T. Ruggeri and T. R. Beck		8. CONTRACT OR GRANT NUMBER(s) N00014-79-C-0021
9. PERFORMING ORGANIZATION NAME AND ADDRESS Electrochemical Technology Corp. 3935 Leary Way N.W. Seattle, WA 98107		10. PROGRAM ELEMENT, PROJECT, TASK AREA & WORK UNIT NUMBERS
11. CONTROLLING OFFICE NAME AND ADDRESS United States Navy Naval Ocean Research and Development Activity Bay St. Louis, MS 39250		12. REPORT DATE October 1981
		13. NUMBER OF PAGES 114
14. MONITORING AGENCY NAME & ADDRESS (if different from Controlling Office)		15. SECURITY CLASS. (of this report) Unclassified
		15a. DECLASSIFICATION DOWNGRADING SCHEDULE
16. DISTRIBUTION STATEMENT (of this Report) Reproduction in whole or in part is permitted for any purpose of the United States Government.		
17. DISTRIBUTION STATEMENT (of abstract entered in Block 20, if different from Report)		
18. SUPPLEMENTARY NOTES None		
19. KEY WORDS (Continue on reverse side if necessary and identify by block number) Paint, polyurethane, vinyl, diffusion, corrosion, mass transport, sodium ion, chloride ion, water, permeation, permeability coefficient, diffusivity.		
20. ABSTRACT (Continue on reverse side if necessary and identify by block number) Since 1979, nine paints meeting military specifications have been studied. Seven of these paints have been formulated with well known chemical compositions. A sequence of tests including dynamic mechanical, IR and UV spectroscopy, and small angle x-ray scattering was performed to determine the physical and chemical structure of the paints. At the same time, new apparatus and techniques were developed to measure the transport of ions and water through paint films.		

DD FORM 1 JAN 73 1473

Unclassified

SECURITY CLASSIFICATION OF THIS PAGE (When Data Entered)

Unclassified

SECURITY CLASSIFICATION OF THIS PAGE(When Data Entered)

In the past year, Hittorf experiments have been conducted to measure the migration of sodium chloride and water through paints. Improved "humidity chamber" apparatus and techniques have been developed to measure the diffusivity and solubility of water in paints attached to metal substrates. Five new mathematical models, developed to interpret the results of these experiments, have been used to deduce the physical form of coatings applied to metals. Preliminary experiments have been conducted to measure the hydraulic permeability of electrolytes through paints. These experiments were performed to obtain coefficients needed for the corrosion model. Also, experiments have been initiated to determine which components of paints have the greatest influence on water diffusivity.

Hittorf Experiments: The transference numbers and permeabilities of ions have been measured in Hittorf experiments. Most experiments were conducted on one type of polyurethane, but three other coatings have also been tested. The most significant finding was that when polyurethane is in NaCl solution, sodium and chloride ions do not carry all the current. The concept that ions other than sodium and chloride carry some current was proposed as a hypothesis in the last annual report. Only indirect evidence supporting the hypothesis was available last year. Since then, measurements have been made of both the sodium and chloride fluxes. These measurements confirm that the total current is greater than that attributable to sodium and chloride migration. Experiments have been conducted to determine which other ions are carrying the balance of the current, but definitive results have not yet been obtained.

Water Solubility: The solubility of water in polyurethane has been measured with the humidity chamber apparatus. Eighteen samples of polyurethane film attached to gold have been tested. Water sorption by the paint was measured at five different relative humidities: 10%, 30%, 56%, 84%, and 98%. The temperature was 29°C. The results obtained with this apparatus are in agreement with those obtained by gravimetric methods using a Cahn electrobalance. The results may be interpreted in two ways; either the solubility increases as the coating thickness decreases, or a water-rich phase exists near the paint-gold interface. Work is continuing to determine which interpretation is correct.

Water Diffusivity: The diffusivity of water in polyurethane has been determined by measuring unsteady-state sorption. It has been determined that the diffusivity is not constant inside polyurethane paint. The diffusivity is now known to be a complex function of the water concentration and passes through a maximum between zero and 100% relative humidity (29°C). Model calculations suggest that the diffusivity may also be a function of position in the paint. Future work will concentrate on identifying features of diffusion generally applicable to paints. The paint components having the greatest influence on water diffusivity will also be identified.

Hydraulic Permeability: Hydraulic permeability experiments were conducted with five types of paint. The paints can be divided into two categories. Some paints exhibit very low permeabilities, on the order of 10^{-5} $\mu\text{l/psig}\cdot\text{cm}\cdot\text{min}$, and others have permeabilities 100 to 1,000 times greater. Some of the high-permeability paint films were nonuniform. Most of the flow was through small "weak" spots. A similar flow mechanism is possible for the low-permeability films, but this was not confirmed. All experiments were conducted in sodium chloride solution, and attempts were made to measure the salt rejection and the water flux. Only high-permeability films could be tested for salt rejection, and no rejection was observed. This result indicates that the "weak" spots in these coatings are relatively porous, and salt, as well as water, can penetrate the films.

Unclassified

SECURITY CLASSIFICATION OF THIS PAGE(When Data Entered)

TABLE OF CONTENTS

	<u>Page</u>
1.0 Introduction	1
2.0 Summary	3
3.0 Results and Discussion	6
3.1 Ion Migration	6
3.1.1 Introduction	6
3.1.2 Apparatus	7
3.1.3 Procedure	11
3.1.4 Results	15
3.1.5 Discussion	15
3.1.6 Conclusions	23
3.2 Diffusivity and Solubility of Water in Polyurethane	25
3.2.1 Introduction	25
3.2.2 Theory	26
3.2.2-1 Crystal Oscillator	26
3.2.2-2 Sorption in a Thin Sheet	29
3.2.3 Apparatus	31
3.2.4 Procedure	35
3.2.4-1 Data Analysis	37
3.2.5 Results	41
3.2.6 Discussion	45
3.2.7 Conclusions	57
3.3 Zero-Capacity Cell	59
3.4 Hydraulic Permeability	60
3.5 Sorption of Radiotracer Ions	60
4.0 Appendices	
A. Paint Formulations	
B. Published Paper	
C. Experimental Results	

Accession For	
NTIS GRA&I	<input checked="" type="checkbox"/>
DTIC TAB	<input type="checkbox"/>
Unannounced	<input type="checkbox"/>
Justification	<i>for on file</i>
By	
Distribution/	
Availability Codes	
Dist	Avail and/or Special
<i>A</i>	



ACKNOWLEDGEMENT

Most of the experimental work in the third year was done in house by chemical technician, J.H. Mabe. The Department of Chemical Engineering, University of Washington, provided facilities for scintillation counting of radioisotope samples. William P. Miller, Assistant Director of Reactor Operations at the University of Washington provided invaluable assistance and hardware required for radiotracer experiments. Professor J.C. Seferis and student, A.R. Wedgewood, continued to provide consulting on physical and mechanical properties of paint films. P. Olson, Experimental Research Equipment Co., made the special equipment necessary to carry out the work. M. Flynn typed the report.

Special appreciation is extended to Dr. Edward J. Green, Program Director, Chemical Oceanography Division, Naval Ocean Research and Development Activity, Bay St. Louis, Mississippi, for his continued support and encouragement of this program.

1.0 INTRODUCTION

There is a need for a more quantitative understanding of the corrosion of painted metals. The electrochemistry of corrosion has been extensively studied, but its application to painted-metal systems has been impeded because the chemical composition and electric potential at the paint-metal interface cannot be measured. Three factors control the local electrochemical conditions at the paint-metal interface: reaction kinetics on the metal, mass transfer through the paint, and the external environment on the side of the paint opposite the metal. A quantitative model of corrosion has been proposed (1). The model describes the mass transfer of ions and water through paint coatings. The current work had two primary purposes: to determine the transport properties of representative types of paint, and to determine the effects of the physical structure and the chemical composition of paints on the transport properties.

It was desired to obtain the required information about the transport properties of paints in a systematic manner. Therefore, the physical properties of nine different paints, of interest to the Navy, were studied. Seven of these paints were formulated in this laboratory and were of known composition (2). The other two were purchased from commercial sources. In order to characterize the physical properties, a sequence of tests was performed. The tests included dynamic mechanical, IR and UV spectroscopy, and small angle x-ray scattering. Quantitative measurements were also performed to determine the effects of external environment on paint adhesion.

The next step was the investigation of the transport properties of the paints (3). In order to simplify the system only the transport of sodium, chloride, and water through paints immersed in sodium chloride solution was studied. The paint film was considered to be a single organic polymer phase in which water and salt were dissolved. The paint was assumed to possess a small bound charge giving it the characteristics of an ion-exchange membrane. Experiments were designed and conducted to measure the migration of sodium and chloride ions, and mathematical models of the paint were used to interpret the data. The net result of this early work on the transport processes was the

hypothesis that sodium and chloride ions were not carrying all the current through paint films immersed in sodium chloride solution (4).

In the past year the work has been concentrated in two areas. First, the hypothesis that ions other than sodium and chloride carry a fraction of the current was investigated more fully than before. The sodium and chloride ionic fluxes have now been measured in a single piece of polyurethane. Experiments have also been conducted to determine which ions other than sodium and chloride carry current, but no definitive results have yet been obtained.

The second area in which recent work has been concentrated is the transport of water through paints. A new apparatus and experimental technique were developed to measure water solubility and diffusivity in paints attached to metals. The key role water plays in the mechanism of corrosion has long been recognized, but it is difficult to study the diffusion of water through coatings attached to metals. The experimental techniques developed here provide the opportunity to evaluate fundamental thermodynamic properties of paint mixtures, the heat of solution of water or salt, for example. Knowledge of these properties is necessary before any comprehensive model of corrosion can be of practical value.

Much has been learned about paint film properties in this contract, but the research program on the effect of composition, structure, and electrochemical mass transport properties on adhesion and corrosion inhibition of paint films as originally envisaged remains to be completed. Work will be continued of funds from other sources.

2.0 SUMMARY

This work was conducted to systematically evaluate the parameters which control the corrosion rate of painted metal. Previously, it was shown that water reduces the adhesion of paint binders to metals in a matter of minutes. When water was removed, the adhesion recovered to nearly its original value (5). It was therefore concluded that the paints which were studied lost adhesion as a result of water penetration to the paint-metal interface, not because corrosion had taken place. Early work also included small angle x-ray studies. The results of these studies were interpreted as evidence of clusters within the paint films. The clusters could be either water or some feature of internal polymer structure. Similar results with Nafion membranes have also been interpreted as evidence of clusters (607).

The diffusivity of water through paint films was also investigated previously. Films unattached to any substrate were used in these experiments. Permeability coefficients were determined for all the paints except the epoxies. The permeability coefficients at 25°C ranged from $2.6 \times 10^{-14} \text{ m}^2/\text{s}$ for a polyurethane (N PUR)¹ and a vinyl resin (VR4) to $7.8 \times 10^{-14} \text{ m}^2/\text{s}$ for VR2. The solubility of water in one type of polyurethane (O PUR) was determined. The diffusivity was determined from the solubility and permeability coefficient to be about $3.5 \times 10^{-12} \text{ m}^2/\text{s}$. The time required for water to penetrate the coating and reach the metal can be calculated from the diffusivity and the coating thickness. The diffusion time for a 50 μm thick coating of polyurethane is about 12 minutes. Similar times can be expected for the other paints if water is about as soluble in them as it is in the polyurethane. These early experiments also provided evidence that the solubility of water in a vinyl resin (VR3) was very sensitive to the plasticizer (tricresyl phosphate) content. This effect is in addition to the changes in diffusivity resulting from increased plasticization. These results indicated that the transport properties of paints were greatly altered by the presence of small amounts of some paint components.

¹ See Appendix A for paint designations and formulations.

Previous work was also conducted to determine the mobility of ions through paint films. The permeability coefficients of sodium and chloride were found to be about $10^{-18} \text{ m}^2/\text{s}$ in polyurethane (O PUR), at 25°C . The dimensionless solubility of sodium chloride in OPUR was measured and found to be on the order of 10^{-3} . A $50 \text{ }\mu\text{m}$ thick coating of OPUR will be penetrated by NaCl in approximately 30 days based on these numbers. Other conclusions drawn from the work on ion transport showed that the transport properties of paints changed significantly with time. This conclusion has been substantiated by the work described in this report, but the cause of the changes is not yet known.

The most recent work has supported the previous conclusion that ions other than sodium and chloride carry some current. The migration fluxes of both sodium and chloride through a single piece of polyurethane (O PUR) were determined in separate experiments. The results of these experiments were consistent with those obtained in other experiments which measured the individual ionic fluxes through separate paint specimens of equal age. It has therefore been concluded that sodium and chloride do not carry all the current through this type of polyurethane. A search was initiated to determine a mechanism to explain this phenomenon, but no satisfactory explanation has yet been found.

Recent work has also been conducted to develop experimental and analytical techniques to measure water diffusion in paints attached to metal substrates. A method was developed using a gold-coated quartz crystal. The diffusivity and solubility of water in polyurethane (O PUR) was determined by measuring the resonant frequency of a painted crystal. The solubility results obtained with this apparatus were in good agreement with data obtained using gravimetric methods. These results also suggest that a water-rich phase exists near the gold-polyurethane interface. This finding is in accord with results obtained by Funke (8).

The diffusivity of water was also measured with the crystal-oscillator apparatus. The diffusivity was found to be a complex function of the water content of polyurethane (O PUR). The diffusivity exhibits a maximum value at about 80% relative humidity at 29°C . A tentative explanation of this behavior is proposed, based on a shift

in the glass transition temperature (T_g) through 29°C.

This work formed the basis for three papers presented to professional groups. "The Transport Properties of Polyurethane Paint" (4) and "An Investigation of the Mass Transfer Characteristics of Polyurethane Paint" (15) are included as Appendix B in the Annual Progress Report No. 2(3). "The Effects of Environment on Paint Adhesion to Steel" is included here as Appendix B (5).

3.0 RESULTS AND DISCUSSION

3.1 Ion Migration

3.1.1 Introduction

The transport of ions through protective coatings on metal has long been recognized as an important phenomenon related to the corrosion rate (9). Generally, protective coatings are dense organic phases relatively impermeable to ionic species. This fact makes measuring ionic fluxes through these coatings difficult. It also obscures the origin of ions at the paint-metal interface. Were these ions simply painted over, or did the ions diffuse through the coating to reach the interface? This work was conducted to help answer these questions and to develop a quantitative description of the transport of ions through paints.

Several investigations of the transport of ions through paints have been conducted in the past (9-17). The paint is usually studied as a membrane separating two electrolyte solutions. In this arrangement, two types of experiments are commonly performed: membrane potential, and Hittorf experiments. The membrane potential experiments are conducted by measuring an electrochemical-potential difference across the membrane which separates solutions of unequal concentration. These experiments have the advantage that they are easy to perform, but the disadvantage that the results depend only on the ratios of ionic mobilities. Hittorf experiments are more difficult to conduct than those measuring membrane potential, but the classic Hittorf analysis allows one to calculate individual ionic fluxes.

In the Hittorf method, the total current through the cell is measured. The changes in electrolyte concentration in the cells are also measured and the ionic fluxes are then calculated. In order to perform this calculation it is tacitly assumed that all mobile ions are known. Then, the total current is the sum of the individual ionic currents. This assumption has been verified for solutions of simple salts and some membranes (18), but it has not been previously tested for transport through dense organic polymers.

In this work modified Hittorf experiments were conducted with a

variety of commercial and military paint coatings. Radiotracers were used to measure both the sodium and chloride fluxes through paint membranes in sodium chloride solutions. Definitive results have been obtained for one type of polyurethane. In this case, the sum of the ionic currents attributed to sodium and chloride was less than the total current conducted through the cell.

3.1.2 Apparatus

Both membrane-potential and Hittorf experiments were conducted in the same apparatus. Figure 1 illustrates the experimental cell which was made of Plexiglas. When assembled, each cell was composed of two cylindrical compartments separated by a paint membrane. The two compartments were aligned vertically. Both compartments were equipped with sampling ports and overflow tubes. The sampling ports were sealed with rubber septums, but the overflow tubes were open to the air. The overflow tubes were made of capillary tubing with one end drawn down to a small diameter. This construction reduced water evaporation to a negligible level. The overflow tubes from both the top and bottom compartments were bent above the cell so they were in the same horizontal plane. In this way the hydrostatic pressure difference across the membrane was minimized.

The cell was constructed in two halves. Internally, each cell was identical, but the external connections (sampling ports, overflow tubes, etc.) were in different positions on the bottom and the top half-cells. The paint membrane was clamped between the two half-cells which were held together by four bolts. Viton O-ring gaskets were used to prevent the chambers from leaking between the paint and the Plexiglas.

Each compartment was equipped with a silver-silver chloride electrode. The electrodes were glued to the Plexiglas with epoxy. The electrode diameter was the same as the "active" diameter of the membrane, and both electrodes were parallel to, and equidistant from, the membrane.

Small Teflon-coated magnetic stir bars were used to stir the solutions in both compartments. The stir bar in the bottom compartment was held above the electrode surface by a circular disc of plastic window screen. Similar screens were clamped on each side of the paint membrane as

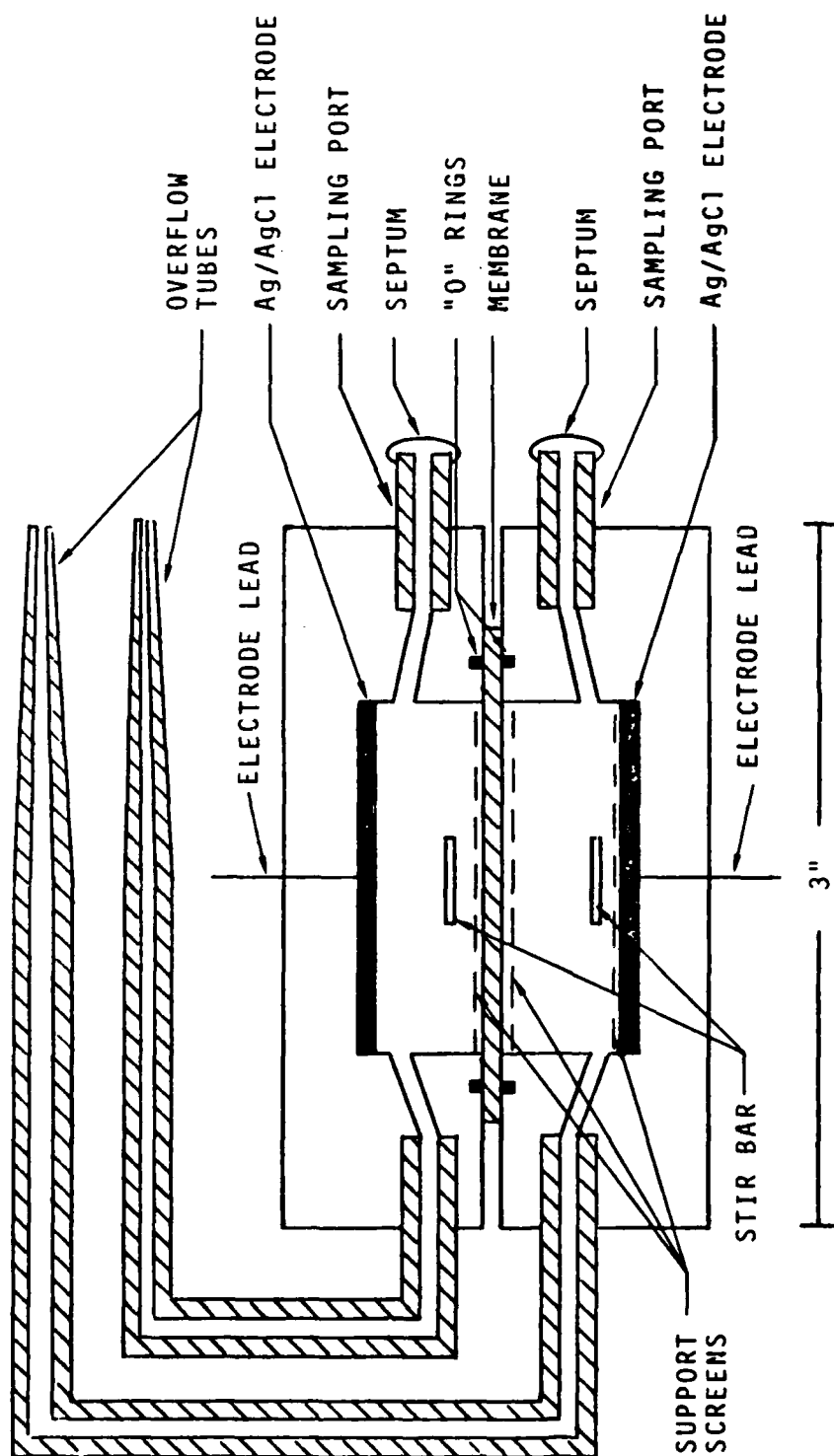


Fig. 1. Hittorf Cell

physical supports. The stir bar in the top compartment rested directly on the upper support screen. Stirring speeds of approximately 100 rpm were achieved with a magnetic stir plate.

The assembled Hittorf cell was placed in a Faraday cage during experiments. A battery was used to control the cell potential between the two electrodes. The voltage difference and electrode current were measured with Keithley electrometers. Fig. 2 is a schematic diagram of the electrical connections. The electrometers contain retransmitting amplifiers with low output impedance. The output of these amplifiers was recorded on an Esterline Angus, model E1124E, strip chart recorder. The output of the electrometer recording the current was also integrated with an Acromag, model 1752-K1-1, integrator. The total charge passed in the course of an experiment was obtained from the integrator. This instrumentation provided a permanent record of the voltage, current, and total charge for each experiment.

The experimental temperature was controlled with an air thermostat. A modified on-off household thermostat was used. Temperatures adjacent to the cell were measured with National Semiconductor, LX5600, temperature transducers. The transducers were purchased in TO-5 packages, and were equipped with radial-finned clip-on heat sinks. The cell temperatures were also recorded on the strip chart. A peak-to-peak temperature excursion of 1°C was observed with this apparatus.

All salts and solvents were ACS reagent grade, and the water was distilled. The paint formulations are included in Appendix A. Radioactive hydrogen (H^3), sodium (Na^{22}), and chloride (Cl^{36}) were purchased in carrier-free form from commercial sources. Radiotracer standards, traceable to the National Bureau of Standards, were purchased and used to make reference solutions. The radiotracer content of samples was measured with a Pakard, model 2002, scintillation counter at the University of Washington.

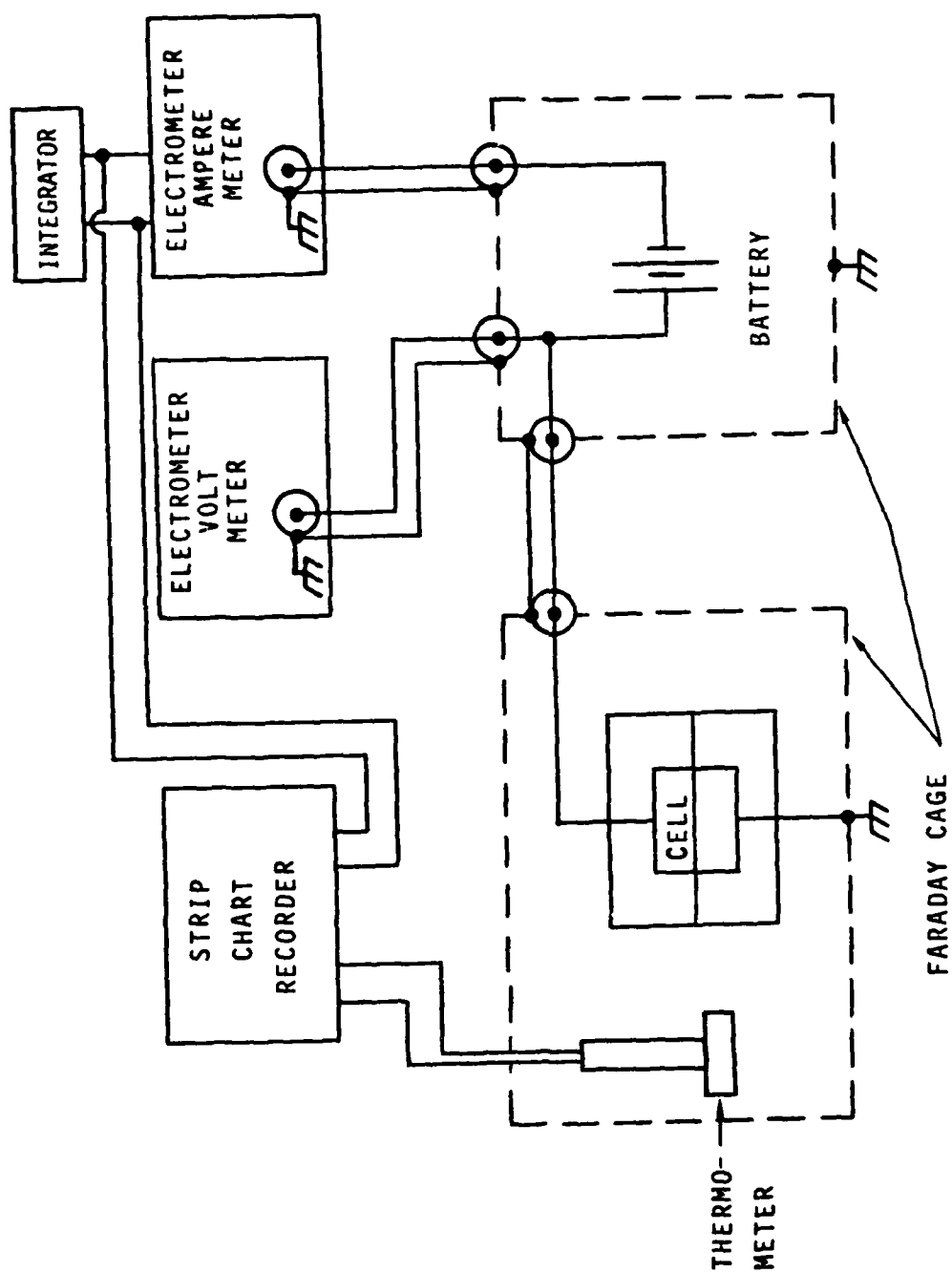


Fig. 2. Electrical schematic and instrumentation for a Hittorf experiment.

3.1.3 Procedure

In order to perform a Hittorf experiment, paint membranes unattached to any substrate were first prepared. Paints were first mixed according to the supplier's instructions. In the case of the polyurethane which was investigated most (O PUR, System VIII), equal parts of catalyst and base were mixed. The paint was then spray applied to sheets of decal paper and allowed to dry. Drying took place in the ambient laboratory air at about 60% relative humidity and 23°C. The paint was protected from dust in a fume hood for about 24 hours. The coated pieces of decal paper were then placed in paper envelopes and stored in a wooden cabinet until needed. Storage times varied from two weeks to two years.

Immediately prior to use, specimens of paint were cut from the large sheets of coated decal paper. The decal paper was soaked in water for a few minutes until the paint could be easily removed. The free paint film was then washed in tap water till no mucilage could be detected by touch. Then the paint was rinsed in distilled water for a few seconds and dried with a paper towel. The dry paint film was allowed to stand in laboratory air for about 15 minutes before the thickness was measured with a micrometer. Twelve to 15 thickness measurements were made in the test area of the sample. The average coating thickness and standard deviations were then calculated. Free films with nonuniform thickness or high standard deviations were rejected. The membrane was next checked optically for defects: holes, dirt or dust particles, etc. Membranes which did not appear to be smooth and free of defects were rejected. The final pre-experiment check was a conductivity measurement. The membrane was mounted in a Hittorf cell and its dc conductivity was determined. If the conductivity differed more than a factor of about three from the average conductivity of similar membranes it was rejected. After a specimen passed all the pre-experiment tests it was ready for mounting in a Hittorf cell.

Prior to an experiment, the Hittorf-cell electrodes were checked. Solutions of differing salt concentration were placed in each half-cell, and the electrode potentials were measured relative to a standard reference electrode. If the "Nernst slope" for the Hittorf electrode exceeded 55 mV/decade, the electrode was considered acceptable. If the

electrode failed this test, the silver chloride layer was removed, and the silver was abraded, cleaned, and reanodized. Also, prior to the experiment the Plexiglas was inspected for scratches. If scratches were found, they were removed by polishing.

After the cell had been polished and the electrodes had passed inspection, both halves of the cell were rinsed in distilled water and then in methanol. The cell was then dried by blowing air through the injection ports and the overflow tubes. When the cell was completely dry, it was ready for assembly.

The cell was assembled in steps proceeding vertically from the bottom to the top. A screen was first placed in the bottom compartment over the silver-silver chloride electrode. A magnetic stir bar was then placed on the screen. Next, a second screen was placed over the mouth of the bottom compartment. The diameter of the second screen was greater than the compartment diameter. This screen supported the membrane. Next, the O-ring was coated with a thin layer of silicone stopcock grease and placed in its groove around the screen. Then the paint film was placed over the O-ring and the support screen. In standard procedure the air-side of the paint film was placed down; the decal-paper side was up. Next, a second support screen was placed on top of the paint, and another stir bar was placed on this second screen. Finally, the top half of the cell was placed on, and the entire assembly was bolted together. After the cell was assembled, a visual inspection was made. The inspection included checking the O-ring seals, the support screens, and the stir bars. If the inspection reveals no defects, the assembly was completed by placing rubber septums over the open ends of the injection ports.

Prior to filling the cell it was weighed. The assembled cell was then filled with electrolyte using a hypodermic syringe. The volume of electrolyte added to each compartment was measured with the syringe. The weight of the cell was also measured after each compartment was filled. This procedure provided two independent measures of the fluid volume in each compartment. The volume of fluid in the overflow tube was determined by the position of the liquid meniscus. Another visual inspection was performed after filling the cell. If bubbles with diameters

greater than about 3mm ($\approx 10\%$ of the diameter of the compartments) were observed, the filling procedure was repeated. If the bubbles could not be removed, the compartments were emptied and the cell reassembled.

Electrolyte solutions were mixed just prior to assembling the cell. Various sodium chloride concentrations from 0.01 N to 3 N were employed. Radiotracers were added just prior to filling the cell. The solution containing the radiotracers was always placed in the bottom compartment. Solutions in both compartments were the same salt concentration, but no radiotracers were used in the top compartment. The bottom compartment always contained two radiotracers: tritium (H^3) and either sodium or chloride. In this way the water flux and one of the ion fluxes could be obtained.

After the cell had been filled, 10 μ l samples were taken from each compartment. The cell was placed on a stir plate inside a thermostatically controlled glovebox. The cell was then connected to the battery and the electronic monitoring equipment. The cell was always connected to the battery with the polarity such that the salt radiotracer (Na^{22} or Cl^{36}) was forced across the membrane. Experiments were conducted for various periods of time up to three months. The cell voltage, current, and temperature were recorded. Radiotracer samples (10 μ l) were periodically withdrawn with Hamilton micro-syringes through the rubber septums. The top compartment was sampled about every three days. The bottom compartment was sampled at two-week intervals. At the end of the experiment three samples were withdrawn from each compartment.

During the course of an experiment the positions of the menisci in the overflow tubes were periodically recorded. By comparing the relative positions of the two menisci, leaks could be detected. Experiments were terminated when leaks developed. At the conclusion of an experiment, the cell was dismantled and each half cell was leached for two weeks in separate distilled water baths.

The radiotracer samples were analyzed by liquid scintillation counting. The scintillation counter was capable of counting two radioisotopes simultaneously. The different isotopes were distinguished by the different energies of their β emissions. Chloride-36 could not

be distinguished from sodium-22 because both radionuclides have similar β -energy spectra. Therefore, tritium and either sodium or chloride were used in each experiment, and sodium and chloride fluxes were determined in separate experiments.

Approximately five standard samples were used to calibrate the scintillation counter during each counting session. The activities of the standards varied, covering a range approximately equal to that expected for the experimental samples. A least-squares matrix inversion method was used to determine counting efficiencies and cross-channel interference coefficients from the calibration data. The accuracy of each calibration matrix was also checked by counting mixtures of known composition. No quenching was observed with the small sample volumes (10 μ l) used.

Transference numbers for sodium and chloride were calculated in the following way. First, the activity of the radiotracer (sodium or chloride) in the top compartment was obtained. These data were converted to equivalents of carrier (n_c) per ml by assuming a specific molar activity equal to that in the bottom cell. Then, the data were plotted as n_c versus charge passed (Appendix C). Different least-squares straight lines were then constructed through the data collected at each cell potential. Finally, the transference numbers were set equal to the slopes of the lines. This method was considered appropriate as long as two conditions were met. The radiotracer flux at zero applied voltage was negligible, and the fraction of radiotracer transported across the membrane was small. Both conditions were always satisfied in these experiments.

The diffusivity of water was calculated from measurements of the tritium concentration. It was assumed that tritium only passed through the membrane as water. This assumption cannot be easily verified. Other assumptions were the same as for sodium and chloride transport except that the fraction of tritium transported was usually large. In order to account for this fact, a differential mass balance was derived for the top compartment.

The equation was solved to yield the tritium activity in the top compartment as a function of the water diffusivity and time. Experimental results were then inserted in the calculated solution, and a diffusivity was obtained for each of n experimental data points. These individual diffusivities were averaged to obtain the tabulated values.

3.1.4 Results

The results of Hittorf experiments conducted in 1980 and 1981 are listed in Table 1. The six experiments, NR-1-80 through NR-6-80, were presented in the last annual report, but they are included here for completeness. The conductivities are average values which were calculated by averaging the mean daily conductivities. Water permeability coefficients are average values calculated from tritium-activity data collected over the course of the experiment. Permeability coefficients of ions and transference numbers were calculated separately at each applied voltage.

3.1.5 Discussion

One of the important objectives of this work was to identify the primary independent variables controlling mass transfer through paint membranes. The data from Hittorf experiments was analyzed to find the effects of time, voltage, and electrolyte concentration on the transport parameters. Three transport parameters were determined in these Hittorf experiments: transference numbers, conductivities, and permeability coefficients. Only two of these three parameters are independent.

The migration flux of species i through a membrane (N_i^m) can be written

$$N_i^m = - \frac{z_i F}{RT} P_i c_i \nabla \phi \quad (1)$$

P_i = the species permeability coefficient (m^2/s)

c_i = the external species concentration (mol/m^3)

Table 1
Results of Hittorf Experiments

Exp. #	Paint	Thickness (μm)	NaCl Conc. (N)	Mean Conductivity ($\Omega^{-1}\text{cm}^{-1}$)	Volts (V)	Transference #		Permeability Coefficient (m^2/s)		
						t_+	t_-	H_2O	Cl^-	Na^+
NR-1-80	VR4	46.6	0.104	5×10^{-11}	1.52			1.59×10^{-14}		
NR-2-80	VR4	70.6	0.099	1×10^{-9}	1.55			2.11×10^{-14}		
NR-3-80	O PUR	57.6	0.037	1×10^{-8}	9.5		0.362	6.12×10^{-14}	3.1×10^{-17}	
NR-4-80	O PUR	38.7	0.009	1×10^{-8}	9.3	0.021		5.61×10^{-14}		8.0×10^{-18}
NR-5-80	O PUR	37.9	0.023	3.5×10^{-10}	4.4		0.268	7.48×10^{-14}	1.0×10^{-18}	
					9.4		0.254		1.1×10^{-18}	
					19.5		0.286		1.7×10^{-18}	
					13.7		0.222		8.33×10^{-19}	
NR-6-80	O PUR	34.5	0.025	5×10^{-9}	4.0	0.021		4.4×10^{-14}		2.7×10^{-18}
					9.9	0.105				4.9×10^{-18}
					19.0	0.009				7.3×10^{-18}
NR-7-80	O PUR	128.	0.30	3×10^{-9}	3.0			5.36×10^{-14}		
					6.25		0.317		8.0×10^{-19}	
					12.5		0.45		1.05×10^{-18}	
					9.5		0.40		1.47×10^{-18}	
					6.3		0.37		2.31×10^{-18}	
NR-8-80	O PUR	37.9	0.023	5×10^{-9}	3.0	.022		1.1×10^{-13}		1.68×10^{-18}
NR-1-81	O PUR	37.9	0.023	1×10^{-9}	3.0	0.366		5.63×10^{-14}		3.32×10^{-18}
					6.1	0.498				6.31×10^{-18}
					9.3	0.493				5.97×10^{-18}
					12.5	0.517				6.45×10^{-18}
					6.1	0.568				6.83×10^{-18}
NR-3-81	O PUR	76.5	1.0	1×10^{-10}	6.2		0.407	4.42×10^{-14}	6.16×10^{-19}	
					9.3	0.315		4.20×10^{-14}		7.9×10^{-19}
					12.5					9.9×10^{-20}
					9.3	0.150				1.0×10^{-20}
					23.5	0.256				1.2×10^{-20}
NR-5-81	VR4	39.8	0.116	5×10^{-9}	3.1		0.342	2.76×10^{-14}	1.7×10^{-17}	
					9.3		0.292		2.2×10^{-18}	
					6.3		0.290		3.1×10^{-18}	

The following equation can also be written

$$N_i^m = \frac{-\kappa \nabla \phi}{z_i F} t_i \quad (2)$$

κ = the membrane conductivity

t_i = the species transference number.

N_i^m can be eliminated from this pair of equations to yield

$$\frac{z_i^2 F^2}{RT} c_i P_i = \kappa t_i \quad (3)$$

Equation 3 shows that, for a given electrolyte concentration (c_i), only two of the three variables (P_i, t_i, κ) are independent.

The conductivity was chosen as one of the independent variables. No systematic variation of conductivity with either time or voltage was observed. Individual paint films did show slight trends, but overall, no significant tendencies were observed. For example, the conductivity in experiments NR-3-81 and NR-4-81 (Appendix C) decreased with time, but in NR-2-81 and NR-7-80 the conductivities were erratic and generally increased. Fig. 3 shows the conductivity of one polyurethane free film over a period of 200 days. Three Hittorf experiments were conducted in that time, and the conductivity varied between about $3. \times 10^{-10} \Omega^{-1} m^{-1}$ and $1. \times 10^{-8} \Omega^{-1} m^{-1}$. No significant trends were identified in Fig. 3 or in the conductivity data from other experiments.

Conductivity experiments were conducted at various values of applied voltage between 2.6 V and 23.5 V. The conductivity did not depend on the voltage in these experiments. This result is in contrast with Cherry's (19) work, and with previous work conducted in this laboratory. In the previous work the dc conductivity was found to be a hyperbolic sine function of the applied voltage. These earlier tests were performed on paint samples exposed to a range of voltages in a short period of time (minutes). One explanation of these two results is that the effects of paint aging are much greater than the effects of voltage. The present experiments were conducted with constant voltages applied for a minimum of six days. Figure 3 clearly shows that very large conductivity changes can be observed in a six-day period. Three conclusions

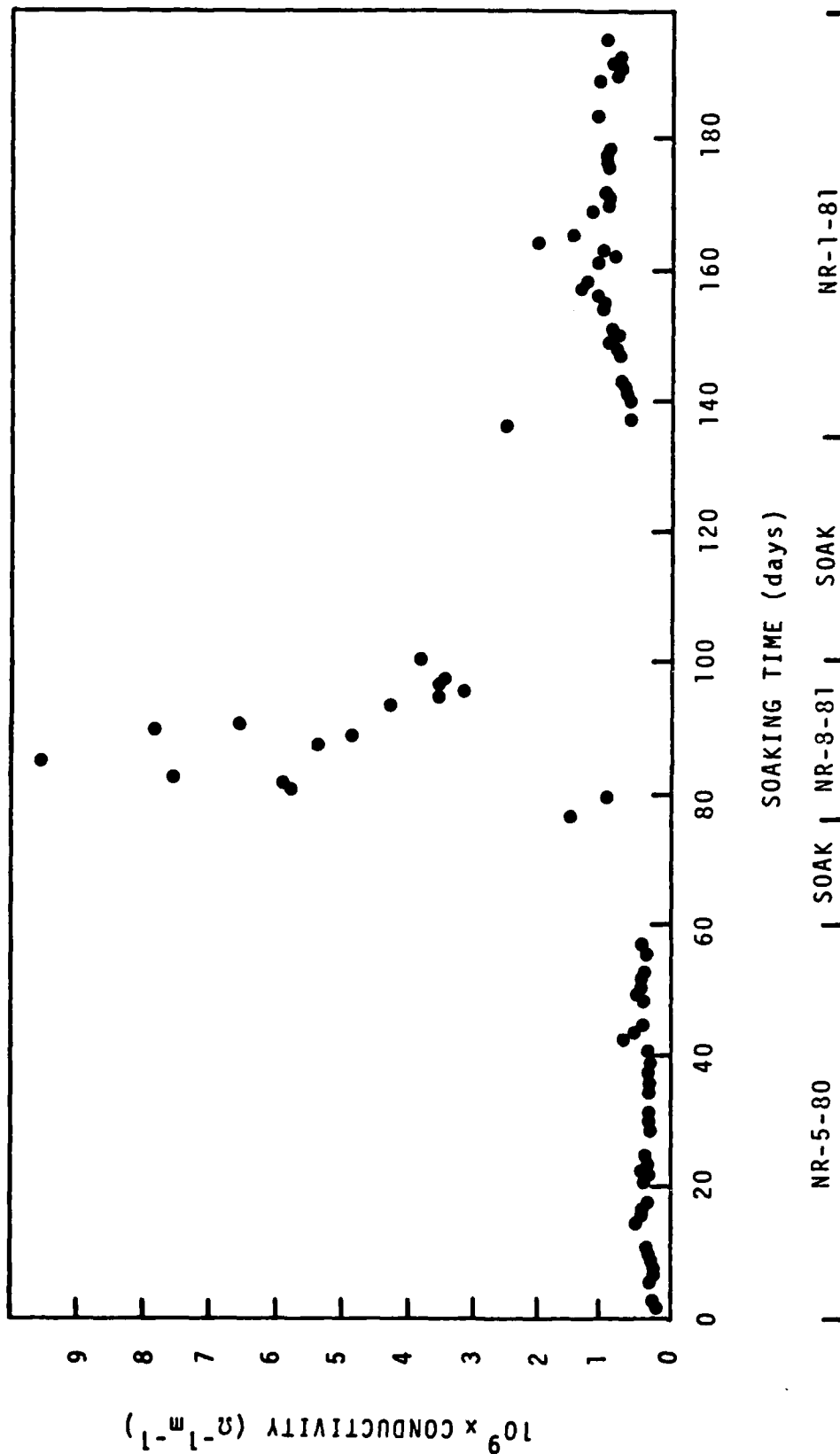


Fig. 3. Membrane conductivity for a single sample of polyurethane (O PUR) during three consecutive Hittorf experiments.

have been drawn from these results.

- Individual specimens exhibit a conductivity which varies as the $\sinh(V)$.
- Different paint samples exhibit variations in conductivity greater than those caused by the application of a few tens of volts.
- For a single specimen, the dependence of the conductivity on voltage is masked by the time dependence, when experiments last more than a few days.

The variation of conductivity with concentration is shown in Fig. 4. The data from Hittorf experiments show no significant trend in conductivity versus concentration. This fact is in contrast to the results of experiments conducted on individual paint samples. The curve in Fig. 4 illustrates the behavior of one free film. The curve has been drawn through four "single-specimen" data points which were measured in about two hours time. The results of the single-specimen experiments suggest the conductivity depends on electrolyte concentration, but in Hittorf experiments these effects are masked by the variation of conductivity with time.

Mayne has suggested that paint films undergo ion exchange (20) and possess small areas of much greater than average conductivity (21,22). Experiments have been conducted in this work which were similar to those described by Mayne. The results of these recent experiments were different from Mayne's results. These experiments do not preclude ion exchange, but they do not support the strong influence of pH, as Mayne's experiments do. However, these experiments do suggest that Mayne's second hypothesis, nonuniform membrane conductivity, could be correct. Despite the fact that Mayne's work was published over ten years ago, the number of conductive sites per unit area and the size of the sites have never been determined. However, the specific area per site can be estimated from the fact that the number of conductive areas in these experiments must be small. The superficial area per conductive site is therefore on the order of 454 mm^2 . This compares to a value of approximately $100 \text{ mm}^2/\text{site}$ obtained by Mayne for three different types of paint.

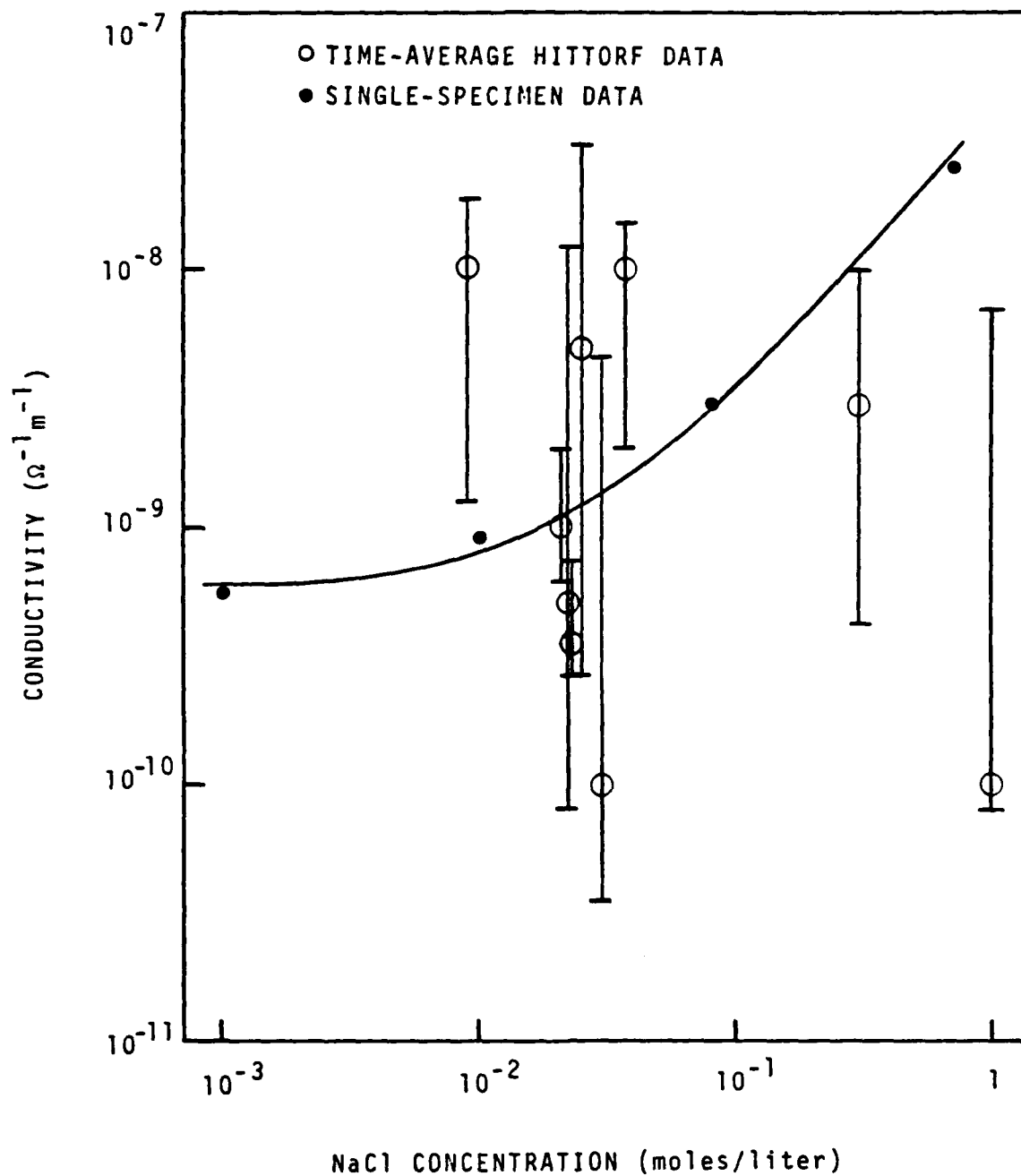


Fig. 4. Polyurethane conductivity in sodium chloride solution. Bars show the variation in each Hittorf experiment. The single-specimen data were collected in 2 hours.

The transference number was chosen as the second independent transport parameter. Table 1 lists the transference numbers of both sodium and chloride ions in polyurethane paint. In general, the sum of these two transference numbers is less than one. This fact means that the transport of sodium and chloride ions is insufficient to account for the total current passed through the paint film. This is a surprising and significant result because most authors assume that sodium and chloride ions carry all the current through membranes in sodium chloride solutions.

The sum of the average transference numbers of sodium and chloride is about 0.6. However, large variations between samples were expected, similar to the observed behavior of the conductivity. A more detailed look at the data revealed larger variations in the sodium ion transference number (t_+) than in the chloride transference number (t_-). The average t_- value was

$$t_- = 0.334 \quad (4)$$

The standard deviation of ten samples was

$$\sigma_-(10) = 0.075 \text{ or } 23\% \quad (5)$$

The corresponding values for sodium were

$$t_+ = 0.275 \quad (6)$$

$$\sigma_+(15) = 0.209 \text{ or } 76\% \quad (7)$$

One explanation of the small standard deviation for chloride ion is that only new membranes were tested for t_- . Six values of t_+ , which contribute significantly to the large σ_+ , were obtained from a membrane which had been soaking more than 142 days. Fig. 5 shows transference numbers obtained with a single specimen of polyurethane (O PUR). The chloride ion transference number was measured first. A nearly constant value of $t_- = 0.258$ was obtained. Then t_+ was measured, and it changed from 0.02 to about 0.55 over a 100-day soaking period. It therefore appears that t_+ can undergo dramatic changes on this time scale.

Experiment NR-4-81 showed relatively high values of $t_+ = 0.25$. This experiment was conducted in 0.3 N NaCl as compared to 0.02 N NaCl for other experiments. This high t_+ could have resulted from the increased sodium chloride concentration, but the results of one experiment were not

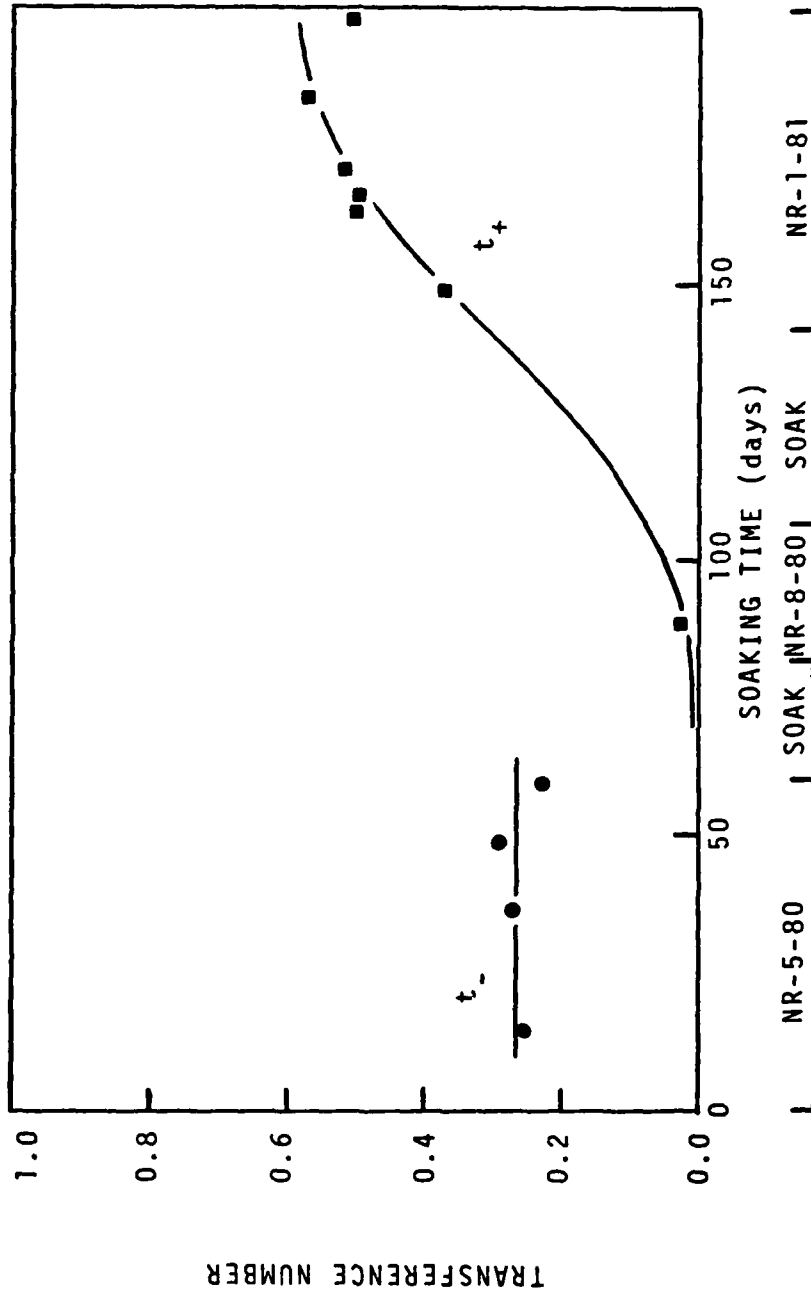


Fig. 5. Transference numbers from three Hittorf experiments with a single specimen of polyurethane (0 PUR).

considered sufficient evidence to draw a firm conclusion. Furthermore, t_- did not show concentration dependence. Experiment NR-3-81 was conducted in 1.0 N NaCl, and $t_- = 0.407$ was within one standard deviation of the mean, $t_- = 0.334$.

Recognizing that only a small number of experiments have been completed, several conclusions were drawn based on these experiments. First, the sodium ion transference number increases dramatically with the time of exposure to NaCl solution. Initially t_+ is approximately 0.04; later it rises to about 0.5. The chloride transference number is initially $t_- = 0.33$. Therefore, the sum of the sodium and chloride initial transference numbers is $t_{\text{sum}} = 0.37$, and about 60% of the initial current is unexplained. It also appears that t_- is nearly independent of the external solution concentration, but t_+ depends strongly on concentration. This work represents a preliminary but relatively thorough look at the transport properties of one type of polyurethane paint. The influence of voltage, electrolyte concentration, and immersion time on the transport of ions and water was investigated. The transport properties were found to be most sensitive to the immersion time and the particular specimen being tested. The transport properties were not sensitive to the applied voltage, and strong evidence supporting ion exchange in this paint was not found.

3.1.6 Conclusions

The following conclusions were based on a limited number of experiments conducted with one type of polyurethane (O PUR), at 25°C. Both the membrane conductivity and sodium ion transference number showed significant variations with time. Chloride ion transference number and the diffusivity of water were relatively constant. These results show that changes are taking place within the paint as it ages, but no mechanism has yet been presented which explains all the facts. Despite the continuing ambiguity regarding ion transport in paints these data clearly indicate that sodium chloride will diffuse through the coating to the metal in a relatively short time (*30 days). It is therefore evident that some mechanism other than reduced ion transport must be provided if corrosion is to be controlled to acceptable levels.

Measurement of the sodium and chloride ionic fluxes with radiotracers has produced convincing evidence that the total current is greater than that attributable to these two ions. Several mechanisms can be proposed to explain the balance of the current, but it is most likely that migration of some other ion is responsible. Identification of the unknown current-carrying ions will be an important step in understanding the corrosion mechanism of painted metals because only when all the migrating species are known can the electrochemical conditions at the metal surface be predicted.

3.2 The Diffusivity and Solubility of Water in Polyurethane

3.2.1 Introduction

Water plays a key role in the corrosion process. The quantity of water at the metal surface affects paint adhesion, electrolyte concentration, and ion mobilities for example. The rate that water can diffuse to, or away from, the metal surface is also of interest because water reactions often form part of the corrosion mechanism. Water can also affect the diffusion of other components, particularly their diffusion through organic polymers. The diffusivities of oxygen or salt could be strongly enhanced by plasticization of the polymer due to water, for example. In order to increase our understanding of corrosion under paints it is therefore important to better understand the thermodynamic and kinetic properties of water in polymers.

Many methods have been used in the past to study water in polymers (23), but most of these methods employ polymer specimens unattached to any substrate ("free" films). These methods therefore have the disadvantage that the free films may be chemically or physically different than coatings attached to metal substrates. A gravimetric method was used in early work on this contract to measure water solubility and diffusivity in free films of paint. More recently our work has concentrated on developing a method of obtaining the same data from films attached to metal substrates. The results of this recent work are described in this section.

The experimental techniques developed for this study were based on those developed earlier. The humidity chamber is unchanged (3), but a crystal oscillator is now used to detect water sorption by the paints. The resonant frequency of crystals coated with a thin layer of paint responds to changes in mass caused by water sorption. This new technique has proved successful for evaluating equilibrium solubility and diffusivities from a single sorption isotherm experiment.

3.2.2 Theory

3.2.2-1 Crystal Oscillator

Quartz crystals have been used to construct highly stable oscillators for many years. The crystal is a low-loss piezoelectric resonator which controls the frequency. The fundamental frequency of a crystal is affected by temperature and several other environmental factors. Generally, however, the physical properties of the crystal have the greatest effect on the frequency.

The mass of the crystal is one property which has a great influence on frequency. This fact is the basis of several unusual uses of crystal oscillators, including sorption detectors (24,25). Highly sensitive sorption detectors have been constructed by coating a quartz crystal with a thin layer of absorbant (paint). The frequency of this "composite" crystal changes as its mass varies. By knowing the relationship between frequency change and mass change, microbalance weighing can be performed. Sensitivities on the order of 10^{-12} g have been estimated (24).

The piezoelectric oscillation of a quartz crystal has been analyzed as an acoustic resonator (26). In this one-dimensional theory, a wave disturbance is introduced at one surface of the crystal. The wave travels through the quartz with a constant velocity and attenuation until it reaches the opposite edge of the crystal. At the edge, the wave is completely reflected. This model is mathematically equivalent to an ideal transmission line with distributed loss, and a complete mathematical description is available.

When a quartz crystal is coated with another substance, a composite is formed. The acoustic resonator theory has been used to describe these composite resonators, but the analysis is more complicated than for the simple resonator. The complexity results from partial reflection of the traveling wave at the boundary between the quartz and the coating substance. Despite the complexity, Miller and Bolef (26,27) obtained an exact solution of the composite resonator. The theory showed that the only major effect of attaching the coating to the crystal was to shift the resonant frequency of the composite resonator relative to the frequency of the simple quartz crystal (f_q).

Miller and Bolef's acoustic resonator theory is based on several approximations and assumptions. The assumptions appear to be appropriate, although they have apparently not been individually checked. However, the applicability of the entire theory to metal-coated crystals was proposed by Miller and Bolef (27), and Lu and Lewis (28) checked this application using three metals: copper, silver, and lead. The theory is in good agreement with experimental data for frequency shifts up to 15% of the "unloaded-crystal" frequency (f_q).

The acoustic resonance theory is based on the following assumptions (In the composite resonator the assumptions apply to the crystal and the coating separately.):

1. The system is one dimensional.
2. End faces are flat and parallel.
3. The wave travels with a constant velocity.
4. The attenuation per unit distance is constant.
5. The density of the medium is constant.
6. The crystal is oscillating at steady state (cw).
7. The coating is uniform over the entire "active" area.

This theory does not treat the effects of crystal mounting or surface nonuniformities.

Lu and Lewis (28) present three relations between the mass change of the composite crystal and the observed frequency shift. The most accurate equation, "exact solution," is based on Miller and Bolef's result (26, Eq.9) with no losses in either the quartz or the coating. The exact equation is:

$$\tan \left[Z\pi \frac{f}{f_q} \frac{m_f}{m_q} \right] = Z \tan \left[\pi \frac{f_q - f}{f_q} \right] \quad (8)$$

where Z = the ratio of the shear-mode acoustic impedance of quartz to that of the coating

f = the frequency of the composite resonator

f_q = the frequency of the uncoated quartz crystal

m_f = the mass of the coating (film)

m_q = the mass of the uncoated quartz crystal

In this instance the composite-resonator frequency (f) depends on the acoustic impedance ratio (Z) as well as the mass of the applied coating (m_f).

The second equation presented by Lu and Lewis is the "period approximation." When $Z = 1$, Eq. 8 simplifies to

$$\frac{m_f}{m_q} = \frac{f_q - f}{f} \quad (9)$$

The period approximation is adequate ($1 < Z < 2.29$) for frequency deviations less than about 5% (28).

When m_f/m_q is small, f has nearly the same value as f_q . Under these conditions Eq. 8 simplifies to the "frequency approximation,"

$$\frac{m_f}{m_q} = \frac{f_q - f}{f_q} \quad (10)$$

The frequency approximation is limited to a deviation of about 2% (28). Once a particular quartz crystal has been selected, m_q and f_q are fixed. Then, f depends only on the mass of the applied coating. Eqs. 9 and 10 show this statement is true for both approximate models, but Eq. 9 is nonlinear.

3.2.2-2 Sorption in a Thin Sheet.

The theory of sorption and desorption in thin sheets has been thoroughly discussed by Crank (29). The basic equation describing the process is:

$$\frac{\partial c}{\partial t} = - \frac{\partial N}{\partial x} \quad (11)$$

where c = the diffusant concentration (mol/m^3)

N = the diffusant flux ($\text{mol/m}^2 \cdot \text{s}$)

t = the time (s)

x = the linear dimension (m)

If the flux obeys Fick's first law,

$$N = - D \frac{\partial c}{\partial x} \quad (12)$$

where D = the diffusivity (m^2/s)

Eq.12 can be substituted into Eq.11 to yield:

$$\frac{\partial c}{\partial t} = \frac{\partial}{\partial x} \left[D \frac{\partial c}{\partial x} \right] \quad (13)$$

This is the basic equation of diffusion in a thin sheet and is equivalent to Fick's second law if the diffusivity is constant:

$$\frac{\partial c}{\partial t} = D \frac{\partial^2 c}{\partial x^2} \quad (14)$$

In general the concentration depends on time, position, and the diffusivity, as well as the boundary conditions of a particular problem. Solutions of Eqs.13 and 14 have been given for a variety of boundary conditions and diffusivities (29,30). Most of the published solutions require knowledge of the functional form of the diffusivity, but Crank and Park (23) and Crank (29) discuss practical ways of using the theory to evaluate the diffusivity from sorption and desorption isotherms.

One set of boundary conditions for which an analytical solution of Eq. 14 is available is:

$$\begin{aligned}\frac{\partial c}{\partial x} &= 0 & @ x = 0, t > 0 \\ c &= 0 & @ 0 \leq x \leq l, t = 0 \\ c &= c_1 & @ x = l, t > 0\end{aligned}\tag{15}$$

These boundary conditions represent a step change in surface concentration, at $x = l$, at time zero. For these conditions, the diffusivity is easily determined by plotting the dimensionless uptake of sorbate (R_w) versus the square root of time.

$$R_w = M_t / M_\infty\tag{16}$$

where M_t = the total amount of sorbate present at time t

M_∞ = the total amount sorbed at long times (equilibrium).

$$M_t = \int_0^l c(x, t) dx\tag{17}$$

This theory is equally applicable to desorption provided M_t and M_∞ represent quantities of diffusant lost.

At $t = 0$

$$\frac{dR_w}{d\sqrt{t}} = \frac{4}{l} \sqrt{\frac{D}{\pi}}\tag{18}$$

The slope $dR_w/d\sqrt{t}$ is nearly constant for $R_w < 0.5$ (23, pl6).

It is also easy to calculate the diffusivity at long time, provided an accurate value of M_∞ is known. At long times

$$\frac{d}{dt} \left[\ln \left(1 - \frac{M_t}{M_\infty} \right) \right] = \frac{-D\pi^2}{l^2}\tag{19}$$

If both Eqs. 18 and 19 are applied to a single sorption experiment, a single value of the diffusivity should be obtained. If this is not found, the diffusivity is not a constant.

3.2.3 Apparatus

The apparatus was designed to subject the coated crystals to an isothermal, step-change in relative humidity. The crystal and the oscillator were suspended inside a metal chamber, and both were inside a thermostatically controlled, Plexiglas, box. The crystal was first allowed to equilibrate with the atmosphere inside the inner (metal), chamber. Then, the inner chamber was opened and the crystal was exposed to the atmosphere in the box. A good step-change in relative humidity was reproducibly produced using this technique.

The "humidity chamber" apparatus is shown in Fig. 6. The outer chamber was constructed of 6.35 mm thick Plexiglas and was insulated with 3 mm thick corrugated cardboard. The volume of the outer chamber was 15 liters. The temperature in the box was controlled with a VWR #13270-030 proportional controller. A long-term temperature fluctuation of 0.5°C was observed. The heater element of the thermostat was outside the box. Water was pumped past the heating coils and through a finned-tube heat exchanger inside the box. The air inside the box was circulated with a fan. Three copper-constantan thermocouples were used to measure the temperature at different locations in the box. The maximum temperature difference between the different locations was 0.1°C.

The inner chamber was composed of two parts: the "cup", and the "lid". The lid was mounted on a metal tube which was attached to the box. The cup could be raised and sealed against the lid to form the inner chamber, or lowered to open the chamber. The cup was aligned with the lid by a Plexiglas tube attached to the box. Both the alignment tube and the tube supporting the lid were perforated with holes (≈ 10 mm diam.) to allow air to circulate completely around the inner chamber. In the raised position, the cup was supported by a Plexiglas column resting on a closed trapdoor. When the door was opened the entire cup-column assembly could be removed from the box. The cup and lid were both constructed of 1 mm thick sheet metal. The cup was 92 mm high and 55 mm in diameter, with a volume of 219 ml.

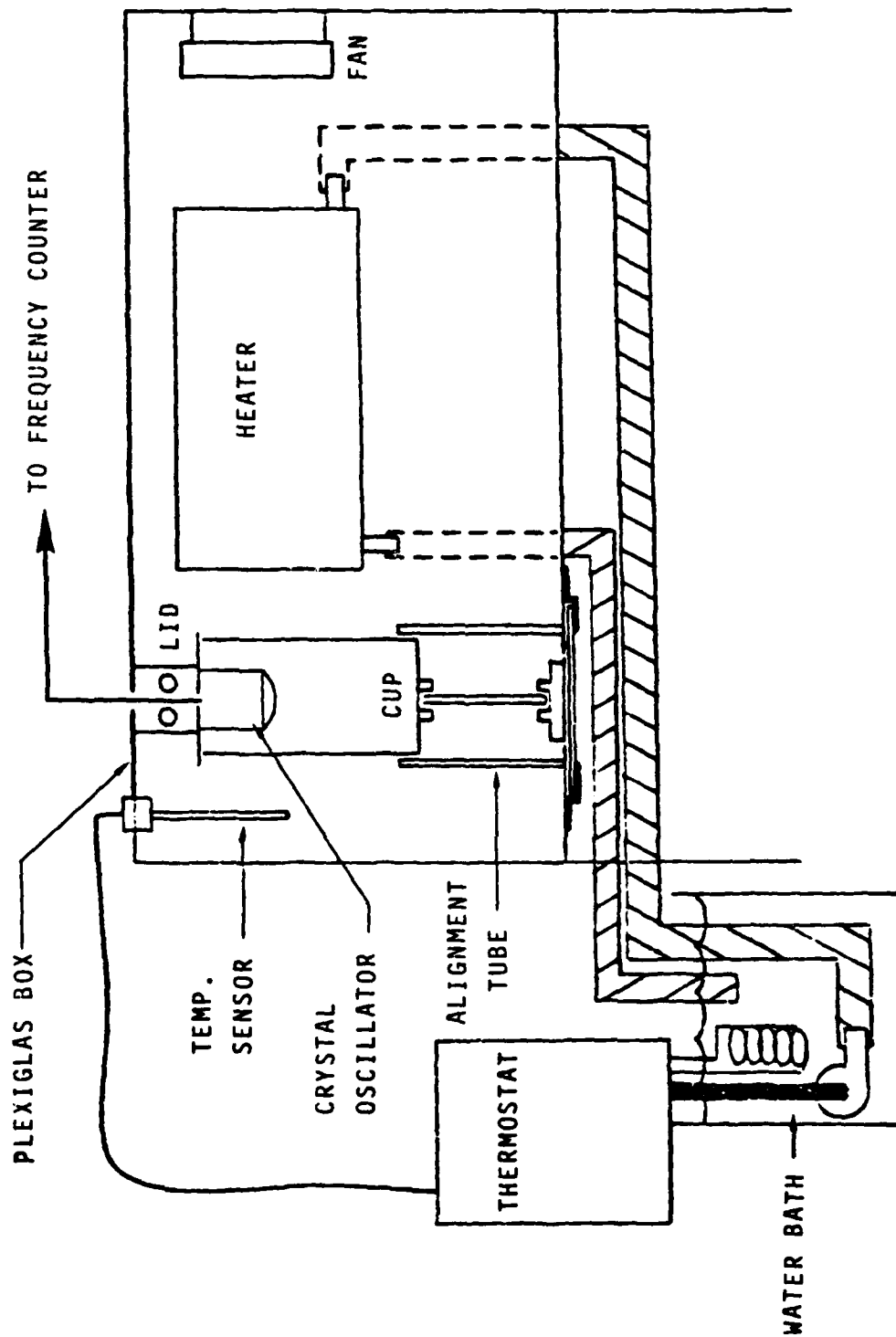


Fig. 6. Humidity chamber and crystal oscillator.

The oscillator and crystal holder comprised a single unit which was mounted on the inside surface of the lid. The oscillator was a "Digital Sensor Head", #900010, Sloan Technology Corp., Santa Barbara, Calif. The oscillator was powered by a 6 V regulated supply (Acopian, model E20D). The frequency was measured with a General Radio, model 1191 frequency counter. Both the frequency counter and the voltage supply were outside the box. The circuit diagram of the electrical connections between the power supply, the oscillator, and the frequency counter is shown in Fig. 7. A low-pass filter (Fig. 7) was used between the oscillator and the frequency counter. The filter was not a necessary part of the circuit, but it reduced the effects of stray capacitance.

The frequency counter operates in the following way. A count is recorded whenever the input signal crosses through a reference voltage. The user can specify whether input signals with positive or negative slopes (dV/dt) are counted. At the end of the counting period the total count is divided by the time period and the resultant, average frequency is displayed. The counting time period is determined by a stable 10 MHz oscillator inside the frequency counter. In automatic operation the frequency obtained in the last time period is displayed while the count for the current time period is taking place. Thus, for a one second counting period, an average frequency is displayed each second. Counting times of 1 s and 10 s have been used in this work.

An accurate, permanent, record of the frequency was obtained with a Datil, model DPP-Q7 thermal printer. The General Radio frequency counter produced a parallel port, BCD code of the frequency. The six most-significant digits of the frequency were fed to the printer which could record four, six digit, frequencies per second.

The crystals for the oscillator were purchased from Sloan Technology Corp. They were AT-cut quartz discs 12.5 mm in diameter and approximately 0.33 mm thick. The nominal frequency was 5.0 MHz. The as-received crystals had been coated on both sides with a thin layer of metal. The metal provided electrical contact with the crystal as it rested in the holder. Crystals with either gold or silver coatings were used. Only part of one surface of the crystal was exposed to air when it was in the holder. The exposed surface was visible through an 8.0 mm diameter

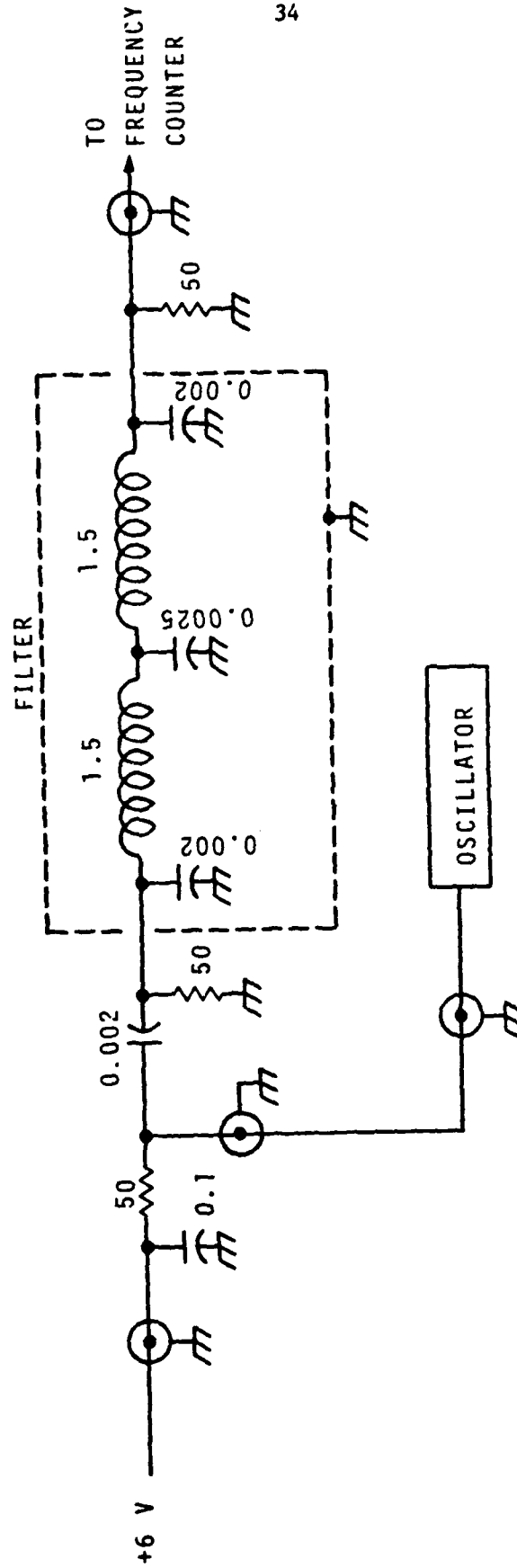


Fig. 7. Crystal oscillator circuit diagram. Resistance values are ohms. Capacitance values are μF . Inductance values are μH .

hole in the crystal holder.

Two types of coatings have been applied to crystals. The first was a polyurethane, designated O PUR (System VIII). This paint was manufactured by Desoto, Inc., Chemical Coatings Div., Berkely, Calif. It was obtained from the Boeing Commercial Airplane Company, Kent, Wash. This polyurethane meets Boeing material specification BMS-10-60D-TYII and military specification C-83286. This paint is a two-part system, and it was supplied and used without pigments or inhibitors. O PUR was mixed with a base to catalyst volume ratio of 1:1. This mixture was then diluted with a solvent having the following composition: 40 V% cellosolve acetate, 30 V% methyl ethyl ketone, 12 V% toluene, 10 V% n-butyl acetate and 8 V% xylene.

The second type of coating was a VAGH vinyl resin designated VR3. This coating was also used without pigments or inhibitors. It consists of a copolymer of vinyl chloride (91 wt%), vinyl acetate (3wt %), and vinyl alcohol (6 wt%). The average molecular weight was 23100. This coating meets military specification P-15929C. The VAGH was purchased from Union Carbide and was used as received. The coating was prepared by dissolving a quantity of VAGH in solvent and adding 10.4 wt% tricresyl phosphatate, based on the weight of VAGH. The solvent was composed of 54 V% methyl isobutyl ketone, and 46 V% toluene. ACS reagent grade chemicals were used throughout this work, unless specified otherwise.

3.2.4 Procedure

The first step in the procedure was to record the base frequency (f_q) of the uncoated crystal in "dry" air at 29°C. Calcium sulfate (Drierite) desiccant was used to maintain dry conditions. Several of the crystals were also weighed on a Cahn, model gram-1501, electrobalance, with a reproducibility of $\pm 10 \mu\text{g}$. The base frequencies (f_q) and base weights (w_q) were measured at least three times for each crystal.

After the base data had been obtained, the crystals were prepared for painting. The crystals were flat only on one face. The other face was slightly convex. Lu and Lewis (28) used similar crystals to confirm the acoustic resonator theory. Tests showed that the crystal could oscillate with the greatest mass attached to the flat side. Masks were used to produce uniform-diameter paint spots which were centered

on the flat side of the crystal. The masks were cut from plastic electricians tape with a cork bore. Various spot diameters were tested, but 5.8 mm was standard. The individual spot diameters were determined by averaging at least six measurements of the diameter (± 0.3 mm) made with a metal rule. The paint was applied to the crystals with a 1 μ l pipet. Different coating thicknesses were achieved by diluting the paints with the appropriate solvent prior to application. The coatings were allowed to dry for several days at ambient conditions. The average laboratory temperature was 23°C and the average relative humidity about 60%. After the coating had dried the mask was removed by soaking the crystal in an organic solvent. Several solvents have been used but hexane was one of the best. It dissolved the sticky side of the tape and had no apparent effect on the coatings. The crystals were soaked in hexane for ten to fifteen minutes; then the mask was lifted off with a pair of tweezers. The mask was inspected for visible traces of metal. If metal flecks were found the crystal was considered defective. Crystals were also classified as defective if any trace of the mask remained imbedded in the paint, or if any part of the paint became detached from the crystal.

After the masks had been removed, the crystals were rinsed with hexane and dried in laboratory air for at least several hours. The frequency (f_d) was then measured after equilibrating the crystals with a dry atmosphere. The crystals were also weighed (w_d) while being desiccated.

At this stage the painted crystals were ready for the diffusion experiments. The crystals were placed in the holder with the paint spot visible through the hole. The holder was then attached to the rest of the oscillator assembly, and oscillation was confirmed with the frequency counter or an oscilloscope. A saturated salt solution was placed inside the cup, and the cup raised to seal the inner chamber. Desiccant, or a second salt solution, was placed in the outer chamber which was then sealed. Thermocouples were used to determine the temperatures in both the inner and outer chambers. When all thermocouples and the frequency had attained a steady state the printer was turned on, and the frequency counter was adjusted for a 1 s time period. A stopwatch

was started, and the cup was dropped at a well-specified time. The frequency (f) was automatically recorded every second for approximately 100 seconds. Then the time period was changed to ten seconds. Frequency measurements were continued in this manner until a total elapsed time of 300 seconds had passed. Most experiments had reached a "steady state" in 300 seconds, but some were extended up to 2 hrs. total time.

Each crystal was tested at least twice for each step change in relative humidity. The standard procedure was to allow the "closed-cup" system 16 hours to reach steady state. The first experiment was then conducted. When this experiment was complete (usually 5 to 20 min.) the cup was raised again and the system was allowed to stand for about 7 hours. A second experiment was then conducted as before. The frequencies obtained from the two experiments were compared at each time interval. If both experiments were in satisfactory agreement, the results of the first run were used to calculate the water diffusivity. If the experiments did not agree the sequence was repeated.

3.2.4-1 Data Analysis

Five different models were used to analyze desorption data. The first four models represent different boundary conditions for which Eq.14 was then solved. Eq.13 represented the fifth model. The boundary conditions for all the models are shown in Table 2. All models describe the desorption of diffusant following a step change in external concentration. The metal surface was considered impenetrable. Crank (29) has presented the solution of the first model in the form of an infinite series (Table 3). The second model was similar to the first but a finite, well stirred, volume existed at the paint metal interface, and a mass-transfer resistance was present at the paint-air interface. Crank (29) discusses both these types of boundary conditions, but he does not consider this model. The third model was the same as model two without the mass transfer resistance at the paint-air interface. The fourth model was also similar to model two, but the mass transfer resistance was between the paint and the volume (capacity) at the paint-metal interface. Table 4 summarizes the mathematical models.

Table 2
Boundary Conditions for Diffusion Models

Model #	Differential Equation	$X=0, t>0$	$X=1, t>0$
1	4	$\frac{\partial C}{\partial X} = 0, (M)^1$	$C = 0, (A)^2$
2	4	$\frac{\partial C}{\partial X} = hC, (A)^3$	$\frac{\partial C}{\partial X} = -\frac{1}{\beta} \frac{\partial C}{\partial t}, (M)^4$
3	4	$C = 0, (A)$	$\frac{\partial C}{\partial X} = -\frac{1}{\beta} \frac{\partial C}{\partial t}, (M)$
4	4	$\frac{\partial C}{\partial X} = -\frac{1}{\beta} \frac{\partial C_s}{\partial t}, (M)^5$	$C = 0, (A)$
5	3	$C - C_g = \frac{1}{\gamma} \frac{\partial C}{\partial t}, (M)^6$	$\frac{\partial C}{\partial X} = -\frac{1}{\beta} \frac{1}{(1+\delta C)} \frac{\partial C}{\partial t}, (M)^7$
1	(M) = metal side of paint		
2	(A) = air side of paint		
3	h = dimensionless mass transfer coefficient		
4	β = the equilibrium ratio of water in the paint to water at the paint-metal interface		
5	C_s = dimensionless surface concentration at the paint-metal interface		
6	γ = dimensionless mass transfer coefficient		
7	δ = dimensionless constant		

Table 3
Functional Forms of the Model Solutions

Model #	Dimensionless Concentration	α_n
1	$C = \sum_{n=1}^{\infty} A_n e^{-\alpha_n^2 t} (\cos(\alpha_n X))^*$	$\alpha_n = (2n+1)\pi$ $A_n = \frac{(-1)^{n+1}}{2n+1}$
2	$C = \sum_{n=1}^{\infty} A_n e^{-\alpha_n^2 t} \left(\frac{h}{\alpha_n} \sin(\alpha_n X) + \cos(\alpha_n X) \right)$	$\alpha_n \tan \alpha_n = \frac{\beta h - \alpha_n^2}{(\beta + h)}$
3	$C = \sum_{n=1}^{\infty} A_n e^{-\alpha_n^2 t} (\sin(\alpha_n X))$	$\alpha_n \tan \alpha_n = \beta$
4	$C = \sum_{n=1}^{\infty} A_n e^{-\alpha_n^2 t} \left(\sin(\alpha_n X) - \left(\frac{\beta}{\alpha_n} - \frac{\beta \alpha_n}{\gamma} \right) \cos(\alpha_n X) \right)$	$\alpha_n \tan \alpha_n = \frac{\beta}{\gamma} (\gamma - \alpha_n^2)$

*Analytical Solution, (29).

Table 4
Diffusion Models of Polyurethane Paint

<u>Model #</u>	<u>Surface Conditions</u>		<u>Diffusivity</u>
	<u>Metal</u>	<u>Air</u>	
1	No Capacity or Resistance	No Resistance	Constant
2	Capacitance	Resistance	Constant
3	Capacitance	No Resistance	Constant
4	Capacitance and Resistance	No Resistance	Constant
5	Capacitance	No Resistance	Linear with water concentration

Approximate solutions of models two through four have been obtained using a CDC 6400 digital computer. The functional forms of the solutions satisfying the boundary conditions were obtained by hand (Table 3). A finite series of n terms with unknown coefficients was then forced to fit the initial condition at n arbitrarily specified positions (collocation points). This procedure allowed calculation of the coefficients in the finite series and an approximate solution was thus obtained. Usually about 20, evenly spaced, collocation points were specified.

In the fifth model the diffusivity was assumed to be a linear function of the concentration. Surface capacity was also considered. This model required the solution of a nonlinear differential equation with nonlinear boundary conditions. The solution was obtained with a computer, using the implicit Crank-Nicolson method (29).

3.2.5 Results

Figure 8 shown the results of typical absorption and desorption experiments. The data are plotted as dimensionless frequency change versus the square root of time. When the "frequency approximation" (Eq.10) is appropriate the dimensionless frequency change is identical to the dimensionless mass charge.

$$\frac{f - f_{\infty}}{f_d - f_{\infty}} = \frac{m - m_{\infty}}{m_d - m_{\infty}} \quad (20)$$

Similar results have been obtained at four different relative humidities. Additional, desorption, experiments have been performed with 15 painted crystals.

Figure 8 shows that the paint has achieved a new "equilibrium" condition after about 300 s. The frequency change $f_w = f_d - f_{\infty}$. This change is proportional to the mass of water absorbed by the polyurethane. Thus, the ratio $f_w(f_d - f_q)$ represents the dimensionless solubility (S') of water. This experimental solubility is a function of the temperature and relative humidity, as expected. Fig. 9 shows the solubility (S') as a function of relative humidity at 29°C.

A different solubility (S) can also be obtained from the data. Fig. 10 shows a plot of the frequency change f_w versus $(f_d - f_q)$. The

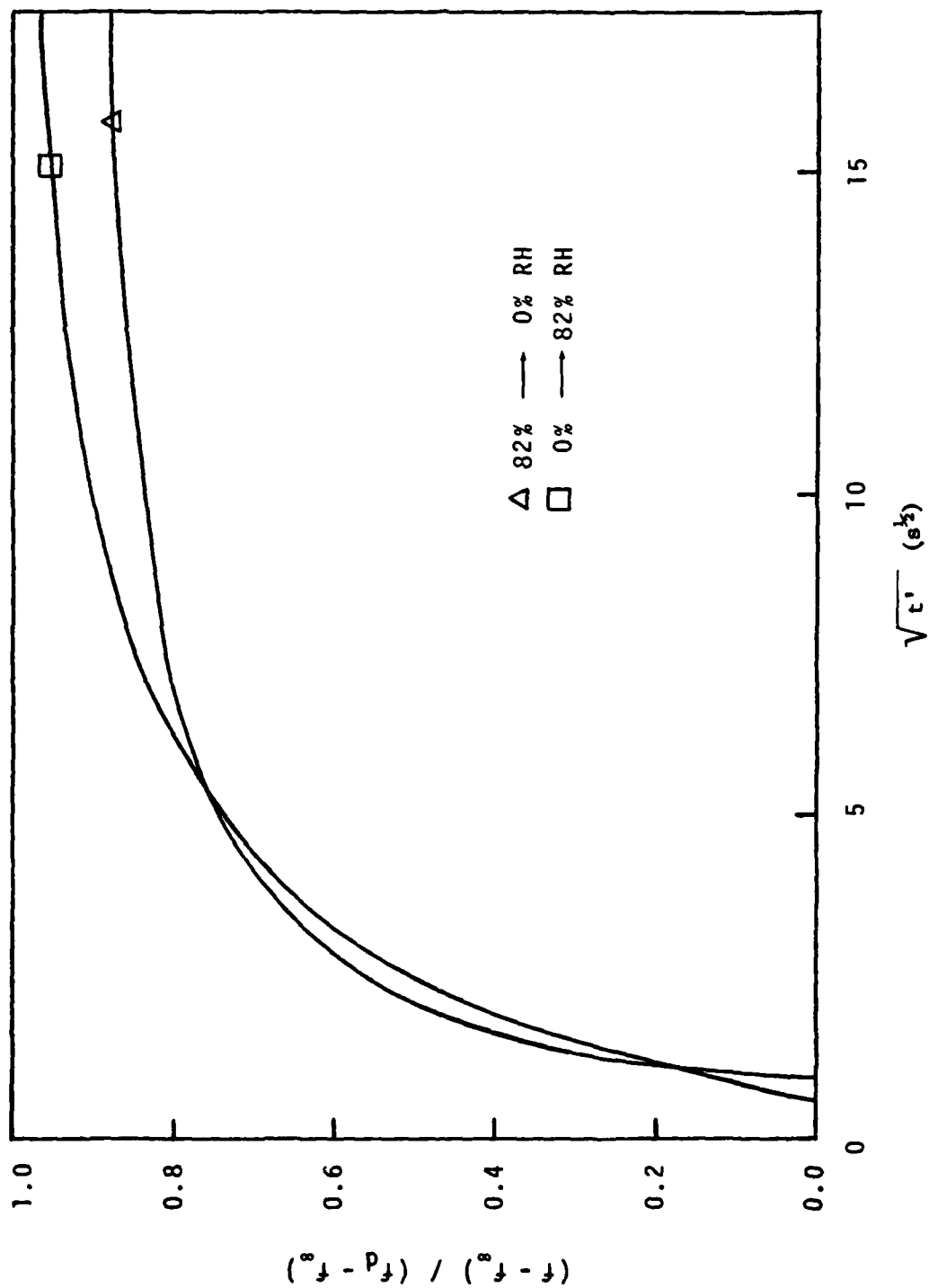


Fig. 8. Sorption and desorption curves for polyurethane (0 PUR) subjected to a step change in relative humidity at 29°C.

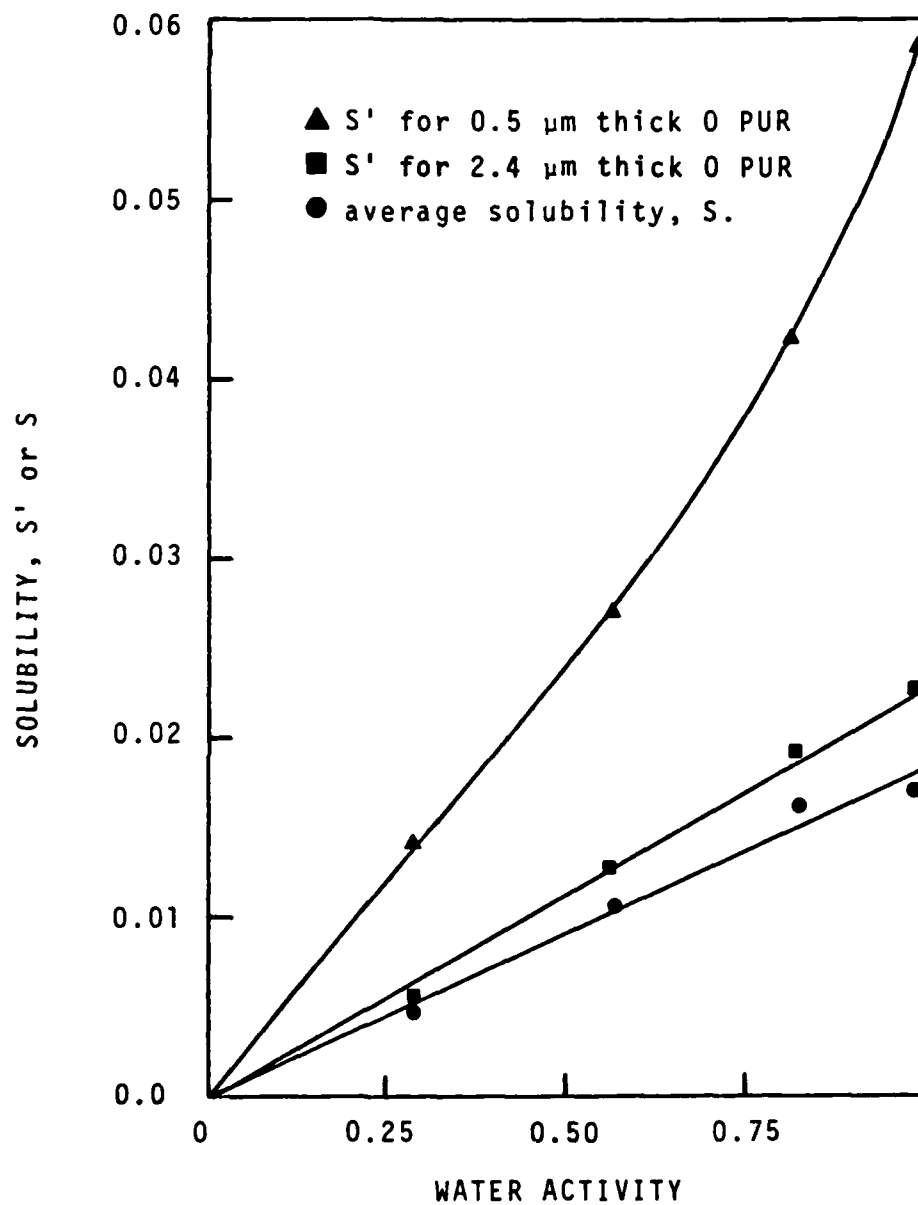


Fig. 9. Different water solubilities in polyurethane (O PUR) at 29°C.

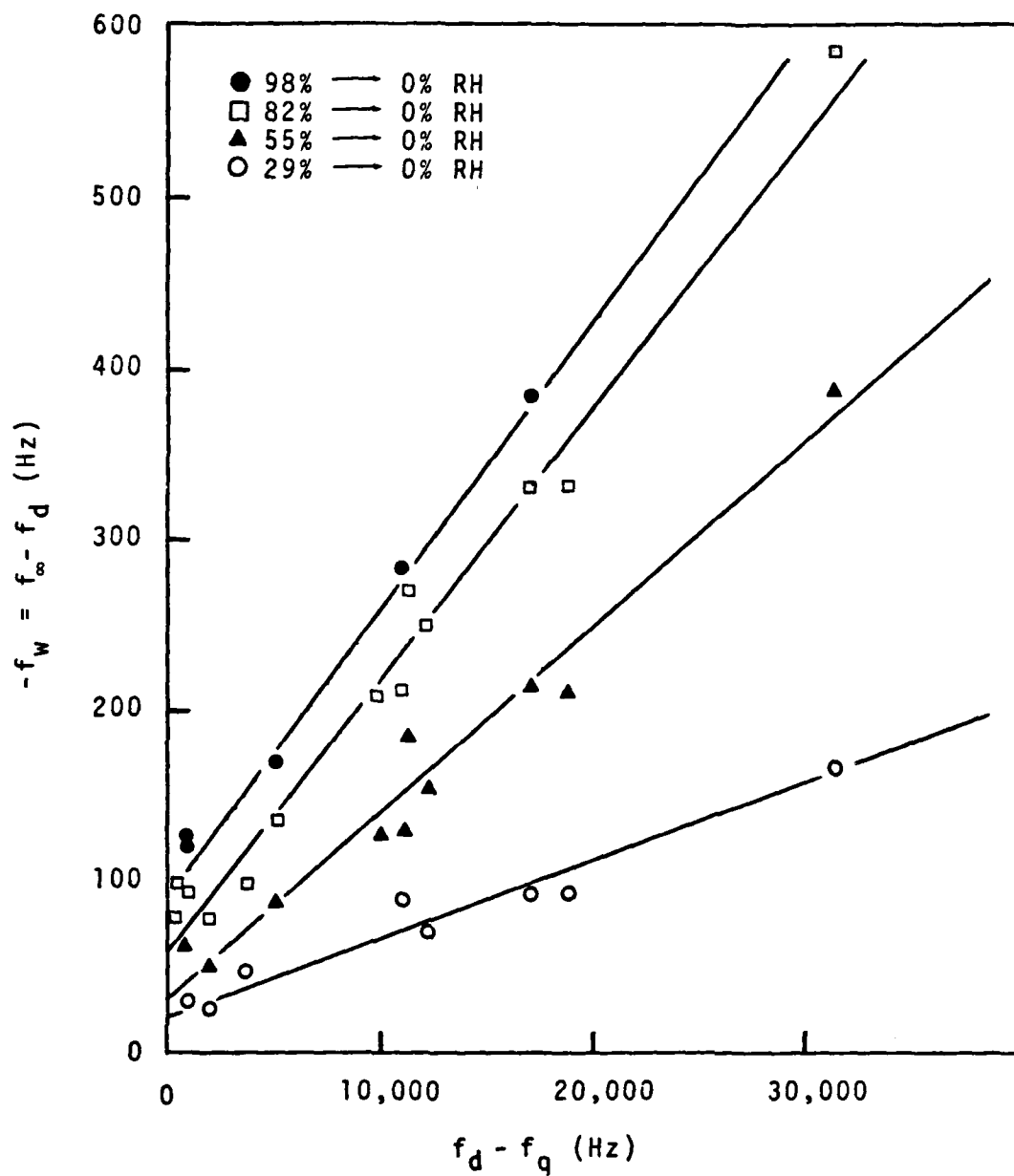


Fig. 10. Results of desorption experiments. The ordinate is the steady-state frequency change for the experiment. The abscissa is proportional to coating thickness, $1.5 \mu\text{m}/10,000 \text{ Hz}$.

slope of the curves represents the differential solubility, S . When the slope (solubility) is a constant, straight lines result. Least-squares straight lines were constructed through the data shown in Fig. 10. The slopes were equated with the solubility and plotted in Fig. 9. versus the relative humidity. In Fig. 10 the original frequency change ($f_d - f_q$) is proportional to the mass of dry paint applied to the crystal. Thus, the abscissa in Fig. 10 represents increasing coating thickness, because the painted area and coating density ($\rho = 1.18 \text{ g/ml}$) were approximately constant for all crystals tested.

3.2.6 Discussion

The first experiments performed with the crystal-oscillator apparatus were analyzed to check the experimental technique. Fig. 11 is a comparison between solubility data collected with the oscillator and data obtained by weighing thin sheets of polyurethane. The gravimetric data were collected over a period of about three months at approximately 23°C . The crystal oscillator data were obtained at 28°C . The data show good agreement between the two methods.

Fig. 9 shows that the average solubility (S') is a strong function of coating thickness. This result suggests that a water rich layer of paint exists somewhere within the coating. Where is the water-rich region located? Many locations are possible, but the most likely appears to be at the paint-metal interface. Fig. 10 is consistent with this view, although the same data would result if a thin, water-rich phase existed on the air side of the coating. Hydration of aluminum oxide layers has been observed under polymer coatings (31), but polybutadiene coatings on steel were observed to degrade in the polymer adjacent to the steel surface (32). Funke (8) has also concluded that a water-rich phase of some sort exists near the paint-metal interface. Therefore, the assumption was made that the water was concentrated near the paint-metal interface.

Attempts were made to determine the approximate thickness of the water-rich phase by coating crystals with different thicknesses of paint. Various thicknesses between $0.2 \text{ }\mu\text{m}$ and $5.0 \text{ }\mu\text{m}$ were tested. It was assumed that significant changes would be observed in both solubilities,

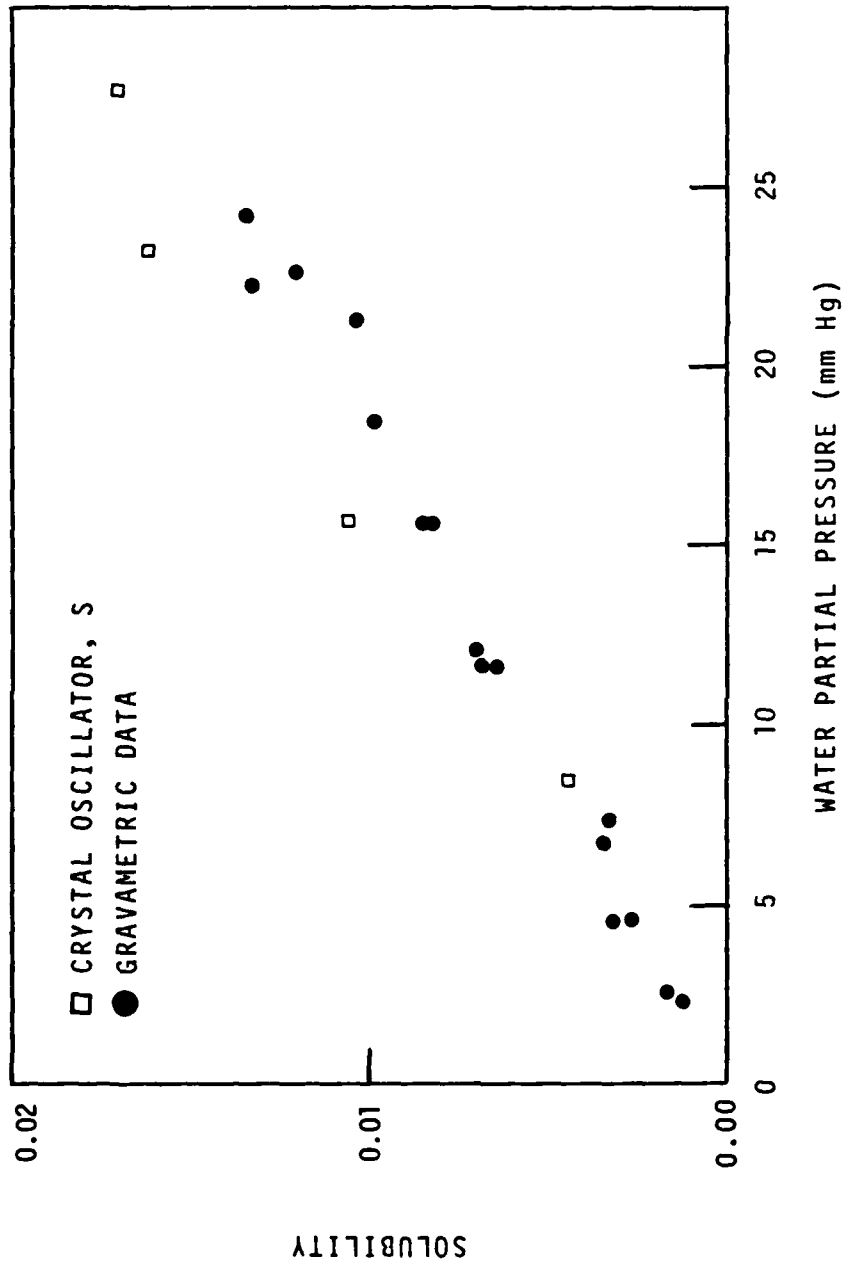


Fig. 11. Water solubility in O PUR

S and S', when the thickness of the coating approached the thickness of the water-rich phase. If the thickness of the water-rich region was independent of coating thickness one would expect S' to approach a constant value as the coating thickness decreased. Also, the differential-solubility curves (Fig.10) would bend and pass through the origin. Neither of these behaviors was observed. It was therefore concluded that, either the water-rich phase was thinner than 0.2 μm or its thickness depends on the coating thickness. The data obtained with the crystal oscillator were insufficient to determine the thickness of the water-rich region, but recent work suggests that the region is probably within a few tens of angstroms of the coating-metal-oxide interface (32).

Evidently a thin water-rich phase exists somewhere near the polyurethane-gold interface. For modeling purposes, it was assumed that the phase could be represented as a plane of finite capacity. This type of model was consistent with the data presented in Fig. 10. The amount of water at the interface (surface water) was determined from the intercepts shown in Fig. 10. Fig.12 shows the quantity of surface water as a function of relative humidity. The error bars represent the one-standard-deviation uncertainty in the calculated intercepts. Each data point presented in Fig. 12 has been reduced 12 Hz to correct for a systematic error which resulted because the temperature inside the cup was 0.5°C warmer than the outside temperature. A surface capacity (q) was defined as

$$q = \frac{\bar{c}}{a_w} \quad (21)$$

where \bar{c} = the water concentration, and a_w = the water activity. Fig. 12 clearly shows that the surface capacity depended on the water activity.

The quantity of surface water shown in Fig. 12 is significant and is difficult to explain. At 98% relative humidity $\bar{c}_o = 0.38 \mu\text{g}/26.4 \text{ mm}^2$. This corresponds to a layer of pure water about 140 Å thick. This represents considerable water, especially on a gold surface which is expected to have a very thin oxide layer. However, this is approximately

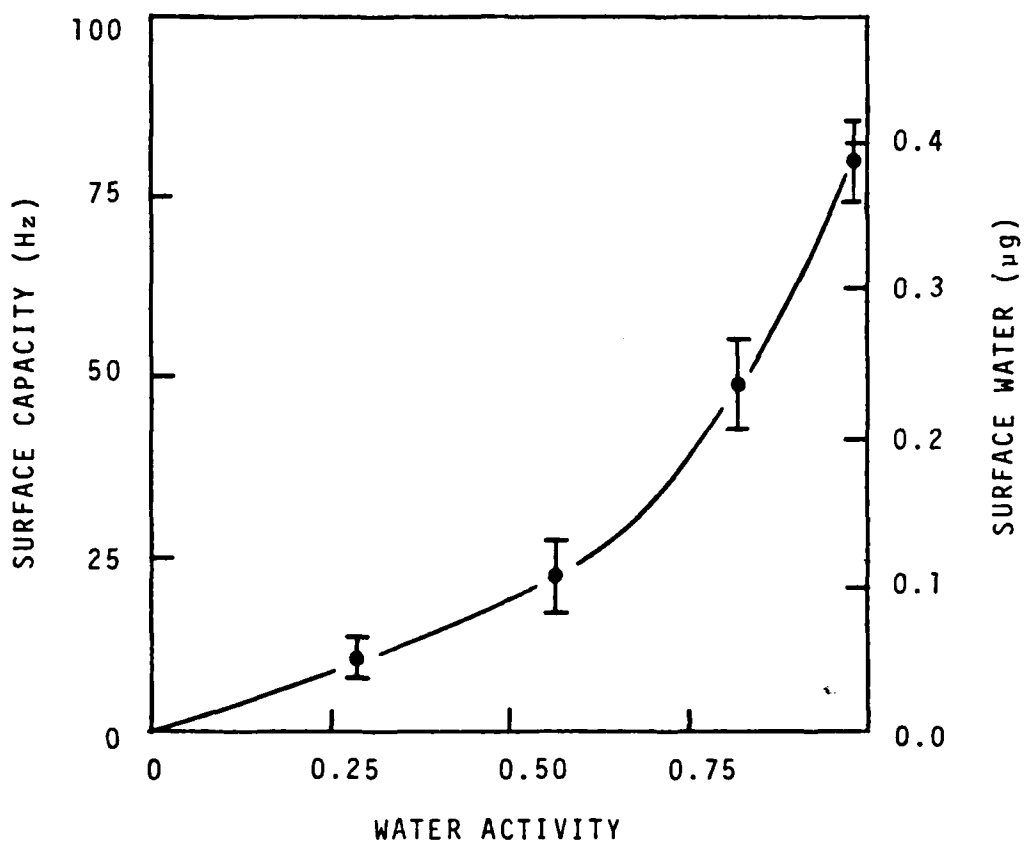


Fig. 12. Water at the polyurethane-gold interface.

1/60 of the maximum surface water Funke (8) found using a different experimental method. It is therefore probable that the quantity of water is correct, but exactly how the water is accommodated at the interface is not yet understood.

A quantitative measure of the surface water was needed for four of the five diffusion models. The method adopted employed a dimensionless variable, β . β is the ratio of the absorbed water, in the polyurethane, to the water at the paint-metal interface. Therefore, in general, β depends on both the paint thickness and the relative humidity. However, β would be independent of the relative humidity if the surface capacity (q) was a constant. A constant surface capacity has been assumed in the appropriate mathematical models. The average surface capacity, $1.47 \times 10^{-2} \mu\text{g}/\text{mm}^2$ (at 29°C), was calculated from the slope of the best straight line through the data shown in Fig. 12. Based on this value of q , average values of β were obtained for five representative crystals. β ranged from 0.41 to 8.25.

The diffusivity experiments were conducted in an attempt to answer two questions:

1. What is the water diffusivity in polyurethane paint, and
2. Does the paint diffusivity change in the direction normal to the plane of the coating ?

In order to quantitatively investigate these questions the five mathematical models were constructed. Table 4 lists the primary characteristics of the coating for each model.

Model 1 was the simplest; it treated the coating as a homogeneous material with constant diffusivity. The mathematical solution for this model is given by Crank (29, Sec. 4.3.2), and Table 3 shows the functional form of the solutions. Model 1 was applied to five representative crystals. The coating thicknesses ranged from $0.53 \mu\text{m}$ to $5.39 \mu\text{m}$. An average diffusivity was obtained for each crystal. The best diffusivity was selected by minimizing the standard deviation (σ) of the desorption isotherm model prediction, relative to the observed data. For the five crystals, $0.07 < \sigma \leq 0.14$.

Two features of this model stand out. First, the calculated diffusivities change systematically with coating thickness. The thinnest

coating (.53 μm) corresponded to the lowest diffusivity ($7.3 \times 10^{-16} \text{ m}^2/\text{s}$), and the thickest coating (5.36 μm) had a thousand times higher diffusivity ($5.8 \times 10^{-13} \text{ m}^2/\text{s}$). This effect appears to have been caused by neglecting the surface water in this model. Furthermore, these results are additional evidence that the water-rich phase is on the metal side of the coating, not the air side. This conclusion follows because the apparent diffusivity would be expected to increase for thinner coatings, if the water was collecting primarily on the air side of the coating. The second feature of this model appears to be a systematic error of some sort. The model calculations predict an initial sorption of water which is slower than the observed rate. Then, at longer times, the predicted sorption isotherm crosses the experimental curve. Similar results were obtained for all five crystals investigated. It was concluded that this model was flawed and contained insufficient detail to warrant further investigation.

The second model differed from the first by including the surface capacitance at the metal interface and a mass-transfer resistance on the air side. The mass-transfer resistance was characterized by a mass-transfer coefficient. In dimensionless form, the coefficient was given the symbol h . Table 3 shows the functional form of the concentration as a function of position and time. An iterative technique was used to search for the best values of h and the diffusivity (D). Table 5 illustrates the results obtained using model 2. The table shows that the diffusivity is a function of coating thickness for this model also, but the variation is now about one order of magnitude. The dimensionless mass-transfer coefficient (h) was always much greater than one. This fact indicated that the air-side mass-transfer resistance was negligible in this model. This conclusion was later confirmed when model 3 gave results nearly identical to those obtained with model 2. In general model 2 predicted the data slightly better than did model 1, but the same systematic deviation of the predicted curve away from the data was observed with both models. It was therefore apparent that model 2 was also deficient in some way. The large change in diffusivity (Table 5) also suggested a deficiency in this model. These considerations lead to the development of model 4.

Table 5
 Model 2 Results for Polyurethane (O PUR)
 Subject to an 85% to 0% Change in Relative Humidity

<u>Crystal #</u>	<u>Coating Thickness (μm)</u>	<u>Beta</u>	<u>Diffusivity (m^2/s)</u>	<u>h^1</u>	<u>Standard Deviation</u>
21	0.53	0.49	5.45×10^{-14}	2.57×10^4	.151
30	0.77	1.33	5.72×10^{-14}	1.59×10^2	.103
5	2.07	3.19	2.72×10^{-12}	2.76×10^6	.108
7	2.42	4.5	2.19×10^{-13}	5.59×10^3	.073
1	5.39	8.25	7.29×10^{-13}	7.39×10^3	.031

¹Dimensionless mass-transfer coefficient on the air side,

$$h = k_m \ell / D.$$

The results of model 2 showed that thick films could be fairly well explained with a single diffusivity and a surface-capacitance parameter. However, models 2 and 3 failed to accurately describe the "thin film" data. Thus, model 4 included a mass-transfer coefficient representing diffusional resistance at a plane between the bulk of the film and the surface capacitance. The dimensionless form of this mass-transfer coefficient was given the symbol γ (Table 3).

Table 6 shows the results calculated for model 4. These results are similar to those obtained with models 2 and 3, but the standard deviation (σ) is better for model 4. Only an approximate value of the diffusivity was obtained for crystal number 21 because the model results were not sensitive to the diffusivity, for that crystal. The same situation holds for the mass-transfer coefficient when considering crystals 1 and 7. It was therefore clear that model 4 represented only a slight improvement over models 2 and 3. The "reliable" diffusivities varied a factor of about 5, and the "reliable" mass-transfer coefficients varied about a factor of 18. This two-parameter model was clearly inadequate to fully describe water diffusion in this paint. On the other hand, model 4 gave the smallest standard deviation of the models tested thus far. It therefore appeared that model 4 incorporated some feature which made it represent the data more closely than the other models. It was apparent that the only significant difference between model 4 and the others was that the mass transfer resistance was inside the paint film. This discovery led to the development of model 5.

Model 5 assumes the diffusivity to be a linear function of the water concentration inside the paint. Under this assumption, both Eq. 13 and the boundary condition at the paint-metal interface are non-linear. Therefore, a finite difference method was used to solve the equations with the prescribed boundary conditions. Some convergence problems were encountered with this method.

Several types of convergence problems are typically encountered when attempting to solve nonlinear differential equations using finite difference methods. The problem encountered in this work was the failure to find a reasonable solution in a region of parameter space

Table 6
 Model 4 Results for Polyurethane (O PUR)
 Subject to an 85% to 0% Change in Relative Humidity

<u>Crystal #</u>	<u>Coating Thickness (μm)</u>	<u>Beta</u>	<u>Diffusivity (m^2/s)</u>	<u>γ^1</u>	<u>Standard Deviation</u>
21	0.53	0.49	8.0×10^{-11}	1.51×10^{-4}	.092
30	0.77	1.33	1.40×10^{-13}	.149	.035
5	2.07	3.19	2.68×10^{-13}	20.8	.107
7	2.42	4.5	2.18×10^{-13}	501	.072
1	5.39	8.25	7.24×10^{-13}	617	.031

¹Dimensionless mass-transfer coefficient on the metal side,

$$\gamma = k_m \ell \beta / D.$$

where the solution was sensitive to both parameters. Model 5 was another two-parameter model. The parameters were: the diffusivity at zero water concentration (D_0) and the dimensionless coefficient of change (δ). Based on the results obtained with model 4, D_0 was expected to be about $1 \times 10^{-13} \text{ m}^2/\text{s}$, and δ was expected to be between zero and about 100. Values in this range were found for the thick coatings on crystals 1 and 7, and in these cases the experimental results were duplicated, within experimental accuracy, by the model. For thinner coatings, the model failed to converge to a "best" D_0 and δ after 200 iterations. This fact is believed to be the result of a propagation of small errors in the calculations. The errors result from the finite difference method of approximating derivatives. At small times the derivatives of concentration are high near the paint-air interface. The errors are highest in this region, and as time passes the errors made at initial time steps are compounded. The method therefore loses accuracy as time passes. For some reason, not fully understood, the errors seem to propagate fastest for thin films. Apparently the final solution is sensitive to the exact value of the initial derivatives. In any event no quantitative results were obtained when model 5 was applied to thin coatings.

Despite the fact that model 5 failed to converge for thin coatings, the ability of the model to accurately describe the results obtained with the two thickest coatings was considered a success. These results clearly showed that the main mass-transfer resistance inside the coating could be explained by a concentration dependent diffusivity. Furthermore, model 5 suggested that the concentration dependence was significant. A factor of ten change in diffusivity could be expected over the activity range, $0 < a_w < 1$. These predictions were later confirmed by experiment.

A series of experiments was conducted to test the conclusions drawn from the model calculations. A series of diffusivity experiments was conducted with small step-changes in relative humidity. The overall relative humidity change of 98% was achieved in six small steps, the largest of which was 26% RH. The results of these experiments were then analyzed using the initial slope method (Eq. 18) to determine the diffusivity. The calculated diffusivities are shown in Fig. 13.

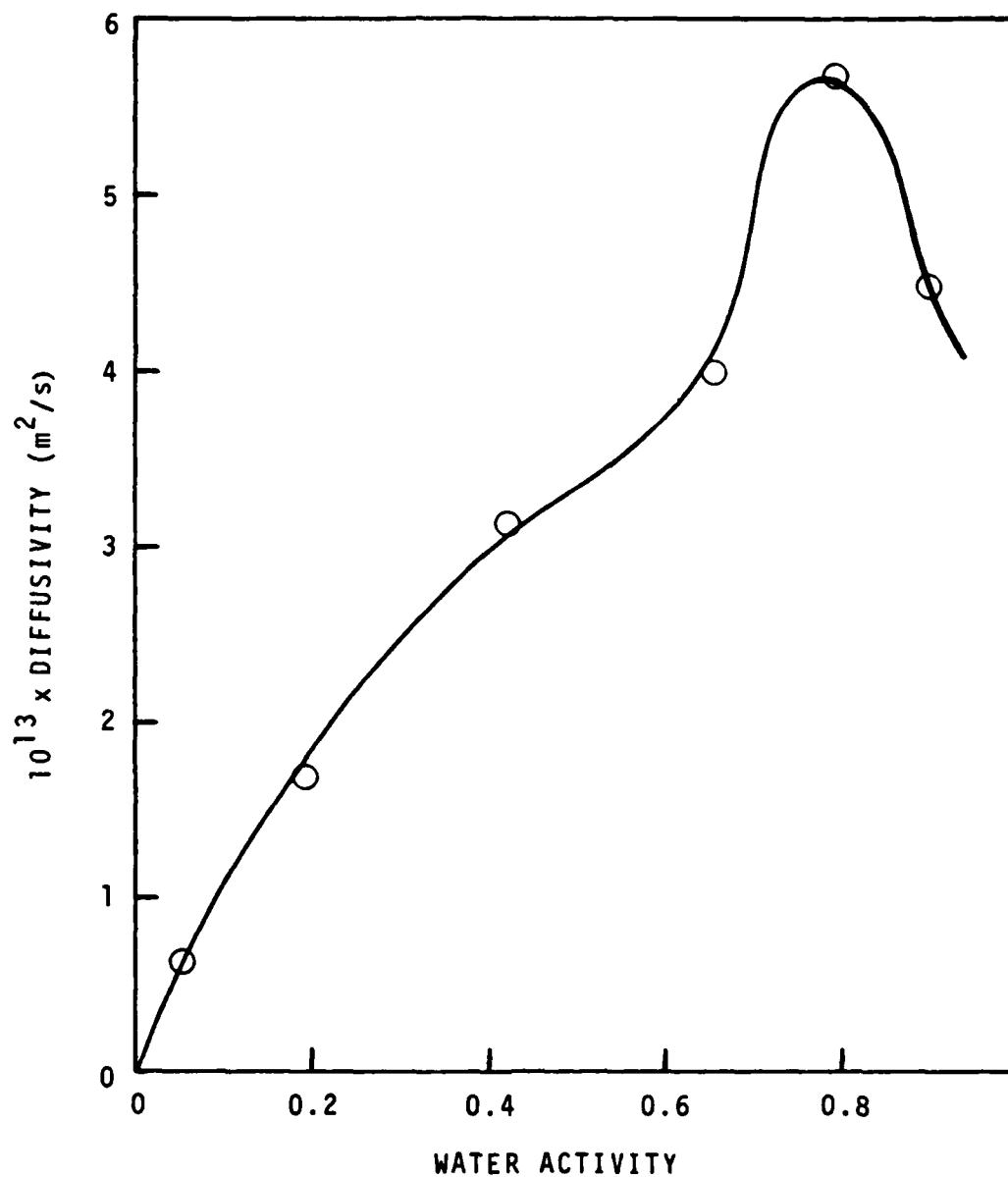


Fig. 13. Diffusivities obtained from a series of experiments subjecting the paint to small step changes in water activity at 29°C. The points (○) are plotted at the midpoint of each step.

The diffusivity passes through a maximum in Fig. 13. Crank (29) has discussed this type of behavior. Crank states the particular experimental evidence suggesting that the diffusivity at $a_w = 1$ is greater than at $a_w = 0$, and the diffusivity passes through a maximum in between ($0 < a_w < 1$). This evidence is that the desorption isotherm be above (faster than) the sorption isotherm at short times, and the relative positions be reversed at longer times. This conclusion follows provided the diffusivity depends only on the sorbant concentration. Both the experimental data (Fig. 8) and the conclusion (Fig. 13) are consistent with Crank's statements. It should be pointed out, however, that the boundary condition describing the water-rich phase is different from the one used by Crank. It is also possible to treat the water-rich phase as a region of very high (infinite) diffusivity. In this case the diffusivity would clearly depend on position as well as concentration. Thus, without further model calculations it is not possible to state conclusively that the data shown in Fig. 8 require the result shown in Fig. 13.

The physical phenomenon causing the diffusivity to pass through a maximum remains unexplained, but one possibility was investigated briefly. It is well known that solvents plasticize polymers, and therefore diffusivities are often concentration dependent. It is also known that plasticizers lower the glass transition temperature (T_g). The T_g of O PUR was measured at 11 Hz using dynamic mechanical methods (2). Similar tests were also conducted for various relative humidities, $0\% < RH < 100\%$, at 22°C . This data was used to estimate T_g for the experimental conditions of the diffusivity experiments (33). The estimated T_g was equal to the experimental temperature (29°C) at about 95% RH. This is slightly higher than the relative humidity of the maximum diffusivity, $\approx 80\%$ RH, but the estimated T_g is probably somewhat high because the results obtained with the dynamic mechanical method are frequency dependent. Thus, it appears that the maximum in the diffusivity occurs very near the relative humidity at which the polyurethane paint passes through the glass transition. Further work will be required to confirm these estimates and investigate further the dependence of diffusivity on T_g .

The maximum value of the water diffusivity obtained in these experiments was about $6 \times 10^{-13} \text{ m}^2/\text{s}$. This is about an order of magnitude smaller than the diffusivity obtained in the previous experiments. This fact suggests that the diffusivity is a function of coating thickness as well as water concentration. Only thin coatings ($< 5 \text{ } \mu\text{m}$ thick) could be tested with the crystal-oscillator apparatus. Thicker coatings ($25 \text{ } \mu\text{m} < \tau < 200 \text{ } \mu\text{m}$) were investigated using other methods. One obvious explanation of these facts is that the paint films possess a dense "surface skin" at the paint-air interface. However, the results of mathematical-model calculations indicate that there is no mass transfer resistance on the air side of the thin coatings on the crystals. This suggests that the thin coatings on the crystals was composed entirely of the "surface-skin" which is therefore thicker than $5 \text{ } \mu\text{m}$. Another possible explanation of the discrepancy in diffusivities is that thicker films have different concentration dependence than thin films. Although the exact nature of these phenomena is not clear it is apparent that thin films behave differently than thicker ones. It appears likely therefore that the paint properties will vary with position across the thickness of these coatings.

3.2.7 Conclusions

The following conclusions were based on experiments conducted with one type of polyurethane attached to gold-coated quartz crystals. All experiments were conducted at 29°C . The reproducibility of the results and the simplicity of the experiments make this technique a satisfactory method for determining mass transport and solubility parameters of thin coatings. One additional advantage is the applicability of the method over wide ranges of humidity and temperature. Another advantage is that the crystals can be coated with many different types of metals. The primary disadvantage is that only thin coatings can be investigated.

Accurate values of the solubility of water in the coating were obtained with this method. Furthermore, the surface effects were easily separated from those attributed to the bulk coating. The

solubility of water in this polyurethane, at 100% RH, was near 0.019 g-H₂O/g-dry paint. Water was sorbed in addition to that attributed to the bulk-coating phase. This water was explained by postulating a thin, water-rich phase at or near the paint-metal interface. This explanation was supported by the work of Funke (8).

Quantitative analysis of the data was performed to evaluate the water diffusivity. These calculations supported the conclusion that the water-rich phase was near the paint-metal interface. They also suggested that the diffusivity was a complex function of the water concentration in the paint, and that no surface "skin" existed at the paint-air interface. A surface skin might be present when the paint is thicker than 5 μm . The concentration dependent diffusivity was verified by experiment. The diffusivity exhibited a maximum value ($5.7 \times 10^{-13} \text{ m}^2/\text{s}$) near 82% RH. This result is in qualitative agreement with loss-modulus data obtained in dynamic mechanical tests and suggests that a change is taking place in the diffusion mechanism around 80% RH.

3.3 Zero-Capacity Cell

The results of Hittorf experiments indicated that some unexplained current was being passed through polyurethane coatings. Several phenomena could explain the findings, and it was desired to investigate which of these was actually taking place. One model which explains the data is that the membrane became a bipolar electrode, i.e., an electronic conductor. A more likely explanation is that some ion other than sodium and chloride carries the unexplained balance of the current. The ion (or ions) could be an organic compound originating from the paint, or some unaccounted for ion in the external solution. One likely possibility is that the ion is hydrogen (4). The diffusion experiments show that water penetrates polyurethane quickly. The permeability coefficients calculated from radiotracer experiments with tritium show even faster transport. Thus, the "zero-capacity" experiments were conducted to determine if the Hittorf results could be explained by hydrogen (or hydroxyl) ion migration.

The theory of the zero-capacity experiments was that hydrogen transport would result in a pH change in the external solutions. The volume (capacity) of the solutions was kept near "zero" to reduce the time required for the experiment. Solution volumes of 10 μ l to 50 μ l were tested. The cell was of the same basic arrangement as a Hittorf cell. Silver-silver chloride electrodes were used, and it was assumed that the only electrode reaction was with chloride. The primary difference between this apparatus and a Hittorf cell was that small volumes were used, and a larger area of solution was exposed to the air. Another difference was that the solutions were held in place by a piece of filter paper or cotton cloth, and they were not stirred. This apparatus had two drawbacks which until now have prevented significant results from being obtained.

The most troublesome problem was that the pH was affected by the paper or cloth blotting material. Several different materials were used as blotters, but none was found satisfactory. It is likely that this problem can be overcome by some kind of washing procedure prior to the experiment, but this has not yet been perfected.

The second problem was caused by absorption of carbon dioxide. This compound tends to buffer the pH at a value near 5.5. This was considered a secondary problem, however, because of the reduced buffering capacity at pH values lower than 5.5. The experiments were designed to produce an acid-side pH in the range, $3. < \text{pH} < 4$. The results of these experiments were inconclusive because any pH change resulting from ion transport through the paint was masked by the effects of the blotter and carbon dioxide.

3.4 Hydraulic Permeability

Seven coatings were tested to determine their hydraulic permeability (HP). The seven coatings included all paints currently under investigation except two of the epoxies. The epoxies were not tested because they were too brittle and did not hold up under pressure. All coatings were tested in 1 N sodium chloride at 23°C.

The results of the HP experiments are shown in Table 7. These results should be considered preliminary because of some experimental difficulties, and because the data are scattered. Table 7 shows that the paint films can generally be divided into two categories: low and high permeabilities. The flow rates through low permeability films ($\alpha < 10^{-17} \text{ m}^2/\text{Pa}\cdot\text{s}$) was so slow that salt rejection coefficients could not be measured. High permeability paints exhibited no measurable salt rejection.

3.5 Sorption of Radiotracer Ions

A single experiment was conducted to investigate the sorption of Cl^{36} by polyurethane (O PUR). The diffusion experiments (Sec. 3.2) had shown the apparent diffusivity of water in thin coatings of polyurethane was about an order of magnitude less than that measured in Hittorf experiments with thicker membranes (Table 1). This fact suggested that a dense "skin" might exist on the air-side of thick coatings. Also, free films used in Hittorf experiments appeared to show preferential absorption of radioisotopes. The results with Hittorf membranes were difficult to interpret, however, because of the past exposure of the membrane to several radioactive solutions. A sorption experiment was therefore conducted to investigate the possibility

Table 7
Hydraulic Permeability Coefficients

Paint	Pressure (kPa)	Permeability Coefficient (m ² /Pa·s)
A Epoxy	690	6.4 x 10 ⁻¹⁷
		3.2 x 10 ⁻¹⁵
	1030	4.5 x 10 ⁻¹⁵
		4.8 x 10 ⁻¹⁶
E Epoxy	690	1.8 x 10 ⁻¹⁷
	1030	5.7 x 10 ⁻¹⁷
	1380	1.4 x 10 ⁻¹⁶
	1720	2.1 x 10 ⁻¹⁶
VR2	690	9.5 x 10 ⁻²⁰
	1380	3.3 x 10 ⁻¹⁸
	2070	2.8 x 10 ⁻¹⁸
	2760	2.6 x 10 ⁻¹⁸
VR2	690	1.2 x 10 ⁻¹⁹
	1030	7.3 x 10 ⁻¹⁹
	1380	1.9 x 10 ⁻¹⁷
	1720	2.8 x 10 ⁻¹⁷
	2070	6.3 x 10 ⁻¹⁷
	2760	7.0 x 10 ⁻¹⁷
VR3	695	8.2 x 10 ⁻¹⁶
		9.9 x 10 ⁻¹⁶
	1030	7.5 x 10 ⁻¹⁶
		9.0 x 10 ⁻¹⁶
	1380	7.0 x 10 ⁻¹⁶
		7.9 x 10 ⁻¹⁶
VR3		7.0 x 10 ⁻¹⁶
	690	6.9 x 10 ⁻¹⁹
	1380	4.8 x 10 ⁻¹⁹
	2070	4.0 x 10 ⁻¹⁹
	2760	4.0 x 10 ⁻¹⁹
	3450	3.5 x 10 ⁻¹⁹
VR4	2070	9.5 x 10 ⁻²⁰
	2760	3.6 x 10 ⁻²⁰
	3450	2.8 x 10 ⁻²⁰
	4140	4.6 x 10 ⁻²⁰
	4830	7.3 x 10 ⁻²⁰
N PUR	1380	7.8 x 10 ⁻²⁰
	2070	8.5 x 10 ⁻²⁰
	2760	5.2 x 10 ⁻²⁰
	3450	5.4 x 10 ⁻²⁰
	4140	4.5 x 10 ⁻²⁰

that ions were preferentially absorbed on one side of thick membranes.

This sorption experiment was conducted by exposing different sides of similar polyurethane films to the same salt solution containing Cl^{36} . Two pieces of polyurethane were cut from a single piece of painted decal paper. The two pieces of paint were as nearly identical as possible. After they had been separated from the decal paper, they were placed on pieces of aluminum, and glass standpipes were clamped against one side of each paint film. The standpipes were then filled with a 0.1 N NaCl solution containing radioactive chloride. The only difference between the two paint samples was that one exposed the air-side to the radiotracer solution, and the other exposed the decal-paper side. Both samples were exposed to Cl^{36} for 46 days. Then the specimens were removed, rinsed briefly in distilled water, and dried.

The paint samples were analyzed by two methods: autoradiography, and beta scintillation counting. The paint specimens were placed near a piece of fast Polaroid film (Type 57, ASA 3000) in the autoradiography experiments. When the film was developed, a qualitative picture of the distribution of chloride across the paint surface was obtained. The scintillation counting technique provided a quantitative measure of all the chloride absorbed by the paint.

Within the statistical counting error, both films absorbed equal amounts of chloride ions, $C_{\text{Cl}} = 1.15 \times 10^{-7}$ mol-Cl/g-paint. The standard deviation was about 13%. This is in close agreement with the results of previous experiments (2-4). A dimensionless solubility coefficient for chloride was calculated from these data.

$$S_{\text{Cl}} = 1.4 \times 10^{-3} \quad (22)$$

This solubility is also in good agreement with the previous results.

On a qualitative basis, these results indicate that no preferential sorption took place. No experiments were conducted at other exposure times so it is not known if equilibrium was achieved. The radiotracer was not absorbed uniformly across the exposed surface, but chloride was present everywhere on the surface. In autoradiography experiments conducted with membranes used in Hittorf experiments, a uniform distribution of radiotracer was generally observed. The Hittorf membranes

were exposed to radiotracers for a longer period than in this sorption experiment, and this result may indicate that equilibrium was not achieved in this case. It does appear once again that variations between individual paint specimens and variations in time are two very significant characteristics of these paint films.

5.0 REFERENCES

1. R.T. Ruggeri and T.R. Beck, "A Model for Mass Transport in Paint Films," Corrosion Control by Coatings, H. Leidheiser, Ed., Science Press, Princeton, New Jersey, 1979, p 455.
2. T.R. Beck, "Determination of the Effect of Composition, Structure, and Electrochemical Mass Transport Properties on Adhesion and Corrosion Inhibition of Paint Films," Annual Progress Report No 1, Contract No. N00014-79-C-0021, Naval Ocean Research and Development Activity, Bay St. Louis, Missouri, 1979.
3. R.T. Ruggeri, and T.R. Beck, "Determination of the Effect of Composition, Structure, and Electrochemical Mass Transport Properties on Adhesion and Corrosion Inhibition of Paint Films," Annual Progress Report No. 2, Contract No. N00014-79-C-0021, Naval Ocean Research and Development Activity, Bay St. Louis, Missouri, 1980.
4. R.T. Ruggeri and T.R. Beck, "The Transport Properties of Polyurethane Paint", accepted for publication in the 2nd Symposium on Corrosion Control by Coatings, Lehigh University, August, 1980.
5. R.T. Ruggeri and T.R. Beck, "The Effects of Environment on Paint Adhesion to Steel", Ext. Abs. No. 124, The Electrochemical Society, May 10-15, 1981, accepted for publication in Symposium Volume, Adhesion Aspects of Polymer Coatings, K.L. Mittal, Ed.
6. R. Duplessix, et al., Water in Polymers, S.P. Rowland, Ed., A.C.S. Symposium Series 127, Am. Chem. Soc., 1980, p 469.
7. B. Rodmacq, et al., Water in Polymers, S.P. Rowland, Ed., A.C.S. Symposium Series 127, Am. Chem. Soc., 1980, p 487.
8. W. Funke, J. Oil Col. Chem. Assoc., 46, 975 (1963).
9. J.E.O. Mayne, J.Oil Col.Chem.Assoc., 32, 481 (1949).
10. B.W. Cherry, and J.E.O. Mayne, Off. Dig., 37, 13-27 (1965).
11. W.W. Kittelberger, J. Phys. Colloid Chem., 53, 392 (1949).
12. W.W. Kittelberger, and A.C. Elm, Ind. Eng. Chem., 44(2), 326 (1952).
13. E.M. Kinsella, and J.E.O. Mayne, Proc. 3rd Int. Congr. on Met. Corros., Moscow, 1966 p 117 (1969).
14. G.W. Rothwell, J. Oil Col. Chem. Assoc., 52, 219-235 (1969).
15. R.T. Ruggeri and T.R. Beck, "An Investigation of the Mass Transfer Characteristics of Polyurethane Paint", American Chemical Society, Division of Organic Coatings and Plastics Chemistry, Preprints of Papers, 43, August, 1980, p 580.

16. C.A. Kumins, Off. Dig. 34, 843, (1962).
17. C.A. Kumins, and A. London, J. Poly. Sci., 46, 395 (1960).
18. N. Lakshminarayanaiah, Transport Phenomena in Membranes, Academic Press, New York, 1969.
19. B.W. Cherry, and J.E.O. Mayne, 1st. Int. Congr. Met. Corros., London, p 539 (1962).
20. J.E.O. Mayne, Br. Corros. J., 5, 106 (1970).
21. J.E.O. Mayne, Anti-Corros., p 3, Oct. 1973.
22. J.E.O. Mayne, and D.J. Mills, J. Oil Col. Chem. Assoc., 58, 155-159 (1975).
23. J. Crank, and G.S. Park, Eds., Diffusion in Polymers, Academic Press, N.Y., 1968.
24. W. H. King, Research and Development, 28, April, 1969.
25. W.H. King, Research and Development, 28, May, 1969.
26. J.G. Miller, and D.I. Bolef, J. Appl. Phys., 39, 4589 (1968).
27. J.G. Miller and D.I. Bolef, J. Appl. Phys., 39, 5815 (1968).
28. C.S. Lu, and O. Lewis, J. Appl. Phys. 43, 4385 (1972).
29. J. Crank, The Mathematics of Diffusion, 2 ed., Clarendon Press, Oxford, 1975.
30. H.S. Carslaw, and J.C. Jaeger, Conduction of Heat in Solids, 2nd ed., Oxford University Press, London, 1959.
31. T.S. Sun, et al., Ext. Abs. No. 125, The Electrochemical Society, May 10-15, 1981.
32. R.A. Dickie, Ext. Abs. No. 122, The Electrochemical Society, May 10-15, 1981.
33. A.R. Wedgwood, J.C. Seferis, and T.R. Beck, "Transport and Related Properties of Paint Films," Part II, submitted for publication in J. Appl. Poly. Sci.

4.0 APPENDICES

- A. Paint Formulations
- B. Published Paper
- C. Experimental Results

APPENDIX A
PAINT FORMULATIONS

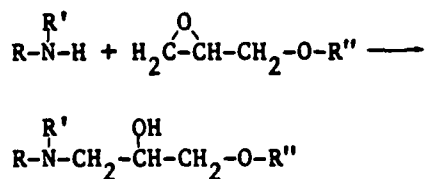
3.1 Formulation of Known-Composition Paints

Two consultants with long-time experience in polymers and paints, Dr. H. A. Newey and Mr. C. J. Busso, provided formulations of known compositions of vinyl, epoxy, and polyurethane paint systems meeting appropriate military specifications. During preparation of the initial proposal (1), it was determined by contacts with paint formulators and raw materials suppliers that the paint industry is extremely competitive and that the only way to obtain known-composition paints was through consultants. Appropriate Military Specification numbers for paints used by the Navy were obtained from NSRDC at Annapolis (2).

The paint systems procured (3, 4) are given in the following subsections. The code name given each paint for internal use at ETC is given in parentheses by each paint.

3.1.1 System I, Epoxy Resin Coating that Meets MIL-P-24441 (E Epoxy)

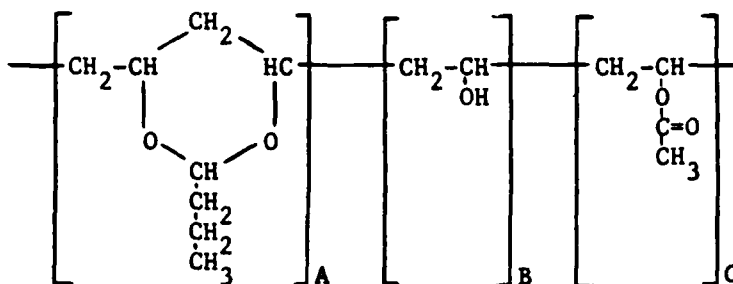
This coating consists of an epoxy resin, Shell EPON 815, and a polyamide curing agent. The epoxy resin is a mixture of the diglycidyl ether of bisphenyl A (90% by weight) and butyl glycidyl ether (10% by weight). The curing agent is a more-complex amine mixture, mainly Versamid 280B75 plus Genamid 2000 and MEK solvent (formulas given). In curing the amine, hydrogens add to the epoxide groups in the epoxy resin by the reaction:



The epoxy group reacts with both amine hydrogen on the terminal primary amine groups. The polyfunctional amines, Versamid 280 and Genamid 2000, react by this simple addition reaction with EPON 815 to give a cross-linked thermoset film.

3.1.2 System II, MIL-P-15328D, Formula 117 (VR2)

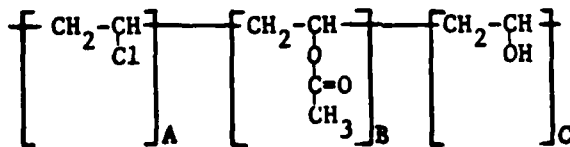
The structure of Bakelite Vinyl Butyral Resin XYGL can be best described by telling how it is made. Vinyl acetate is polymerized to a linear polymer and then saponified to remove most of the acetate groups leaving hydroxyl groups. Part of these hydroxyl groups is reacted with butyraldehyde, which forms an acetal with adjacent hydroxyl groups. The final product may be represented by the following structure:



Units of A, B, and C are randomly distributed along the molecular chain. In Bakelite XYHL there is approximately 80% by weight A, 19.5% by weight B, and 0.5% by weight C. The molecular weight is about 30,000.

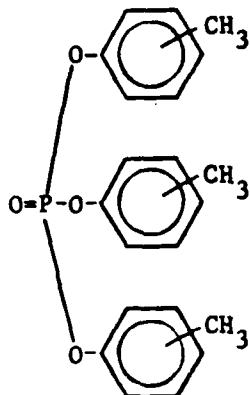
3.1.3 System III, MIL-P-15929C, Formula 119 (VR3)

Bakelite vinyl resin VAGH is a copolymer of vinyl chloride and vinyl acetate where a fraction of the acetate groups have been saponified to hydroxyl groups. It can thus be described as a copolymer of vinyl chloride, vinyl acetate, and vinyl alcohol, and can be represented by the formula:



These units are randomly distributed along the molecular chain. Bakelite VAGH is 91% by weight A, 3% by weight B, and 6% by weight C. The average molecular weight is 23,100 and it has a glass transition temperature of 79°C.

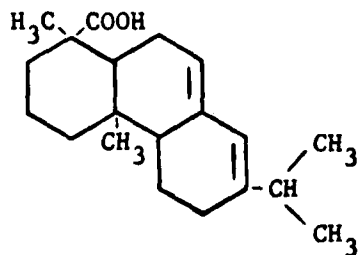
Tricresyl phosphate is a plasticizer for the resin. It has the structure:



It does not react chemically but only dissolves in the vinyl resin.

3.1.4 System IV, MIL-P-15931, Formula 121 (VR4)

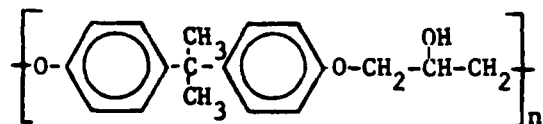
Bakelite Vinyl Resin VYHH is a random linear copolymer of vinyl chloride (86% by weight) and vinyl acetate (14% by weight). Again, tricresyl phosphate is the plasticizer. The rosin in the formula is largely abietic acid with other related compounds. Abietic acid has the following structure:



The rosin contributes to the hardness of the coating and helps adhesion. The coating dries by the evaporation of the solvent and no chemical reaction takes place between the components.

3.1.5 System V, EPONOL Resin Coating (A Epoxy)

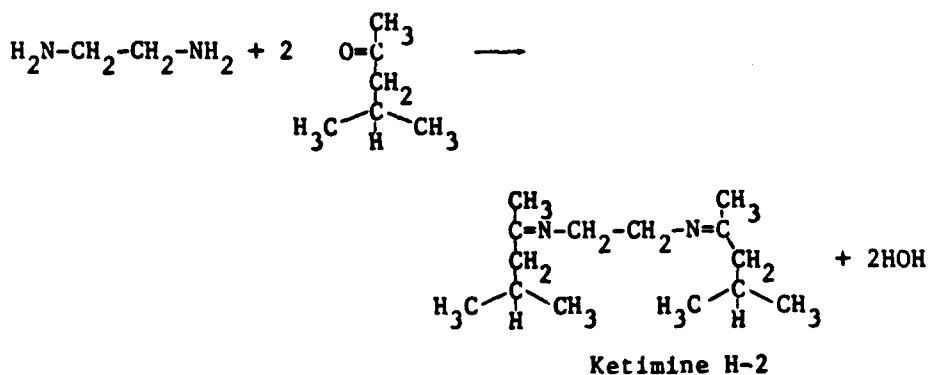
EPONOL 55 is a thermoplastic resin related to epoxy resin. The structure of the repeating unit is generally represented by the formula:



where n is about 25. There is some branching of the chain and the end groups are probably phenol or alcohol groups. While the chemical structure is similar to the epoxy resins, the molecular weight is high enough that good films are formed merely by evaporation of the solvent without the need of a curing agent.

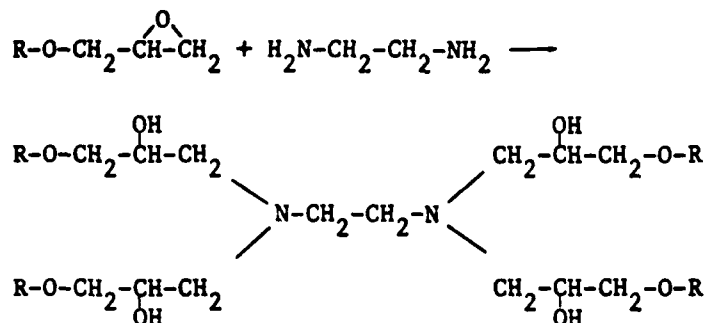
3.1.6 System VI, Ketimine-Epoxy Coating (K Epoxy)

To explain the chemical composition of this coating we must first explain what a ketimine curing agent is, and how it works. The ketimine H-2 is formed from ethylenediamine and methyl isobutyl ketone by the splitting out of water as follows:



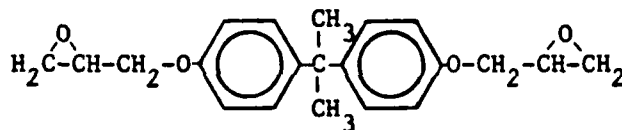
When applied in a coating, this ketimine readily reacts with the moisture of the air which breaks it back to ethylenediamine and methyl isobutyl ketone. (The reverse of the above equation.) The methyl isobutyl ketone evaporates from the coating and the ethylenediamine is the real curing agent. Ethylenediamine cures epoxy resins by a simple, clean-cut addition

of the amine hydrogen to the epoxide groups. This reaction is shown in the following equation using a monoepoxide for illustrative purposes:

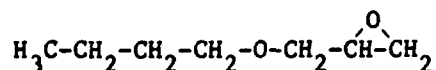


Since in the actual coating the epoxy resin is close to difunctional and the ethylenediamine is tetrafunctional, the addition reaction gives a cross-linked system with well-defined structure.

The epoxy resin in this coating consists of two parts. It is mainly the diglycidyl ether of bisphenol A.



To lower the viscosity and cut down the cross-link density, this diglycidyl ether of bisphenol A is diluted with a minor amount (about 10%) of a monofunctional epoxy compound, butyl glycidyl ether.

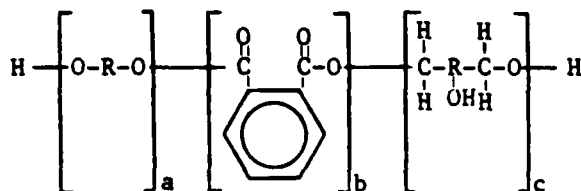


The phenol in the formula is merely present as a catalyst to speed up the reaction between amine hydrogens and epoxy groups.

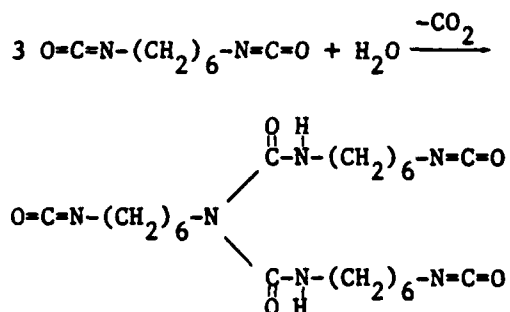
3.1.7 System VII, MIL-C-81773B A/S (N PUR)

This is a two part coating. Part I is a solution of polyester resin having free hydroxyl groups. A typical product of this type would be

prepared by reacting a glycol, phthalic anhydride and a triol to yield the following resin structure:

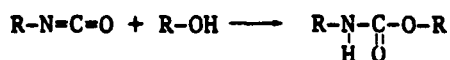


Component II is a solution of Desmodur N. This is a biuret derived from hexamethylene diisocyanate:



Desmodur N is sold by Mobay Chemical as a 75% solids solution in 1/1 by volume ethylglycol acetate/xylene solvent; designation of the solution is Desmodur N-75.

Cross-linking these systems results from the isocyanate-hydroxyl reaction to produce a urethane linkage:



Stoichiometry for this system is 1:1, Component I:Component II, by volume. Films of these coatings should be fully cured after eight hours at 77° F.

All of the components for the seven paints were procured and free films of all were made by spraying on decal paper and stripping in water. To date only unpigmented films have been made.

In addition to these systems, some testing was done on two airplane paint systems studied on another contract. These were both commercially

important, modern, two-part polymer systems, without pigments, obtained from the Boeing Commercial Airplane Company, Kent, Washington. One was a polyurethane, Desoto, Inc., Chemical Coatings Div., Berkeley, California, meeting Boeing material specification BMS-10-60D-TYII and Mil C-83286. The code name given to this system was System VIII or O PUR. The other paint was an epoxy, Koppers Co., Andrew Brown Div., Kent, Washington and was given the code name System IX or O epoxy. No information was obtainable on the exact formulations of these systems.

REFERENCES (Section 3.1)

1. Electrochemical Technology Corp., proposal 7803, "Determination of the Effect of Composition, Structure, and Electrochemical Mass Transport Properties on Adhesion and Corrosion Inhibition of Paint Films," April 1978.
2. T. R. Beck, Telephone call to H. Preiser, NASRD, Annapolis, MD, February 23, 1978.
3. Letter, Newey & Busso Associates, to Electrochemical Technology Corp., December 11, 1978.
4. Ibid, January 29, 1979.

APPENDIX B
PUBLISHED PAPER

THE EFFECTS OF ENVIRONMENT ON PAINT ADHESION TO STEEL

R. T. Ruggeri and T. R. Beck
Electrochemical Technology Corp.
3935 Leary Way N.W.
Seattle, WA 98107
(206) 632-5965

ABSTRACT

Painted steel specimens were exposed to six different environments to determine which surroundings had the greatest effect on paint adhesion. The adhesion of seven different paints to a steel substrate was quantitatively measured using a mechanical cutting device. The paints were unpigmented and contained no corrosion inhibitors. One-coat systems without primers were investigated. Tests were conducted to evaluate the effects of water, sodium chloride solution, anodic or cathodic currents, and various solvent-cleaning methods on paint adhesion. Results indicate that water had the most disruptive influence on adhesion, but at short times the effects were reversible when water was removed.

INTRODUCTION

The corrosion rate of painted metals is influenced by many factors. Two important factors are, the local electrolyte concentration and potential, at the corroding surface. Another is the adhesion of the paint to the metal surface. Adhesion is also influenced by the local conditions at the paint-metal interface. A quantitative study of adhesion should therefore yield valuable information on the mechanism of corrosion and the interfacial conditions.

A series of experiments was conducted to quantitatively measure adhesion under wet conditions, conducive to corrosion. The experiments were designed to answer three questions related to the overall corrosion inhibiting performance of paints. What conditions in the external environment have the greatest influence on paint adhesion? Could adhesion measurements be used to measure effects of interfacial concentrations or potential? Does the loss of adhesion promote corrosion, or is corrosion a necessary precursor of adhesion loss? Preliminary answers to these questions have been obtained, but additional work will be required before the relationship between adhesion and corrosion is fully understood.

In order to perform the experiments, a quantitative method of measuring adhesion was required. Various methods of measuring adhesion have been described (1, 2), but none has received universal acceptance. All methods disrupt the coating-metal bond by applying a force to the coating. At least six different ways of applying force to the coating have been used: acceleration, tension, backside hydrostatic pressure, cutting or scraping with a knife blade, friction on the coating surface, and bending of the substrate. Asbeck (3-5) describes the cutting method used in this work.

A machine was constructed to measure the force exerted on a knife as it cut strips of paint off a metal substrate. Results were obtained for seven different types of paint on one type of steel. The paints included three vinyl resins, two epoxies, one methacrylate, and a polyurethane. Surface energies were determined for all paints exposed to the ambient laboratory environment. In addition, the cutting force was measured to determine the effects of five other environments: distilled water, 1.0 N and 0.2 N sodium chloride solution, and 0.2 N sodium chloride after passing either anodic or cathodic currents. The results of these experiments can be interpreted on a semiquantitative basis to provide insight into the mechanism of corrosion under paint films.

THEORY

Asbeck proposed a method of measuring the surface energy of adhesion between paint coatings and their substrates (3-5). He used a knife to remove the paint from the substrate and observed both cohesive and interfacial separation of coatings. Cohesive failure took place when the knife cut through the coating. When interfacial separation was observed, the paint disbonded from the metal in front of the knife tip. This interfacial separation was called peeling. Asbeck used a theory of cutting (6, 7) to calculate the forces acting at the coating-substrate interface when the transition from cutting to peeling occurred. He then applied a theory of fracture mechanics to obtain a relationship between the forces required to propagate a crack and the cohesive energy of the material being fractured. He reasoned that, at the transition from cohesive failure to adhesive failure, the force in the coating was equal to that required to separate the coating from the substrate. Thus, the adhesive surface energy of a coating can be calculated from knowledge of the forces acting on the coating at the transition from cutting to peeling.

Merchant developed the theory of orthogonal cutting used by Asbeck. Merchant originally used the theory to describe the cutting of metals, but he later applied it to celluloid. Asbeck used the theory as the basis for his work on paint adhesion.

Fig. 1 shows the force vectors acting on the coating during cutting. Primed vectors denote reaction forces acting on the knife. The total force is denoted by the vector R which has been resolved into three pairs of orthogonal components in Fig. 1. F_T and F_C compose one pair of components. F_C is the cutting force acting in the plane of the substrate, and F_T acts normal to the substrate surface. The normal component, F_T , is required by the fracture mechanics theory. Experimentally, F_C is measured as a function of the initial coating thickness t_1 . The friction angle, τ , the blade angle, α , and the chip thickness, t_2 , are also measured. Merchant's theory is then used to calculate F_T at the transition from cutting to peeling, and the surface energy is calculated using the theory from fracture mechanics.

The normal force, F_T , depends on coating thickness. In thin coatings, F_T is too small to propagate a crack ahead of the knife tip, and cutting takes place in thin coatings. As the coating thickness, t_1 , increases, so does F_T . Eventually a point is reached where a crack propagates by peeling at the coating-metal interface. The transition from cutting to peeling takes place at a particular value of cutting force and thickness called the critical point.

Fig. 2 shows idealized data for a cutting experiment. Merchant's theory predicts that the force during cutting is a linear function of coating thickness. Line ab represents cutting. A discontinuity in the force is observed at b , and from c to d peeling takes place. The line ai

represents an extrapolation of the force from the linear region to zero coating thickness. The critical cutting force is the net increase in force between i and b. The surface energy is easily calculated once the critical force is known (5).

APPARATUS & PROCEDURE

A cutting machine was constructed to measure the surface free-energy of the paint-metal interface. It was similar to one described by Asbeck (3, 8). The machine consisted of a 0.64 cm wide knife, held at a fixed angle (α). The knife traveled 8.9 cm across a stationary test specimen at a constant cutting speed of 31.9 cm/min. The knife was attached to a hinged arm which allowed vertical movement. The vertical force on the knife was controlled by placing weights on the arm. When the proper weight was used, the knife would cut through the coating near the paint-metal interface. The horizontal cutting force (F_C), coating thickness, and knife position were measured with transducers and recorded on a Hewlett Packard, model 7046 A, XY recorder.

The shear angle, ϕ (Fig. 1), depends on the thickness ratio, t_1/t_2 , which is difficult to measure. Asbeck used the chip-length ratio instead of the thickness ratio to determine ϕ ; the chip-length ratio is the ratio of the length of the chip to the length of the coating before cutting. The chip-length ratio is equivalent to the thickness ratio if the density and width of the coating remain constant during cutting.

The chip-length ratio was determined in the following way. Five or six lines were drawn on the coating perpendicular to the direction of travel of the knife. The distance between the lines was measured before and after cutting, and the ratio of distances between adjacent lines was used as the chip-length ratio for the region between the lines.

All experiments were conducted on 15 cm square test panels of type 1018, cold-rolled, mild steel. The panels were 1.25 cm thick. The steel surface was abraded with a wire brush and 400 grit abrasive paper to remove all visible surface contamination. The panels were then rinsed alternately in hexane, methanol, and again in hexane. The panels were spray painted immediately following surface cleaning. The coating thickness (t_1) was made to vary across one width of the panel. The thickness usually varied, in the direction of cutting, between 1.2×10^{-3} cm and 1.3×10^{-2} cm. The coatings were allowed to dry in laboratory air at about 63% relative humidity ($55\% < RH < 83\%$), and $22^\circ\text{C} \pm 3^\circ\text{C}$. Drying times ranged from 16 hours to five weeks. Immediately prior to testing, the coatings were cut into knife-width strips. A single experiment involved cutting a coating strip off the steel substrate with the knife held at a specified angle α .

Dry Adhesion Measurements

Surface-energy measurements were successfully completed for seven different paint coatings. The paints were unpigmented and contained no

corrosion inhibitors. Only one-coat systems without primers were investigated. All surface energy measurements were conducted in the ambient laboratory environment. Coefficients of friction were obtained by drawing the knife backwards across the coating surface and measuring the horizontal force as a function of the vertical force. The vertical force was changed by placing weights on the hinged arm holding the knife. Knife angles were measured from photographs of the edge of the knife blades. Experiments were conducted with various knife angles (α) between 9° and 66° . Three to five cutting experiments were conducted at each knife angle for which the transition from cutting to peeling was observed.

The abrupt transition at the critical point (Fig. 2) was not usually observed in experiments performed in this laboratory. A linear dependence between F_c and thickness was observed when cutting was taking place, but the abrupt discontinuity was usually missing. In order to establish an unambiguous method of determining the critical cutting force, the following procedure was adopted. An approximate critical thickness was chosen, representing the boundary between cutting and peeling. Coatings thinner than the approximate critical thickness appeared to fail only by cutting. A least-squares straight line was then constructed through the data in this cutting region, and the point at which the experimental cutting force fell 5% below the straight line was identified as the critical point. The critical cutting force was then used to calculate the surface energy according to Asbeck's theory.

Coatings Exposed to Test Environments

One of the primary objectives of these experiments was to test the effects of external environments on coating adhesion. Several environments were tested; all included exposure to high activities of water. In order to establish an experimental control, only half of each steel panel was exposed to the test environment. The cutting force results obtained from each half panel were compared to determine the effect of the applied environment. In short experiments, water or salt solutions were held in contact with the coating by saturating a paper towel with the appropriate solution. This method was satisfactory for experiments lasting no more than eight hours, or when no current was passed. For longer experiments and whenever current was passed, solutions were held in place by a dam of silicone rubber around the test area, as shown in Fig. 3.

Cutting experiments have been conducted under five environments other than ambient laboratory conditions: distilled water, 0.2 N and 1.0 N sodium chloride solution, and 0.2 N sodium chloride solution after passing either anodic or cathodic current. Reagent grade, ACS specification, sodium chloride was used. For experiments in which current was passed, a Wenking model 68TS3 potentiostat was used in the galvanostatic mode. The counter electrode was a platinum sheet with an area of 6.5 cm^2 . The total charge passed through the steel electrode was varied from about $6 \times 10^{-4} \text{ C/cm}^2$ to $6 \times 10^{-1} \text{ C/cm}^2$, and current densities ranged from

$3 \times 10^{-8} \text{ A/cm}^2$ to $1 \times 10^{-5} \text{ A/cm}^2$, based on a superficial area of about 100 cm^2 for the steel. The paint-film resistance is high compared to the solution resistance, and the current density was assumed to be independent of the position of the counter electrode.

In all experiments conducted with wet coatings, rapid changes in the cutting force were observed following exposure to the test environment. These variations in the cutting force precluded determination of the optimum blade angle, α . Alpha could only be optimized by trial and error, and the best angle under wet conditions was invariably different from that for dry coatings. In addition, the cutting force changed rapidly for about thirty minutes following wetting, and twenty to thirty minutes were required to change knife blades. In order to obtain data in the time period immediately following a change of environment, a single knife was used. Experiments were conducted at various times, and comparisons were made between the cutting forces obtained.

RESULTS AND DISCUSSION

Dry Adhesion

Surface energies were measured for seven coatings on steel. Table 1 shows the results. Table 1 also lists data obtained by Asbeck as well as data obtained by others, cited by Asbeck, using different methods. The high and low surface energies obtained in this study are shown in

Table 1. Two factors were responsible for most of the variation in surface energy: changes in the chip-length ratio, and differences in cutting force. The chip-length ratio appeared to depend on coating thickness and to some extent on coating age. No mention of either of these two effects has been found in the literature. The chip-length ratio also depended on the time that elapsed between cutting and measuring the distance between the lines drawn on the chip. This behavior was more pronounced with polyurethane than with other paints tested, and it may depend on the viscoelastic properties of the paints. Asbeck does not mention this phenomenon. The second factor affecting the surface energies was variation of cutting force. When two adjacent strips of paint were cut off a steel panel, the cutting force and thickness were reproduced within approximately $\pm 5\%$. Most of the variations in cutting force resulted from testing the same type of paint on different steel panels. Experiments were conducted to see if the variations between panels resulted from variations in the method of preparing the steel for painting. Different abrasion times and solvent rinses were tested. No significant variations in cutting force were observed in these surface-preparation tests. At this time, the variations in surface energies of methacrylate and XYHL vinyl resin remain unexplained, but the results obtained in this study are in general agreement with Asbeck's data.

Wet Test Environments

When experiments were conducted in wet environments, rapid changes in cutting force occurred. Under these conditions, true critical cutting forces could not be observed, and surface energies could not be calculated. Consequently, the changes in cutting force were compared directly without using Asbeck's theory. Fig. 4 shows cutting-force data for a methacrylate-coated panel after exposure to distilled water. Each curve represents a single coating thickness. The curves connect data points, but the points have been omitted to promote clarity. A cutting experiment was always conducted immediately prior to introducing the test environment. Thereafter, data were collected at regular intervals of approximately 15 minutes. In Fig. 4, the cutting force declined to approximately 36% of its original "dry" value after only 30 minutes exposure to the water. It took less than 75 minutes exposure to water to reduce the cutting force to a nearly constant, low level. This same specimen remained in contact with water for 15 hours. Fig. 5 shows the cutting force following removal from the wet environment and exposure to the ambient laboratory atmosphere. The initial cutting force in Fig. 5 is about the same as that measured after 75 minutes of exposure to water, Fig. 4. Fig. 5 shows that, after exposure to laboratory air for 90 minutes, the cutting force has returned to roughly 90% of its original "dry" value. These results suggest that the mere presence of water at the paint-metal interface is sufficient to reduce the cutting force substantially. Furthermore, the recovery of the cutting force after the water was removed suggests that the interfacial region between

the coating and the metal had not been permanently disturbed. This indicates that no significant amount of corrosion had taken place in 15 hours. Similar results for shorter soak times have been obtained for vinyl resin and epoxy coatings as shown in Figs. 6 and 7.

A quantitative evaluation of the surface energy was not possible when the cutting force was changing rapidly with time. Asbeck's theory can be used to establish a qualitative relationship between cutting force and adhesion, however. Qualitatively, high cutting force is usually associated with good adhesion (2). A comparison of the curves in Fig. 2 shows that this may not always be true. Curve abcd in Fig. 2 represents a dry cutting experiment. The surface energy of adhesion depends on the critical cutting force and the cutting geometry. Curve a'b'c'd' represents one possibility when the coating is in a wet environment. In this case, the polymer coating will be plasticized by water, and in general, the slope of cutting force versus thickness will change. The curve a'b'c'd' has the same critical cutting force as abcd, however. Since invariant cutting geometry is assumed, the surface energy is the same as for the dry coating, but the cutting force at a prescribed thickness is always less for a'b'c'd' than for abcd. In this case, a reduced cutting force does not coincide with reduced adhesion.

Curve a'b''c''d' represents a second possibility for a wet coating. In this case, the slope of cutting force versus thickness is the same as

in the previous case of a wet coating, but the critical cutting force is much less than before. The surface energy is therefore much smaller in this case. In these examples, whenever the coating was wet, the cutting force was reduced, but the adhesion fell only if the critical cutting force declined. A reduction in the coating adhesion coincides with a reduction in critical thickness. The ratio of the wet critical thickness to the dry critical thickness can be used to qualitatively describe adhesion. If this critical-thickness ratio is less than one, adhesion has been reduced. In wet environments, the cutting force curve changed with time, and identification of the critical point was not always possible. However, the cutting force under wet conditions was often a low and nearly constant value. This indicates a reduction in the critical thickness and a corresponding loss of adhesion.

Coated panels were exposed to 0.2 N sodium chloride solution for up to 15 hours. No distinguishable difference from the behavior in distilled water was observed. A difference was noticed when similar experiments were conducted in 1.0 N sodium chloride, however. Data obtained with VAGH vinyl resin are illustrated in Fig. 8. The cutting force and coating thickness are shown as functions of position on the steel panel. Before wetting, the cutting force was a linear function of the thickness, indicating a cutting process. After exposure to sodium chloride solution for 5.5 hours, the cutting force was very low and uniform. This type of behavior indicated reduced adhesion. After the panel was allowed to dry overnight, non-uniform recovery of the cutting force was observed. Areas of permanent adhesion loss were

observed under thick as well as thin coatings, but a greater fraction of the surface area lost adhesion under thin coatings. No absolute correlation between adhesion loss and coating thickness existed in this test, but a statistical correlation does appear likely.

Permanent loss of adhesion was only observed when the panels were exposed to 1.0 N salt solutions. In all cases, the permanent adhesion loss was accompanied by corrosion of the iron substrate. Rust colored spots were visible through the coatings, and the cutting force was always low in the areas where rust was observed. Similar panels generally showed no loss of adhesion when exposed to 0.2 N salt solution for 15 hours. Strong salt solutions accelerated the rate of adhesion loss, but a quantitative explanation of this phenomenon and the role of corrosion remain to be determined.

A series of experiments was conducted to test the effect of electrolysis on adhesion. In these experiments, the test coating formed a barrier between a 0.2 N sodium chloride solution and the steel substrate. Current was passed between the steel panel and a platinum counter electrode. The cutting force results obtained in these experiments were indistinguishable from those conducted in 0.2 N salt when no current was passed, or those conducted in distilled water. Various anodic and cathodic currents were passed. The average iron equivalent of the total charge ranged between 1 and 1,000 monolayers. The results were independent of the charge passed.

One of the objectives of this work was to find a quantitative relationship between corrosion and the loss of coating adhesion. It was initially assumed that the moles of corroded iron would correspond to the charge passed through the coating. However, no permanent adhesion loss was observed after passing an average charge corresponding to 1,000 monolayers of corrosion. Three explanations are consistent with the observations.

1. Limited corrosion can take place without reducing adhesion.
2. Corrosion did not take place in these experiments.
3. Adhesion loss occurred only in a small area which was undetected in the cutting experiments.

The first explanation is considered unlikely. The second is possible if a charge transfer reaction other than corrosion takes place. Such a reaction could be the oxidation or reduction of an organic species in the paint. The third explanation is possible because the current density through the coating was not known. The current density depends on two factors: the thickness, and the conductivity of the coating. The thickness can be controlled, and was easily measured, but the conductivity varied unpredictably. Thus, even though the average current density through the coatings represented significant corrosion, the area actually experiencing corrosion could have been less than a millimeter in diameter. Disbonding of the coating in such a small spot could have gone unnoticed in the cutting experiments.

Additional work will be required to determine which of the three explanations is correct.

CONCLUSIONS

The conclusions are based on observations of the force required to cut paint off type 1018, cold-rolled, mild-steel panels. Seven different coatings have been investigated. Asbeck's theory has been used to calculate surface energies at room temperature when the relative humidity was near 63%. The cutting force dropped rapidly to a low value following contact of the coatings with aqueous solutions. During the time when the cutting force was changing, the cutting method could not be used to calculate surface energies. Nevertheless, the cutting force measurements indicate that water quickly penetrates the coating and substantially reduces paint-metal adhesion. The initial reduction in cutting force was reversible following removal of the aqueous environment. If corrosion permanently destroys adhesion, one must conclude that the reversible loss of adhesion was not caused by corrosion. This conclusion is further supported by the fact that only near-zero cutting forces were observed in all regions where rust was visible.

Permanent loss of adhesion occurred when the test panels were exposed to 1.0 N NaCl solution. The permanent adhesion loss was localized in small regions which were distributed across the entire wet

area. The regions of low adhesion were more common under thin coatings than under thick coatings. These observations suggest that spots of relatively high salt-permeability exist in these coatings, and the number of spots per unit area is statistically related to the coating thickness. No significant permanent adhesion loss was observed following exposure of the panels to distilled water or 0.2 N NaCl solution. The corrosion rate under these coatings was highly dependent on the external salt concentration.

We conclude from these experiments that corrosion is not a necessary precursor of adhesion loss, and that the cutting method could be used as a qualitative test for water at the paint-metal interface. However, further efforts will be required to determine a more quantitative relationship between coating adhesion and the mechanism of corrosion.

ACKNOWLEDGMENT

This work was supported by the Naval Ocean Research and Development Agency, Contract #N00014-79-C-0021. The contributions of Mr. Ricky Chan, who performed the cutting experiments, and Mr. Paul Olson, who constructed the cutting machine are appreciated.

AD-A113 975

ELECTROCHEMICAL TECHNOLOGY CORP SEATTLE WA
DETERMINATION OF THE EFFECT OF COMPOSITION, STRUCTURE AND ELECT-ETC(U)
OCT 81 R T RUGGERI, T R BECK

F/6 11/3

N00014-79-C-0021

NL

UNCLASSIFIED

2 OF 2

NO. 1
18474



END

DATE

FILED

5-82

DTIC

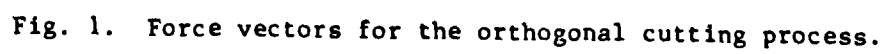
REFERENCES

1. N. Hamner, Materials Protection, May, p.31 (1970).
2. G. G. Sward, Ed., Paint Testing Manual, 13 ed., ASTM Special Technical Publication 500, Americal Soc. for Testing and Materials, Philadelphia, PA, 1972, Ch. 5.3.
3. W. K. Asbeck, "Adhesion and Cohesion," Philip Weiss, Ed., Elsevier, New York, 1962, p. 101.
4. W. K. Asbeck, IX FATIPEC Congress, p. 78, 1968.
5. W. K. Asbeck, J. Paint Tech., 43, (556), 84 (1971).
6. M. E. Merchant, J. Applied Phys., 16, 267 (1945).
7. M. E. Merchant, J. Applied Phys., 16, 318 (1945).
8. W. K. Asbeck, Paint Varn. Prod., 60, (3), 23 (1970)

Table 1
Characteristic Surface Energy for Paints on Steel

<u>Type of Paint</u>	<u>Surface Energy (kJ/m²)</u>			<u>Reference</u>
	<u>High</u>	<u>Low</u>	<u>Average</u>	
XYHL (VR-2)*	2.75	-	2.44	this work
VAGH (VR-3)	1.28	0.72	1.03	this work
VYHH (VR-4)	1.85	1.30	1.62	this work
Polyamide Type Epoxy	0.76	0.70	0.73	this work
Ketamine Type Epoxy	-	-	0.95	this work
Methacrylate	3.46	0.66	1.52	this work
Polyurethane	0.60	0.50	0.55	this work
Methyl Methacrylate			0.53	Asbeck (5)
Methyl Methacrylate			0.14 to 0.49	Other Investigators (5)
VMCH (VR)			3.00 2.79	Asbeck (3) Asbeck (3)

* VR = vinyl resin



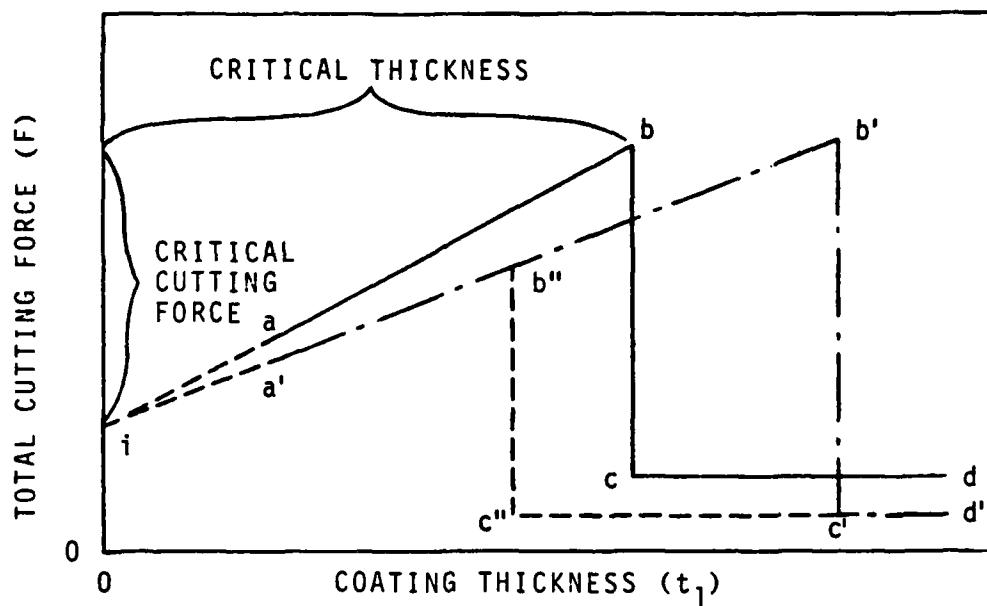


Fig. 2. Qualitative representation of cutting force versus coating thickness. Critical cutting force and critical thickness are shown for data following the path abcd. Other pathways represent data for removal of wet coatings (see Results and Discussion).

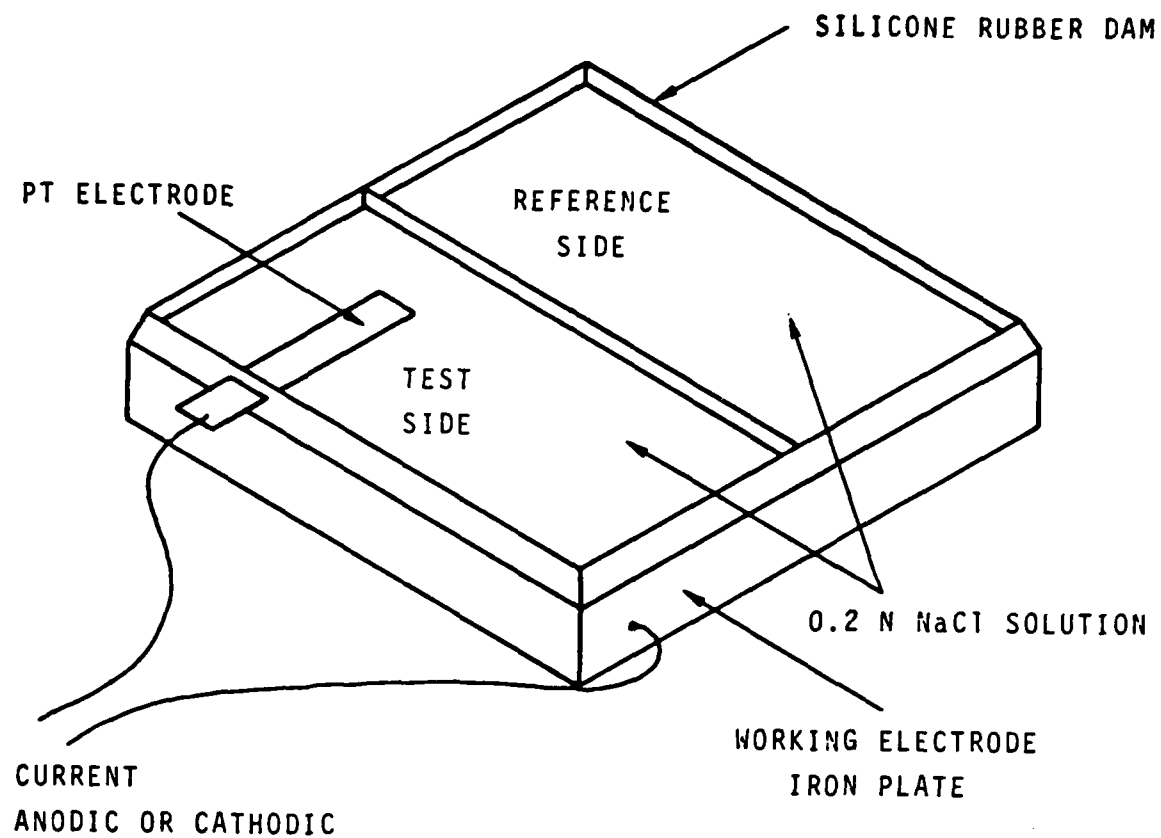


Fig. 3. Test panel as prepared for a constant current experiment.

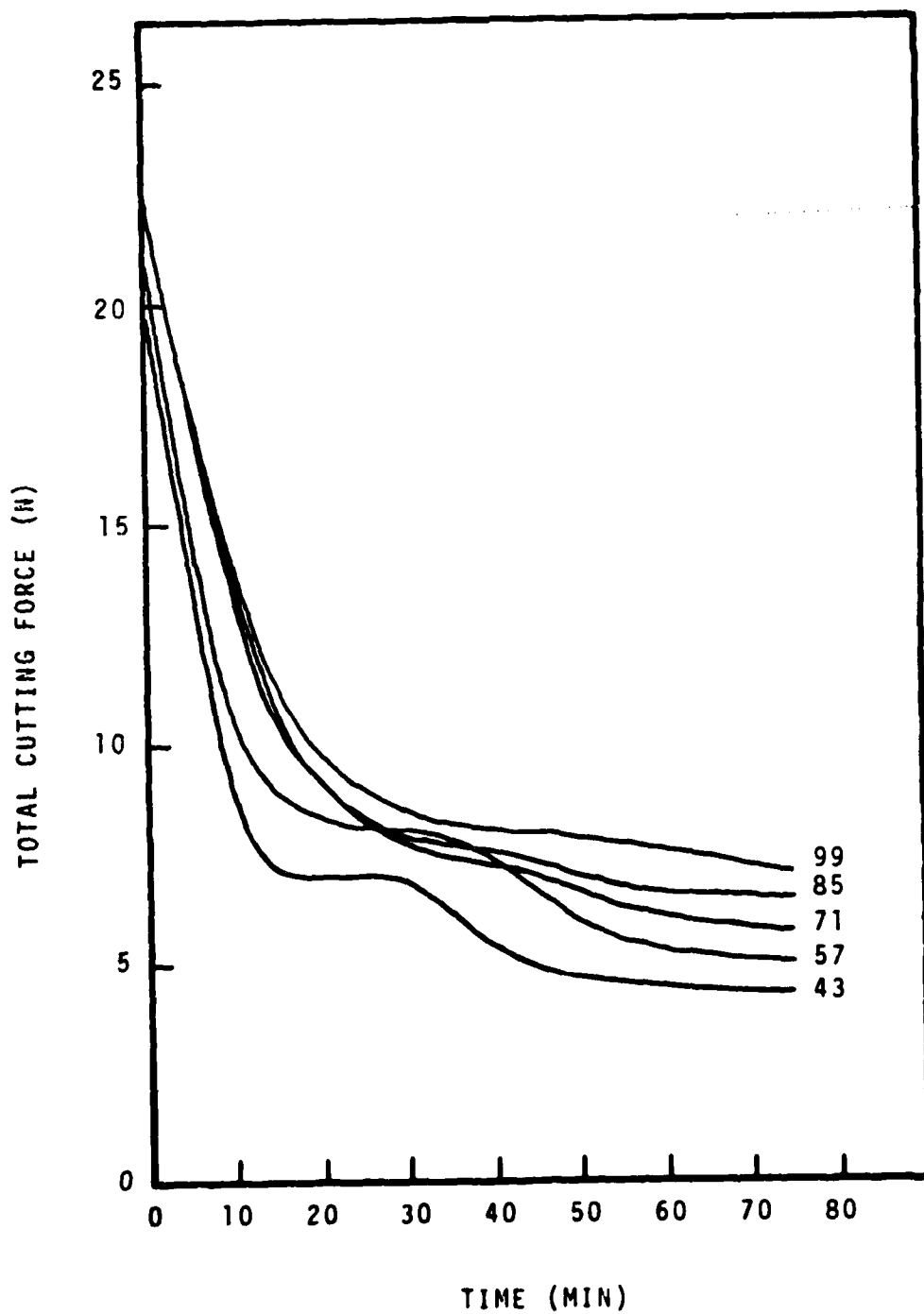


Fig. 4. Cutting force vs time of exposure of methacrylate to water. Five paint thicknesses are shown in μm. (Blade #14, $\alpha = 24^\circ$, w

4 mm).

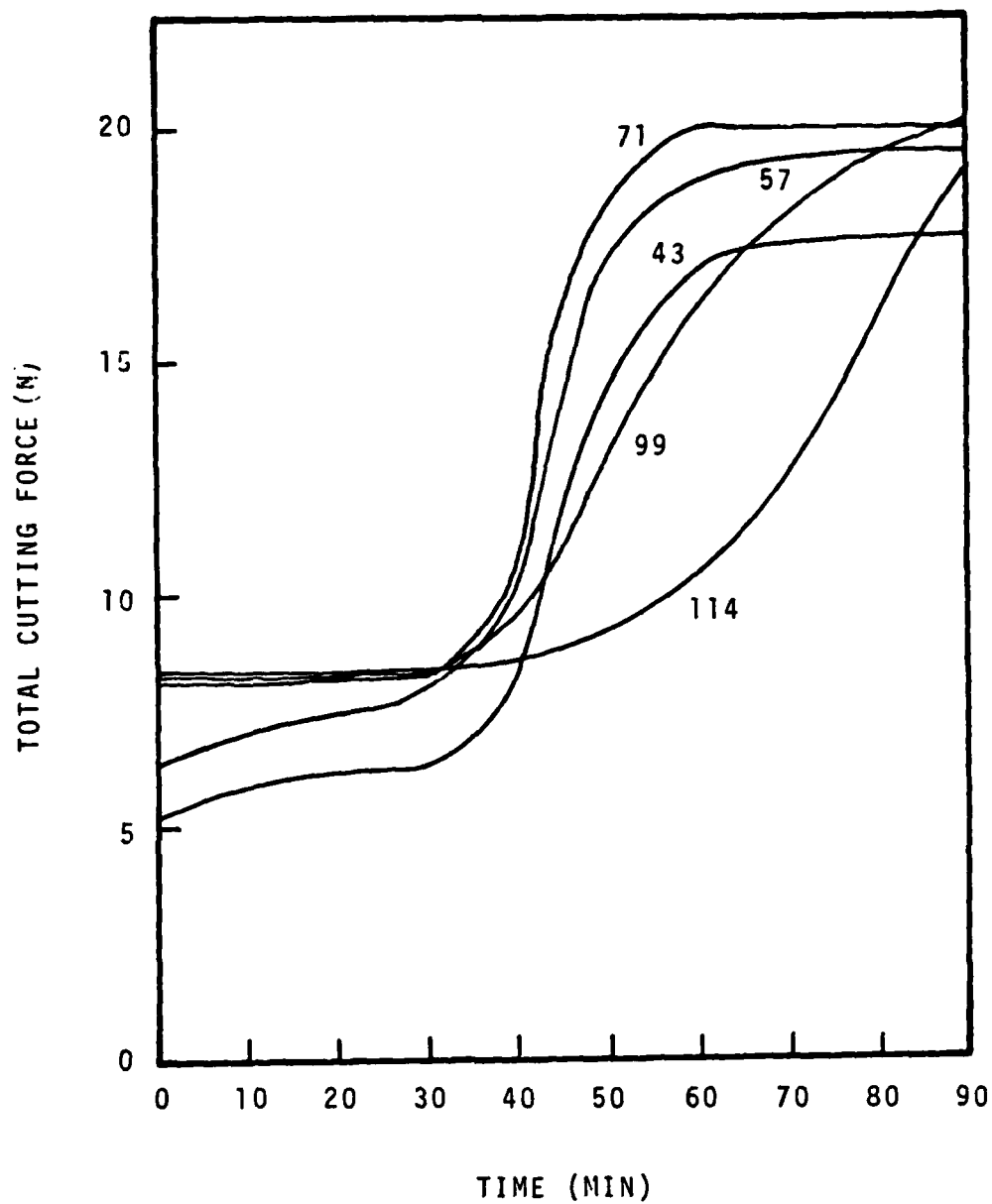


Fig. 5. Cutting force vs drying time after exposing methacrylate paint to water for 15 hours. Five paint thicknesses are shown in μm (Blade #14, $\alpha = 24^\circ$, width = 6.4 mm).

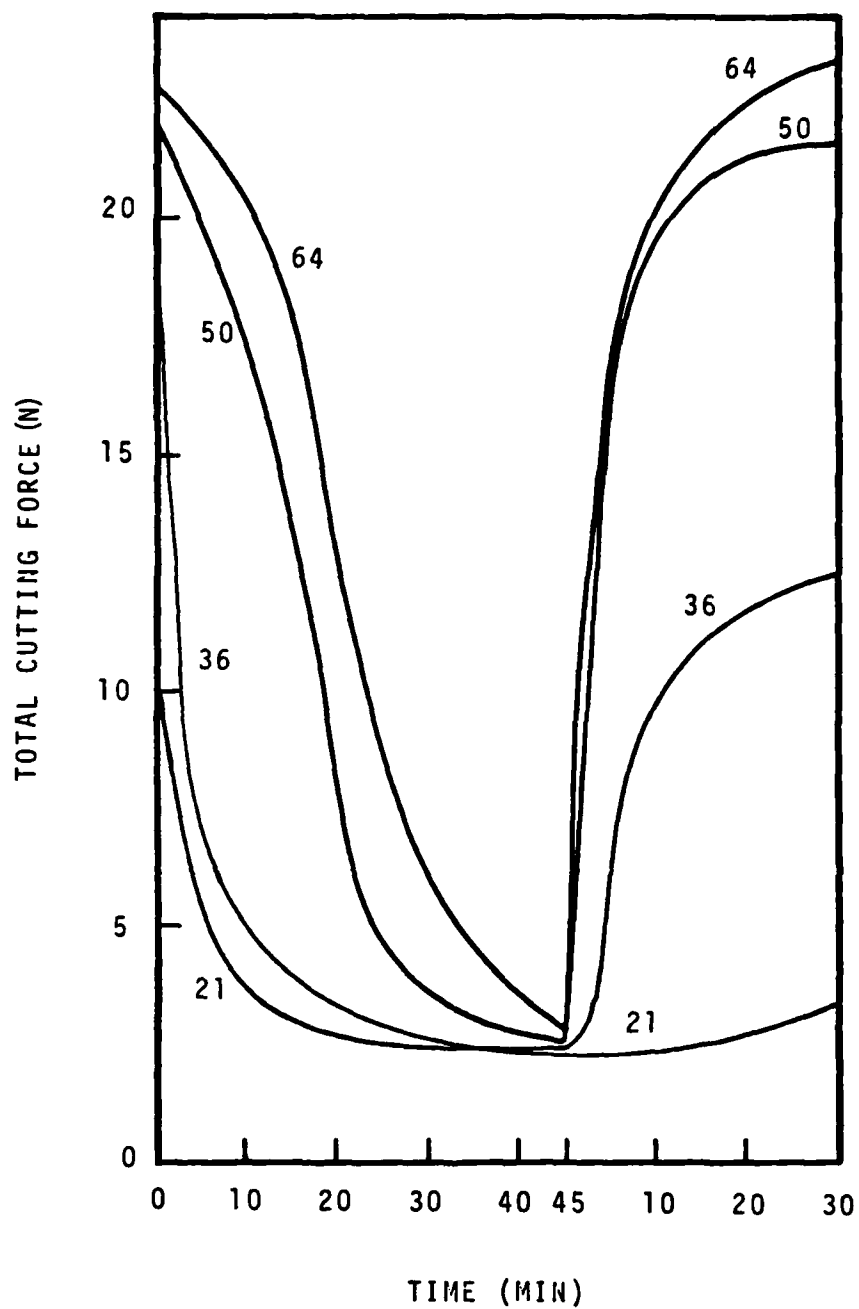


Fig. 6. Cutting force vs time following exposure of a VAGH vinyl resin first to water then to laboratory air. Four paint thicknesses are shown in μm (Blade #14, $\alpha = 24^\circ$, width = 6.4 mm).

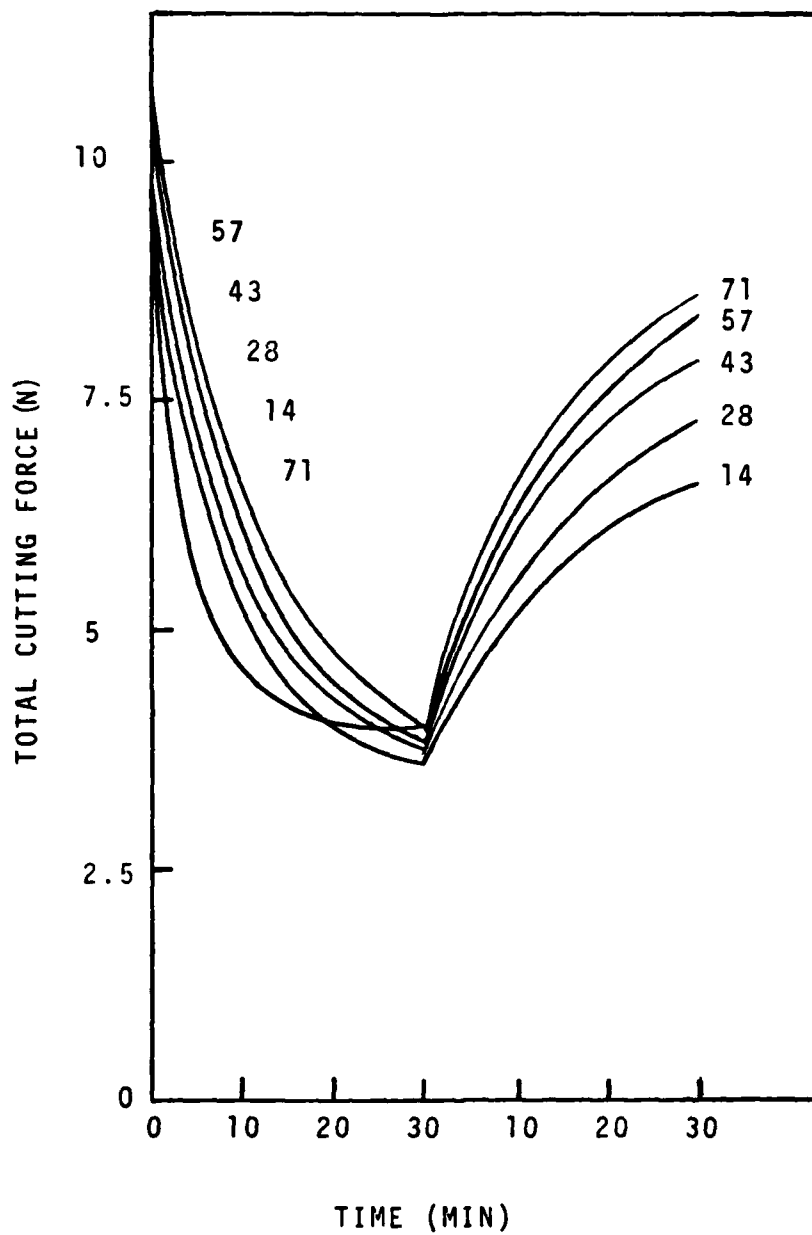


Fig. 7. Cutting force vs time following exposure of a polyamide epoxy first to water then to air. Five coating thicknesses are shown in μm (Blade #14, $\alpha = 24^\circ$, width = 6.4 mm).

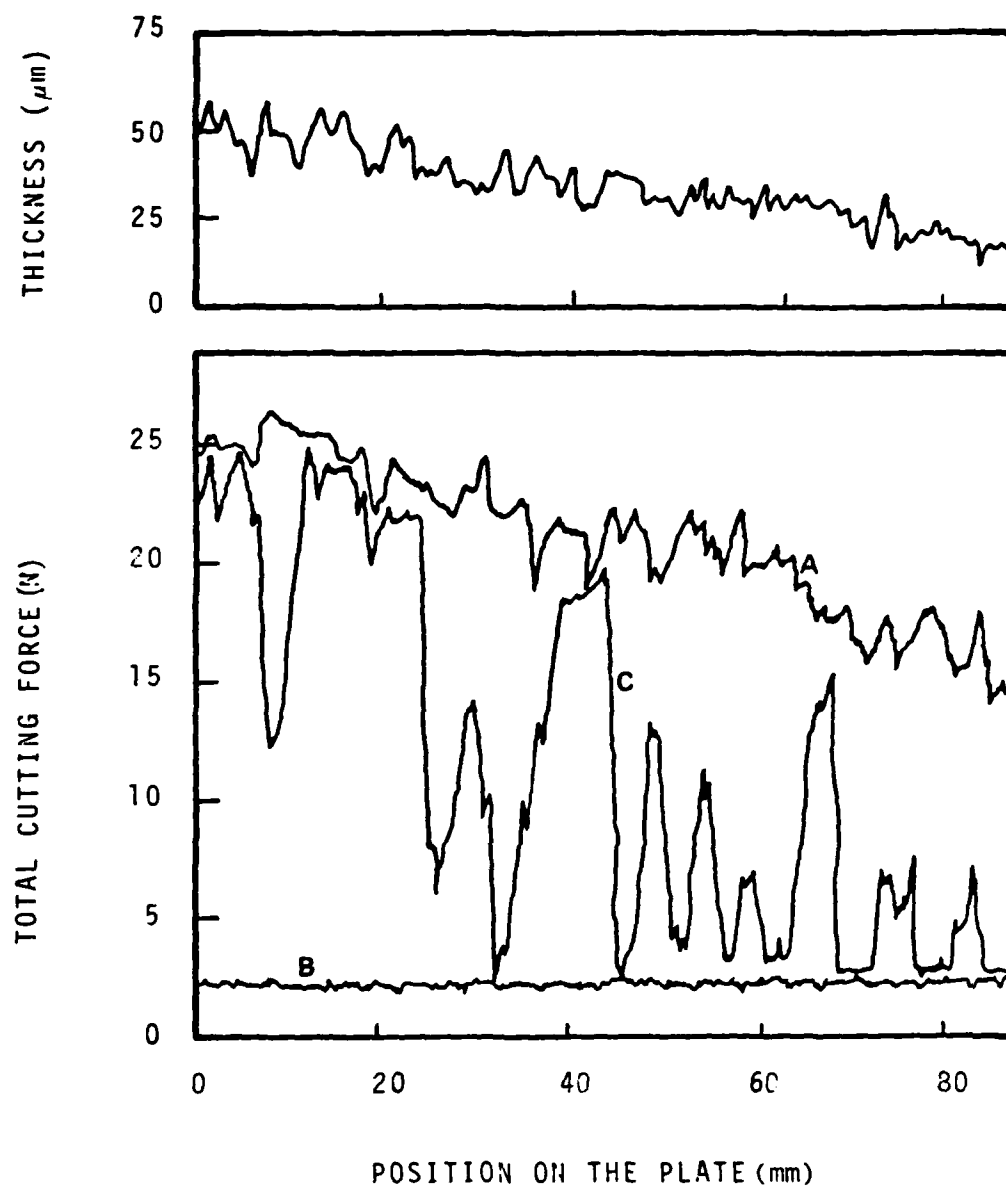


Fig. 8. Effect of wetting a VAGH vinyl resin with 1 N NaCl solution: A = before wetting; B = wetted with 1 N NaCl solution for 5.5 hours; C = dried for 17 hours after B. Knife width = 6.4 mm.

APPENDIX C
EXPERIMENTAL DATA

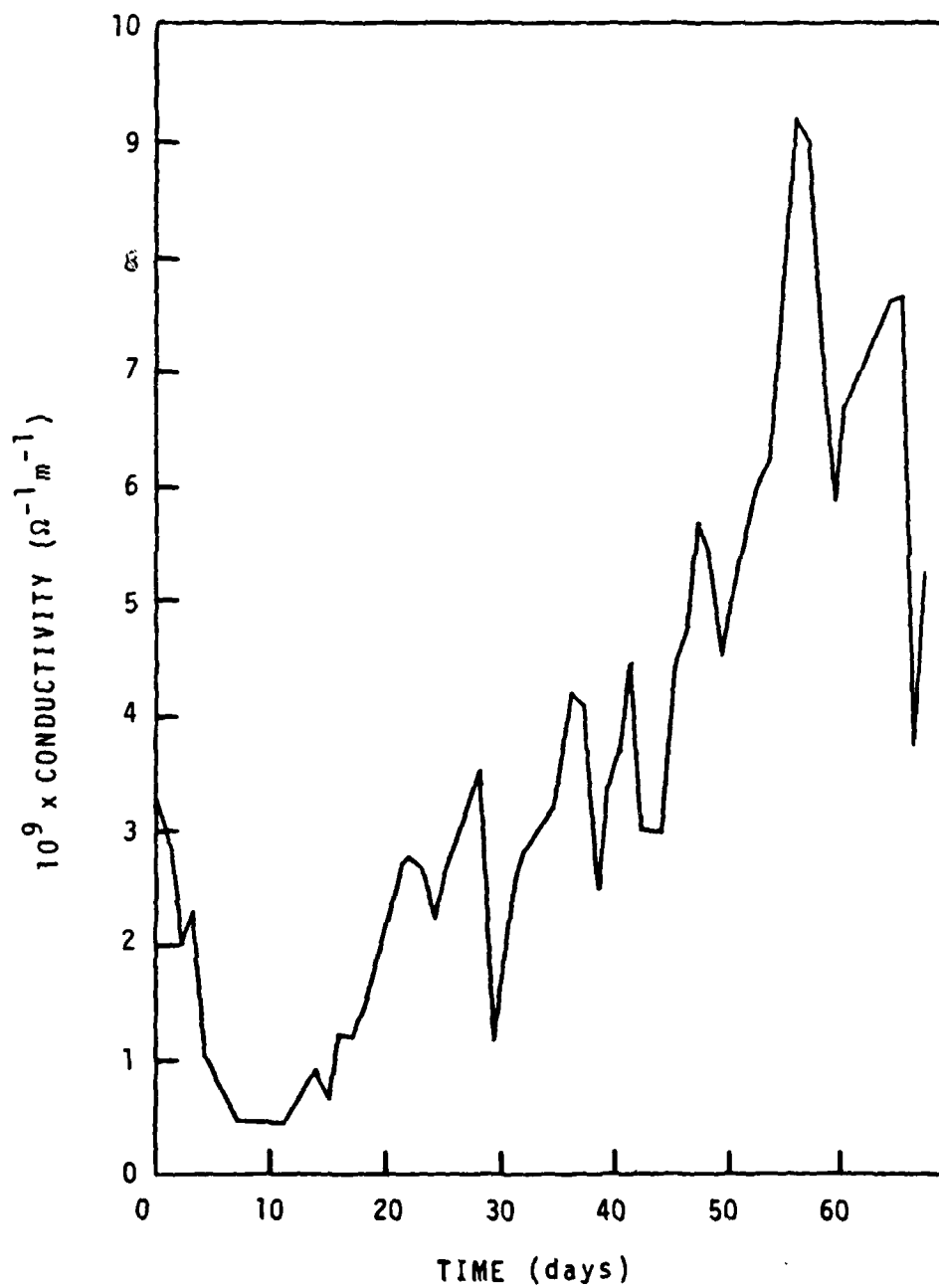


Fig. C-1.1 Membrane conductivity for polyurethane (O PUR)
in 0.3 N NaCl, at 25°C (NR-7-80).

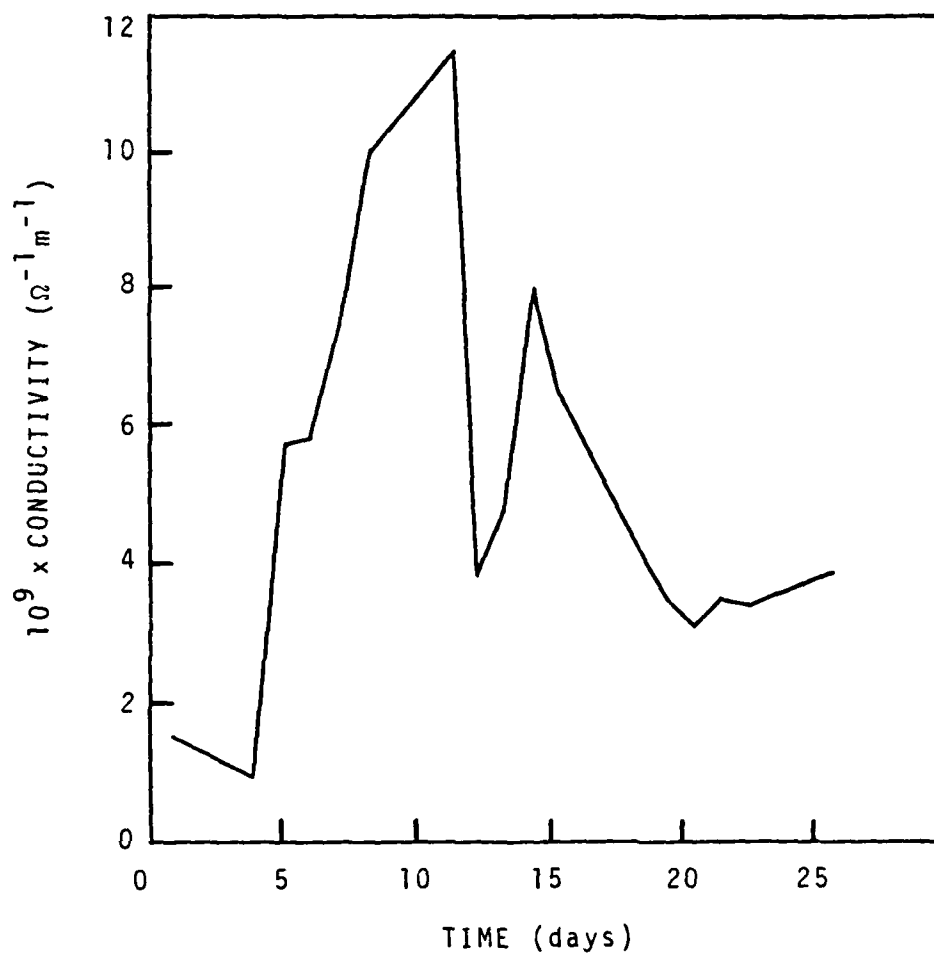


Fig. C-1.2 Membrane conductivity for polyurethane (O PUR) in 0.023 N NaCl, at 25°C (NR-8-80).

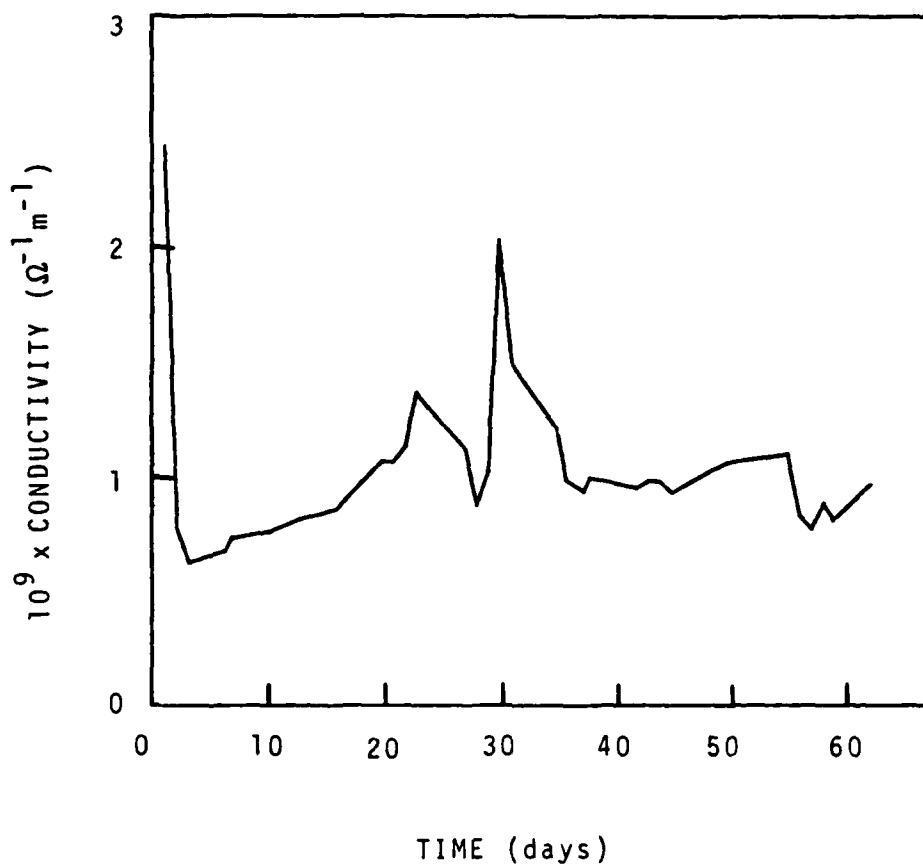


Fig. C-1.3 Membrane conductivity for polyurethane (O PUR) in 0.023 N NaCl, at 25°C (NR-1-81).

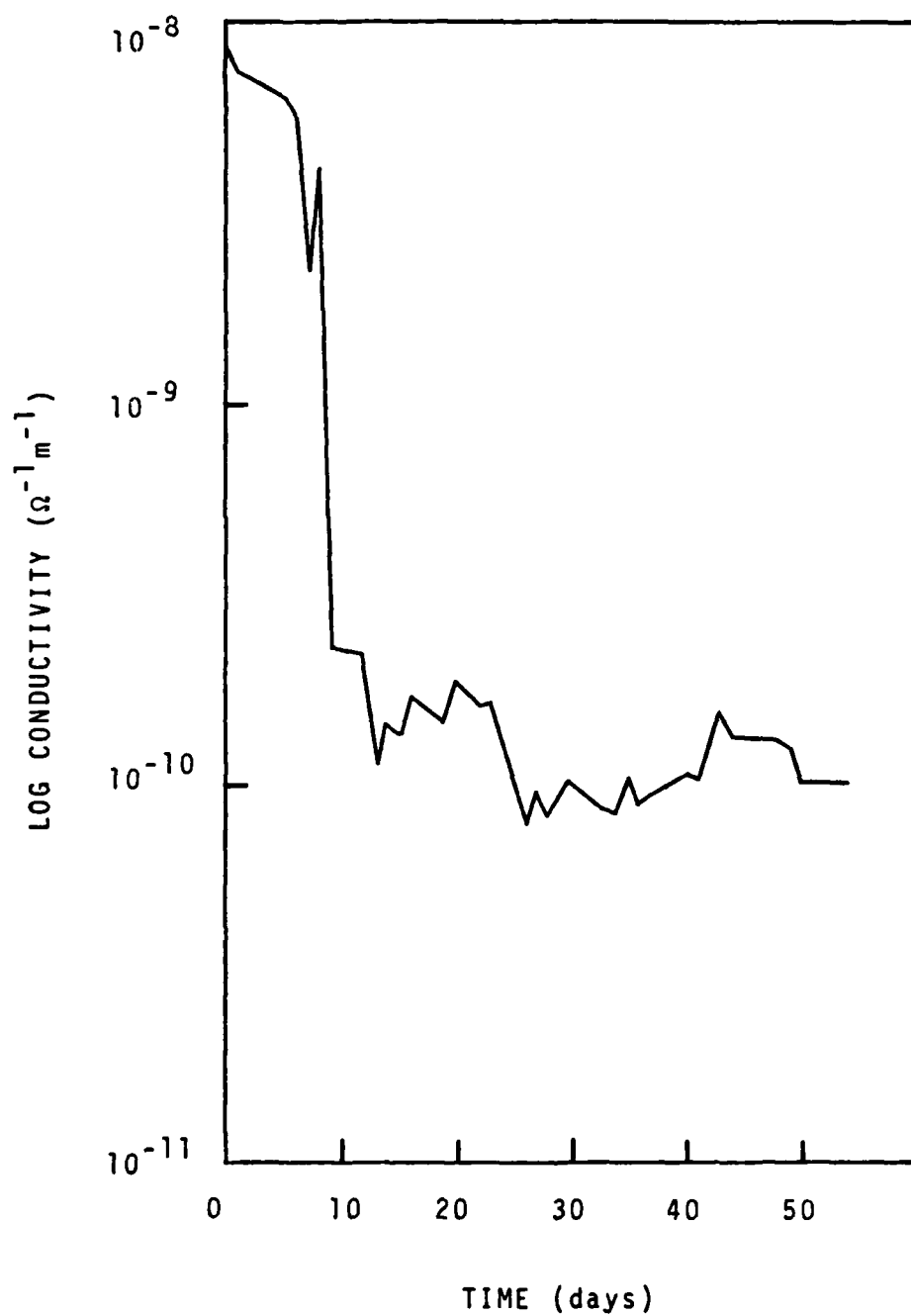


Fig. C-1.4 Membrane conductivity for polyurethane (O PUR) in 1.0 N NaCl, at 25°C (NR-3-81).

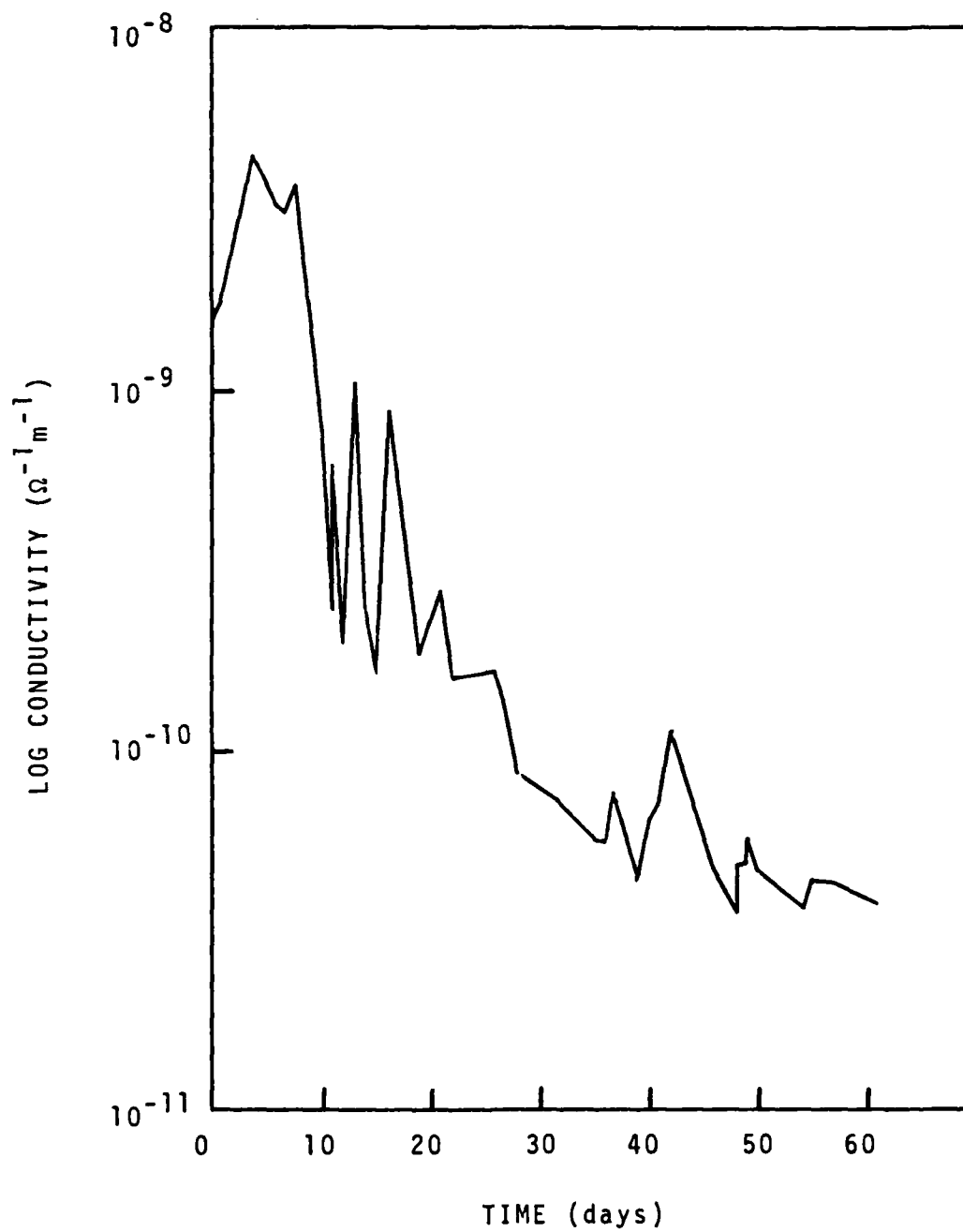


Fig. C-1.5 Membrane conductivity for polyurethane (O PUR) in 0.3 N NaCl, at 25°C (NR-4-81).

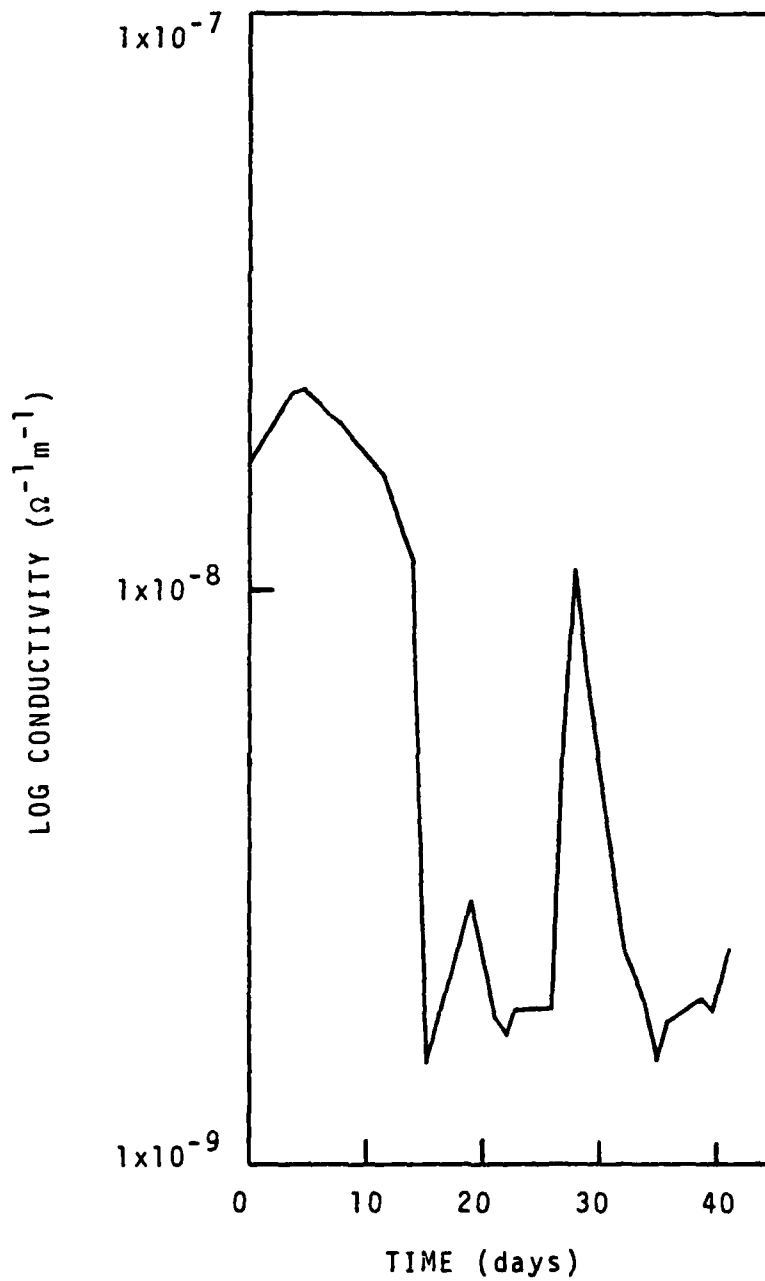


Fig. C-1.6 Membrane conductivity for a vinyl resin (VR4) in 0.012 N NaCl, at 25°C (NR-5-81).

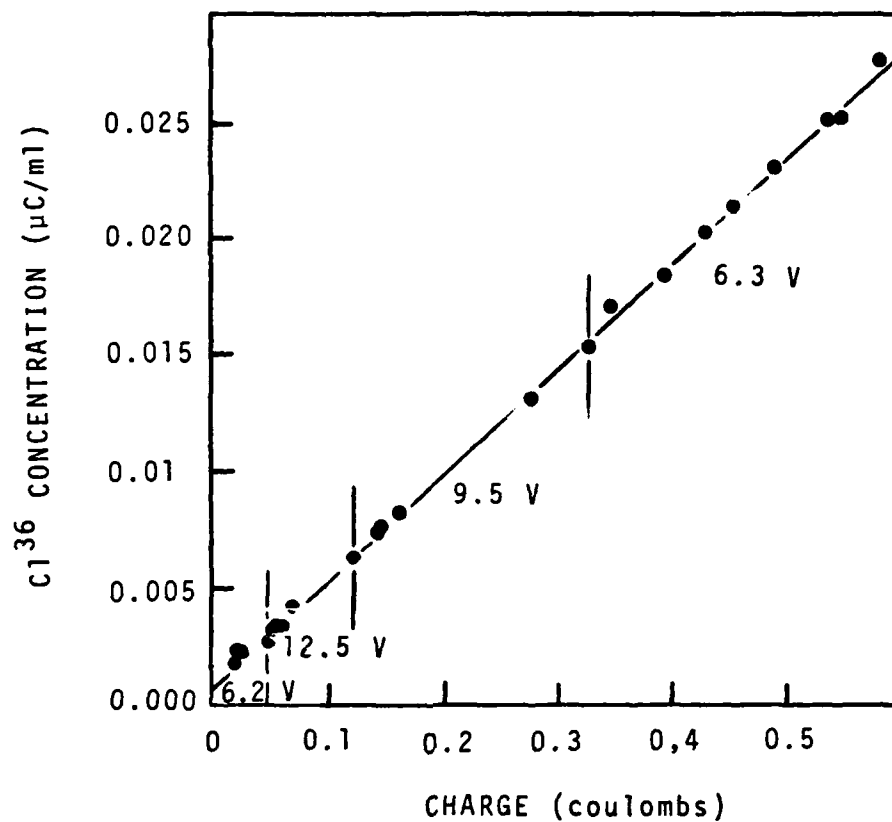


Fig. C-2.1 Radiotracer activity versus charge for NR-7-80. Specific chloride activity $2.08 \times 10^4 \mu\text{C}/\text{mol-Cl}$.

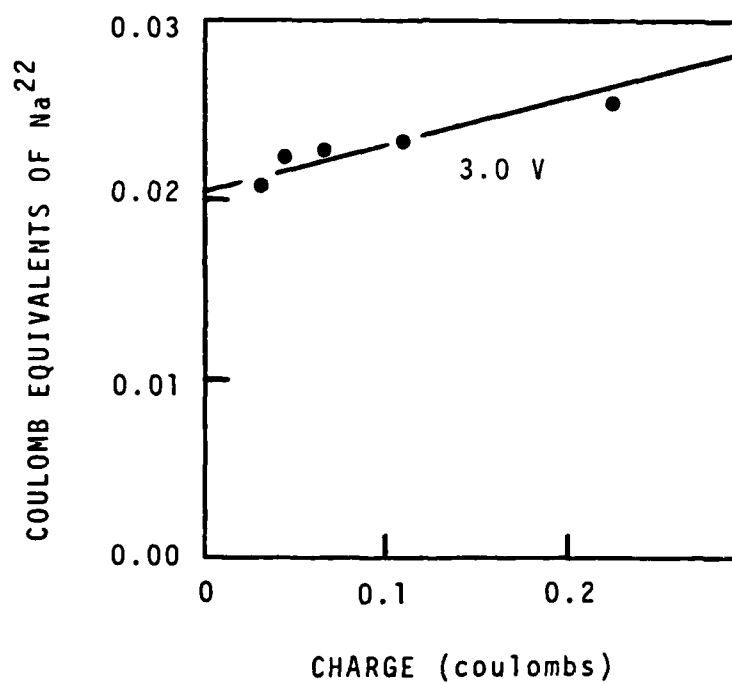


Fig. C-2.2 Equivalent sodium current versus charge for NR-8-80. Specific sodium activity $9.652 \times 10^{-4} \mu\text{C}/\text{mole-Na}$.

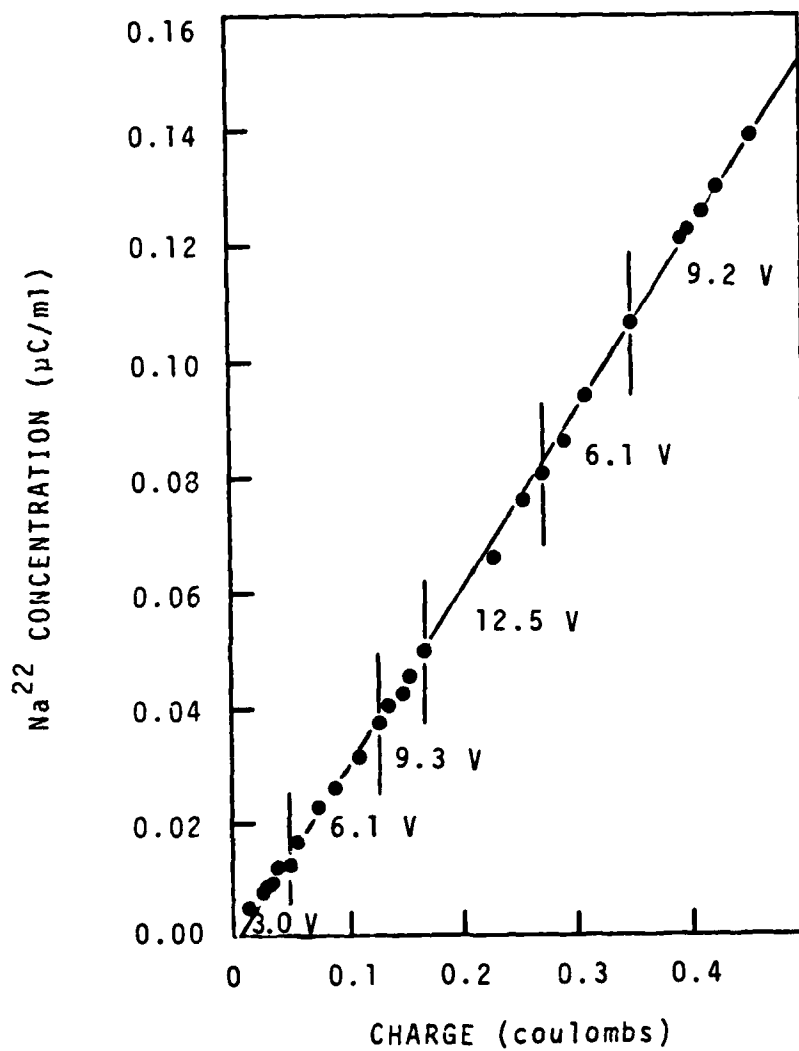


Fig. C-2.3 Radiotracer activity versus charge for NR-1-81. Specific sodium activity $1.224 \times 10^5 \mu\text{C/mol-Na}$.

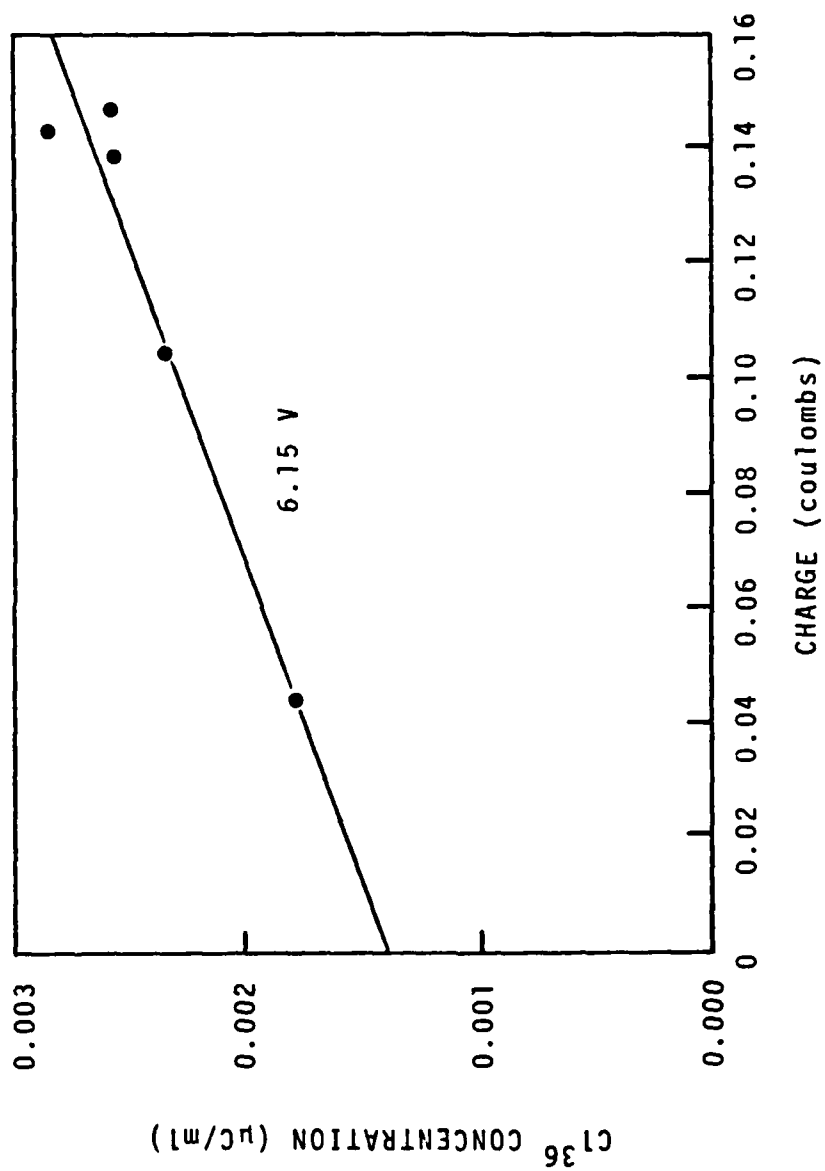


Fig. C-2.4 Radiotracer activity versus charge for NR-3-81. Specific chloride activity $4.572 \times 10^5 \mu\text{C}/\text{mol-Cl}$.

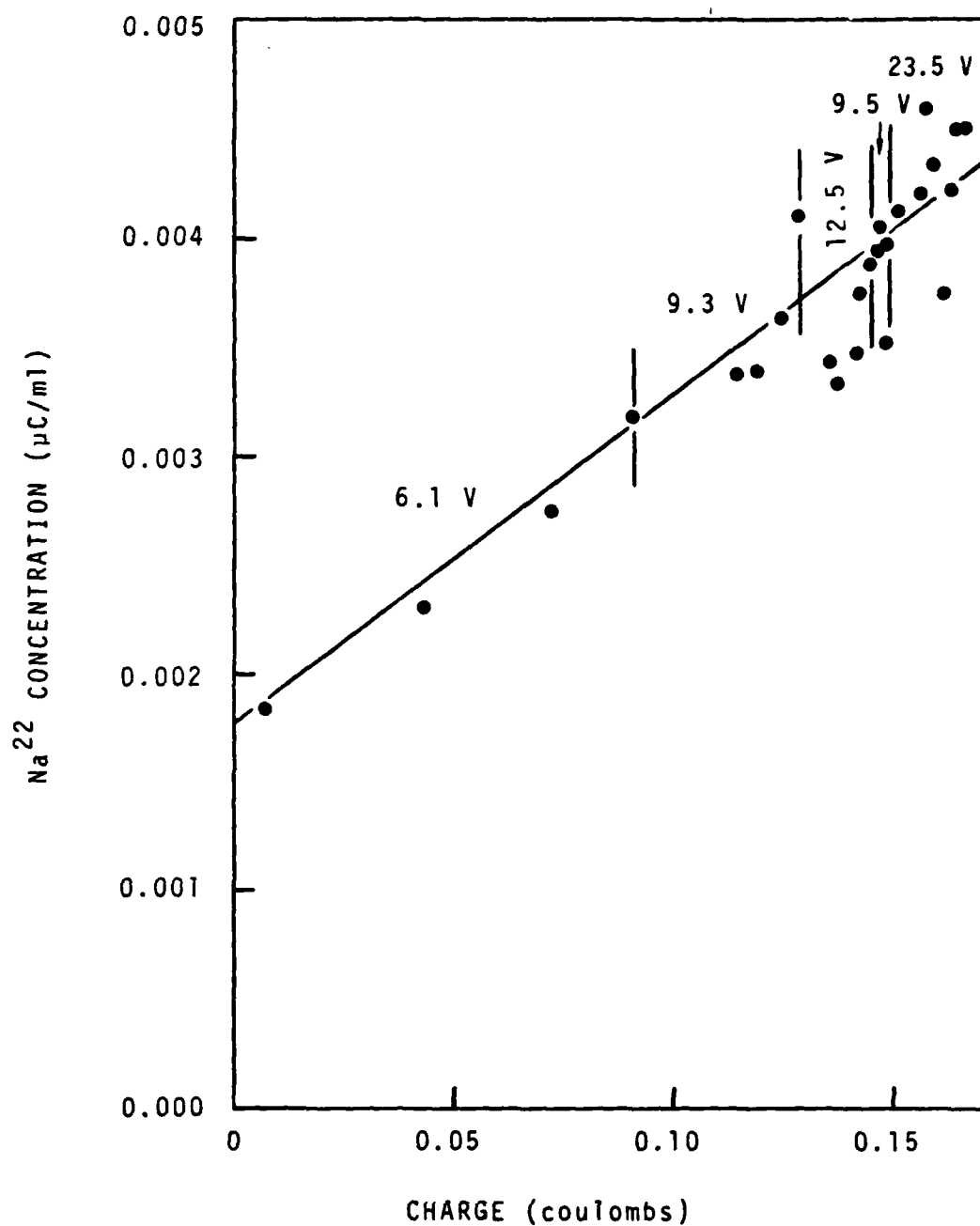


Fig. C-2.5 Radiotracer activity versus charge for NR-4-81.
Specific sodium activity $1.35 \times 10^4 \mu\text{C}/\text{mol-Na}$.

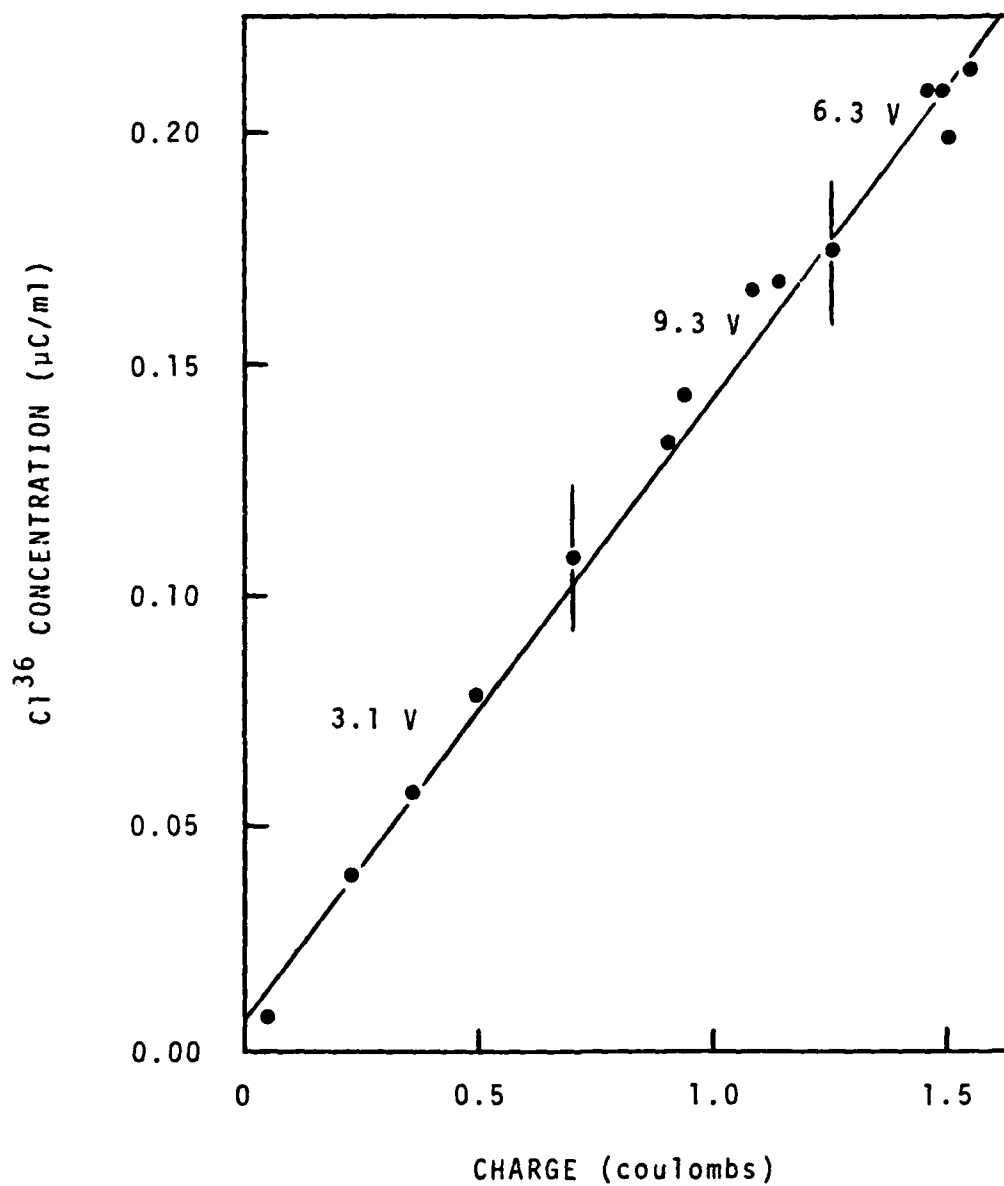


Fig. C-2.6 Radiotracer activity versus charge for NR-5-81.
Specific chloride activity 1.554×10^4 $\mu\text{C/mol-Cl}$.